Doctoral thesis submitted for the degree of Doctor of Philosophy in Telecommunication Engineering

Postgraduade programme: Communication Technology

Plasmonics and Metamaterials at Terahertz Frequencies

Presented by:

Víctor Torres Landivar

Supervised by:

Dr. Miguel Beruete Díaz and Dr. Miguel Navarro Cía

Pamplona, 2014

Acknowledgements

First of all, I wish to express my gratitude to Dr. Miguel Beruete and Dr. Miguel Navarro, who supervised this work, for their continuous support, constant advice and transferring me their knowledge and passion in this fascinating field. They always pushed me in the right way and they never let me lose the motivation during these years. I also thank to Dr. Francisco Falcone for introducing me in the research world and for his priceless advices regarding to research topics and life in general. Moreover, I have had the profound honor of working with the late Prof. Mario Sorolla who taught me the importance of humility and hardworking and who I consider one of the best examples of how a researcher must be. Also to my fellows from the Teralab, Pablo, Pacheco, Unai, and Baha for all moments spent together.

I would like to thank to Prof. Nader Engheta from University of Pennsylvania, Prof. Stefan A. Maier from Imperial College London and Prof. Alejandro Martínez from Universitat Politècnica de València for giving me the opportunity of being part of their research groups and so improving my quality as a researcher. Thanks to all people that I met in Philadelphia, London and Valencia, particularly to Pak, Jero, Marco, Lupe, Yoan, Rubén, Jose María and Álvaro, for making me feel like if I never would have left home.

Finally, I would like to acknowledge my family, especially my parents and brother for their unconditional support and trusting in me completely; my friends from Marcilla, for helping me to disconnect every weekend; all Telecos spread around the world, particularly Alberto M. for his unquestionable friendship; my flatmates, especially Andres for encouraging me to find the perfect wave; all colleagues from UPNA, and anyone who has played any role during these years. Thanks to all of you, today I am the person who I am.

Table of Contents

Introduction

This thesis describes the research work performed under the doctorate program "Communication Technology" from Universidad Pública de Navarra (UPNA), for the degree of Doctor of Philosophy (PhD) in Telecommunications Engineering. The guidance and supervision of this doctoral thesis has been conducted by Dr. Miguel Beruete Díaz from UPNA and Dr. Miguel Navarro Cía from Imperial College London. This work has been partially developed during three stays performed by this doctoral student in three additional institutions: at University of Pennsylvania under the guidance of Prof. Nader Engheta (3 months), at the Imperial College London under the supervision of Prof. Stefan A. Maier (3 months) and at Valencia Nanophotonic Technology Center, Universitat Politècnica de València, under the supervision of Prof. Alejandro Martínez (2 months).

Field of study and objectives

The research presented in this manuscript falls under the framework of metamaterials and plasmonics. It is mainly focused on applications at terahertz (THz) frequencies, a spectral band located between microwaves and infrared.

Metamaterials are advanced materials able to synthesize electromagnetic properties hardly found in natural materials by means of engineering their meta-atoms. Metallic inclusions are commonly used in metamaterials design. At low frequency bands such as microwaves and millimeter-waves, metals behave fundamentally differently than at infrared and optics. Plasmonics sets the theory of the interaction processes between electromagnetic radiation and conduction electrons of metals at such high frequencies.

The objective of this thesis is to devise, design, analyze and, whenever possible, experimentally realize and measure new metamaterials and plasmonics devices for free-space quasi-optical applications. Particularly, field concentrators in the form of advanced lenses and nanoantennas as well as advanced polarizing devices are targeted. The contributions presented here start from the specific theory of the field and the

results are supported by numerical simulations, analytical calculations and/or measurements of real prototypes.

Structure of the thesis and personal contributions

The manuscript begins with this *Introduction* where the research line and objectives are defined and the relation between the different works is established. The personal contribution of this author to each work is also highlighted here. This section is followed by four chapters which describe the main contents of the thesis.

In *Chapter 1* the fundamentals of plasmonics and metamaterials are described in order to present the foundations for the rest of the thesis. After some basic theory of electromagnetism, metamaterials are presented as effective media able to achieve intriguing electromagnetic properties. Next, the modeling of metals putting emphasis in the plasmonics effects is shown. Extraordinary transmission (ET), a phenomenon connected to both metamaterials and plasmonics, is presented at the end.

Chapter 2 describes the extraordinary transmission phenomena through subwavelength hole arrays (SHAs) from an equivalent circuit perspective. Three original contributions related with the circuital modeling and applicability of ET through mono- and bi-layer SHA are included:

- PAPER A: presents a mid-infrared inductor based on meandering lines that when applied to a regular SHA produces an inductance enhancement which causes a redshift of the resonant frequency and an enlargement of the operational bandwidth. This author performed the experiment and data analysis; contributed to the numerical results, the equivalent circuit analysis and the discussion; and wrote the paper.
- PAPER B: provides an equivalent circuit of the double-layer fishnet metamaterial based on the interpretation of the underlying physics. This model serves as a tool for designing and optimizing metamaterials with negative refractive index. This author conceived and analyzed the circuit, performed the numerical simulations, contributed to the discussion, and wrote the paper.
- PAPER C: shows a very compact quarter-wave plate metasurface that consists of a mono-layer SHA with modifications based on slits and meandering lines. This device operates at 1 THz and 2.2 THz with narrow and wide fractional bandwidth, respectively. This author conceived the idea, designed the metasurface, performed the numerical analysis and the experiment, contributed to the discussion, and wrote the paper.

Chapter 3 presents the squeezing energy principle in epsilon-near-zero (ENZ) metamaterials for focusing applications. Two original contributions are included:

- PAPER D: shows the experimental demonstration of a plano-concave ENZ metamaterial lens comprised of an array of very narrow metallic waveguides working, under the energy squeezing principle, at the lower part of the THz band. This author performed the experiment, analyzed the data, contributed to the numerical results and the discussion, and wrote the paper.
- PAPER E: presents the design guidelines of ENZ graded-index lenses of planar faces based on the energy squeezing through arrangement of metallic waveguides to be used at the THz band. The designs show a good performance in terms of impedance matching and focusing enhancement. This author performed the theoretical analysis and the numerical simulations, designed the structures, contributed to the discussion, and wrote the paper.

Chapter 4 introduces the initial work of the author in modeling nanoparticles to be used as plasmonics nanoantennas. One contribution is included:

- PAPER F: presents a plasmonic nanoantenna for multispectral surface-enhanced spectroscopy. This author performed the modeling and optimization of the nanoantennas and participated in the discussion.

The main body of the thesis is concluded with a final section of *General discussion of results and future lines* where a summary of the thesis is reported.

At the end of the manuscript, the *References* section lists all works that are cited throughout the text. After the references, the complete list of *Author's merits* is given, including the main contributions to international journals [PAPER A]-[PAPER F], the additional contributions to international journals [Paper 7]-[Paper 11] and the conference proceedings resulting from oral and poster presentations [Conf 1]-[Conf 28].

Chapter 1

Fundamentals of metamaterials and plasmonics

This chapter is an overview of metamaterials and plasmonics to put the thesis in its context. Starting from the basis of electromagnetics through Maxwell's equations, we will see how metamaterials can be seen as effective media which exhibit enthralling properties by means of tailoring the values of the constitutive electromagnetic parameters. Secondly, the modeling of the electromagnetic behavior of metals, which are crucial elements in the design of metamaterials, is analyzed from the Terahertz band up to the visible. In the latter domain, plasmonics effects play a key role, and thus, a detailed description of them will be given. Finally, extraordinary transmission, a phenomenon connected to both metamaterials and plasmonics, is described from a historical perspective, to show different theoretical explanations and experimental demonstrations that have flourished over more than a decade to describe it.

1.1 Introduction to metamaterials

Providing an exact and worldwide accepted definition for the term *metamaterials* is not an easy task due to the wide variety of contexts where this concept is used. In general, one might define metamaterials as artificially made materials which exhibit engineered electromagnetic properties that do not occur or may not be readily available in nature or in their constituent materials [SOLY 09], [SIHV 07]. This definition, which tries to embrace the most common uses of the term, is a derivation of

the original definition stated by Rodger Walser who coined the term metamaterials in 1999:

> "Metamaterials are macroscopic composites having man-made, three-dimensional, periodic cellular architecture designed to produce an optimized combination, not available in nature, of two or more responses to specific excitation."

The idea behind the metamaterial concept can be inferred from the understanding of how natural materials behave when they are excited with an electromagnetic field. As it is well known, the interaction of an electromagnetic wave with a material is totally determined by the atomic structure of that material. In other words, it is the atoms and the bonds among them which determine the response. When the wavelength of the electromagnetic wave is larger than 10 nm (which corresponds with the border between ultraviolet and X-rays in the electromagnetic spectrum), quantum effects can be neglected and the response is governed by macroscopic Maxwell's equations [JACK 98]:

$$\tilde{N}\acute{}\ \boldsymbol{E} + \frac{\P \boldsymbol{B}}{\P t} = 0 \tag{1.1}$$

$$\tilde{N}\acute{}\ \boldsymbol{H} - \frac{\P \boldsymbol{D}}{\P t} = \boldsymbol{J} \tag{1.2}$$

$$\tilde{N} \times \boldsymbol{B} = 0 \tag{1.3}$$

$$\tilde{N} \times \boldsymbol{D} = r \tag{1.4}$$

where $\boldsymbol{E}$ and $\boldsymbol{H}$ are the electric and magnetic field respectively, $\boldsymbol{B}$ is the magnetic flux density, $\boldsymbol{D}$ is the electric displacement, r is the free charge density and $\boldsymbol{J}$ is the free current density[1]. Both r and $\boldsymbol{J}$ are external sources to the material but the material itself generates new sources due to the interaction with the electromagnetic wave through the polarization $\boldsymbol{P}$ and magnetization $\boldsymbol{M}$ of the material. Actually, $\boldsymbol{H}$ and $\boldsymbol{D}$ are auxiliary fields defined as:

$$\boldsymbol{D} = e_0 \boldsymbol{E} + \boldsymbol{P} \tag{1.5}$$

$$\boldsymbol{H} = \frac{1}{m_0} \boldsymbol{B} - \boldsymbol{M} \tag{1.6}$$

[1] Symbols in bold type represent vector quantities, whereas symbols in normal type represent scalar quantities.

where ε_0 and μ_0 are the electric permittivity and magnetic permeability of vacuum[2], respectively. If we consider a linear media, the above equations can be written in terms of ε and μ, the constitutive parameters of the material[3], as follows:

$$\boldsymbol{D} = \varepsilon \boldsymbol{E} \tag{1.7}$$

$$\boldsymbol{H} = \frac{1}{\mu} \boldsymbol{B} \tag{1.8}$$

Therefore, the permittivity ε and permeability μ define all electromagnetic properties of the material according to the above equations. It must be highlighted that for isotropic materials, ε and μ are scalars, whereas for anisotropic materials, they are tensors. Moreover, materials are generally dispersive, so ε and μ depend on the frequency of the incident electromagnetic wave. This aspect is crucial in metals, as it is described later.

Up to this point, it has been stated that the elementary particles of the material, molecules and atoms, define its electromagnetic behavior. Metamaterials are based on the idea of engineering artificial elementary particles in order to achieve certain desired electromagnetic response. The size of these meta-atoms, also called unit cells, should be smaller (typically one order of magnitude) than the operation wavelength, so that homogenization of the macroscopic fields inside the metamaterial is valid [JACK 98]. The meta-atoms have a specific geometry and they are made of natural materials with certain ε and μ. However, a periodic (or quasi-periodic) disposition of the meta-atoms allows characterizing the whole structure with an effective permittivity ε_{eff} and permeability μ_{eff}. These effective parameters are different from the original ε and μ because the unit cell produces a specific electric and magnetic response where its geometry plays a role as important as the constituent materials. This way, it is possible to achieve values of ε and μ not available in nature and design tailor-made medium properties. Figure 1.1 illustrates these ideas.

---

[2] $\varepsilon_0 = 1/(\mu_0 / c_0^2) \approx 8.854 \cdot 10^{-12}$ F/m, $\mu_0 = 4\pi \cdot 10^{-7}$ H/m, $c_0 = 299792458$ m/s.

[3] $\varepsilon = \varepsilon_0 \varepsilon_r$ and $\mu = \mu_0 \mu_r$ where ε_r and μ_r are the relative permittivity and permeability of the medium, respectively.

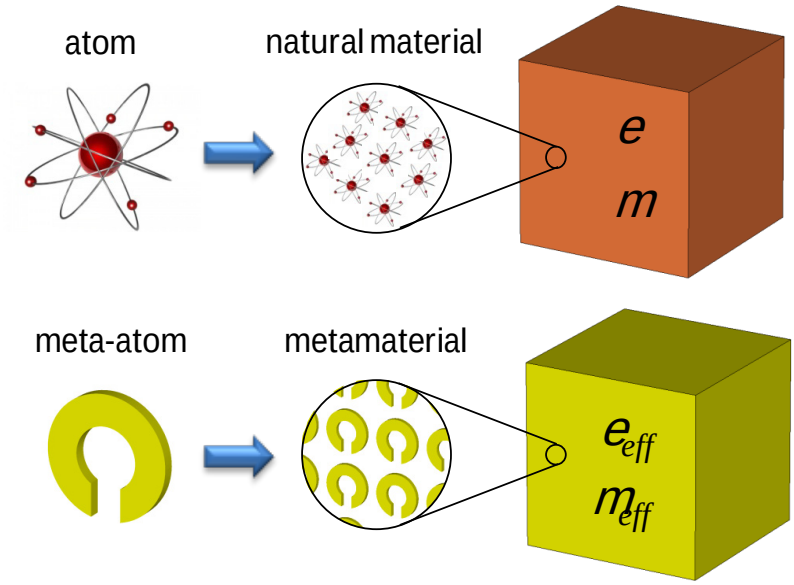

Figure 1.1. Analogy between natural materials (top) and metamaterials (bottom), composed by atoms and meta-atoms, respectively, which define the constitutive parameters of the whole structure.

Some scientists assign the term *metamaterials* also to artificial periodic composites where the size of the unit cell is comparable to the operation wavelength. In this case, a homogenization process would not be correct although precise control over propagation waves can be achieved as well. These kind of artificial structures are the so-called photonic crystals (PhCs) or photonic bandgaps (electromagnetic bandgaps in the microwave and millimeter-wave regime). They were initially proposed to control spontaneous emission of atoms [BYKO 72] [YABL 87], and shortly thereafter, they were suggested to manipulate the flow of light in a similar fashion as the flow of electrons in a solid-state crystal [JOHN 87] [YABL 91]. Since then, PhCs became a very dynamic research field due to their ability of inhibiting propagation in some frequency bands or space directions [JOAN 95], i.e. bandgap phenomena, and light confinement [JOHN 97]. With the advent of metamaterials similar capabilities of tailoring the electromagnetic response can be achieved but in a more reduce space, with the consequent technological implications .

1.2 Metamaterials as effective media

Metamaterials are engineered so that the unit cell of the periodic structure is much smaller than the operation wavelength. Therefore, the incident electromagnetic wave effectively sees a homogenous medium that can be analyzed by means of effective electric permittivity and magnetic permeability.

Metamaterials have their origins in artificial dielectrics. Probably, we owe the first attempt of an artificial material to Jagadis C. Bose, who conducted, in 1898, the first microwave experiment with artificial chiral elements [BOSE 98]. Of indubitable relevance is also the work of Karl F. Lindman in artificial chiral media conducted during the first twenty years of the past century. A brief summary of the life and work of this "last Herztian physicist"[4] can be read in [LIND 92]. Afterwards, in 1946, Winston E. Kock synthesized the first artificial dielectric medium using a periodic arrangement of spheres, disks and strips to tailor the index of refraction for constructing lightweight metallic lenses [KOCK 48]. Specially, artificial dielectrics came into use in the context of microwave technology between the 1950s and 1970s [BROW 53], [ROTM 62], [COLL 61].

Finally, the meaning of metamaterials was not completed until the development of artificial magnetic media. Initially investigated by Sergei A. Schelkunoff in the 1950s [SOLY 09], [MARQ 08], artificial magnetic media relaunched the interest of the scientific community in metamaterials after John B. Pendry, in 1999, proposed a subwavelength particle with a strong magnetic response, the Split-Ring Resonator (SRR) [PEND 99].

The combination of artificial dielectric and artificial magnetic media makes it possible to achieve effective metamaterials[5] with almost any desired value of permittivity ε and permeability μ and thus, obtain intriguing electromagnetic properties. Depending on the sign of ε and μ, we can distinguish four types of media: double-positive (DPS), epsilon-negative (ENG), mu-negative (MNG) and double-negative (DNG). In Figure 1.2 a scheme illustrating this classification is depicted.

[4] Lindman's aims were physical, in a purely Hertzian manner: to demonstrate an effect and increasing knowledge of it, rather than to find practical applications, using essentially the same methods as Heinrich Hertz did in his time.

[5] From now on, ε_{eff} and μ_{eff} in metamaterials will be denoted as ε and μ for clarity and to avoid ambiguity when we refer to normal (i.e. non-metamaterials) media.

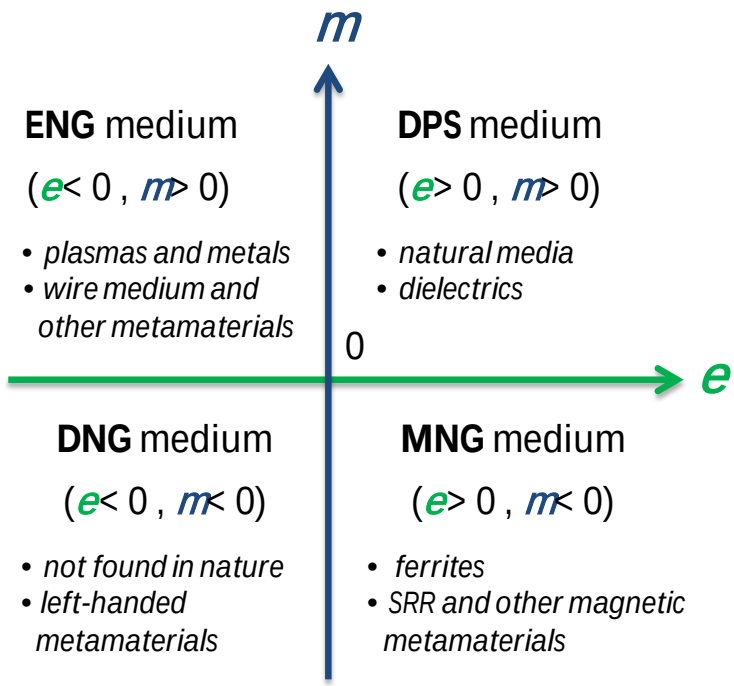

Figure 1.2. Permittivity-permeability diagram. The most relevant natural and artificial materials which fulfill the condition for the real part of ε and μ are indicated in each quadrant.

The values of the material constitutive electromagnetic parameters have a direct consequence in the propagation of a wave traveling through it. A plane wave propagates in a homogeneous, linear and isotropic medium[6] according to the equations:

$$\boldsymbol{E}(\boldsymbol{r},t) = E_0 e^{j(\omega t - \boldsymbol{k}\cdot\boldsymbol{r})}\hat{\boldsymbol{p}} \qquad \boldsymbol{H}(\boldsymbol{r},t) = \frac{1}{\mu} E_0 e^{j(\omega t - \boldsymbol{k}\cdot\boldsymbol{r})}(\hat{\boldsymbol{k}} \times \hat{\boldsymbol{p}}) \tag{1.9}$$

where E_0 is the complex magnitude of the field, ω is the angular frequency, t expresses the temporal dependence, $\hat{\boldsymbol{p}}$ is the unitary polarization vector and $\boldsymbol{k}$ is the propagation (or wave) vector whose magnitude is the wave number $k = \omega\sqrt{\varepsilon\mu}$. As the wave travels, it transports energy. The energy flux density is given by the Poynting vector $\boldsymbol{S} = \boldsymbol{E} \times \boldsymbol{H}$. Moreover, the wave travels with a phase velocity defined as $v_p = \omega/\boldsymbol{k} = 1/\sqrt{\varepsilon\mu}\hat{\boldsymbol{k}}$. Additionally, another material parameter is defined: the index of

[6] The analysis here avoids nonlinear and anisotropic considerations while giving the essentials for understanding the most important phenomena. In [RAMO 94] a full analysis can be read.

refraction. This magnitude relates the phase velocity in vacuum to the phase velocity in the material:

$$n = \frac{c_0}{v_p} = \frac{\sqrt{\varepsilon\mu}}{\sqrt{\varepsilon_0\mu_0}} = \sqrt{\varepsilon_r\mu_r} \tag{1.10}$$

Therefore, from the cross product of Eq. (1.9), it is deduced that vectors ***E***, ***H*** and ***k*** form an orthogonal triplet. Furthermore, vector ***S*** and ***k*** are parallel although they can be point to opposite direction depending on the sign of ε and μ. Next, we analyze more deeply the different kinds of media and present some of their most representative natural materials or metamaterials.

Double-positive media (DPS)

In DPS media $\varepsilon > 0$ and $\mu > 0$ and thus the index of refraction is positive, $n > 0$. Hence, vectors ***E***, ***H*** and ***k*** form a right-handed triplet and ***S*** and ***k*** points in the same direction. This means that the energy flows in the same direction as the phase propagation. This kind of propagation is called right-handed propagation and most natural materials present it. Regular dielectrics fall under this designation.

Mu-negative media (MNG)

Also called negative magnetic permeability media since $\varepsilon > 0$ and $\mu < 0$. Under this condition, wave vector ***k*** is imaginary and, according to Eq. 1.9, the complex exponential turns into real and the fields show an exponential decay, forbidding propagation of the electromagnetic wave. In certain frequency regimes, ferrites and some gyrotropic materials exhibit this characteristic. Metamaterials also comprise $\mu < 0$ and the SRR is the most widely-used elementary particle (unit cell).

- *Split-Ring Resonator*: is a non-magnetic subwavelength particle formed by two metallic concentric rings with slits (Fig. 1.3 (a)), although in its simplest form is just one ring. The incident axial magnetic field induces currents on the rings which produce a local magnetic moment that can balance the incident field giving rise to a Lorentz-like resonant effective permeability. This response shows a negative μ between the quasi-static frequency of the particle and the magnetic plasma frequency. In [MARQ 08], [PEND 99] a more rigorous analysis can be found where the bi-anisotropy of the particle is analyzed.

Epsilon-negative media (ENG)

In ENG media $\varepsilon < 0$ and $\mu > 0$. Therefore, similar to MNG media, the wave vector is imaginary and the fields suffer an exponential decay. A negative permittivity can be found in a plasma medium where the ionization of the molecules or atoms produces a

non-negligible volume of free charges which make the plasma electrically conductive so that it responds strongly to electromagnetic fields [STUR 94]. For instance, metals exhibit a negative permittivity below their plasma frequency [JACK 98]. Metals are the preferred material for the unit cell of metamaterials and it is the basic ingredient in the field of plasmonics. Hence, a more profound analysis of metals is provided in the next section. Two metamaterials structures with $\varepsilon < 0$ are highlighted here (Fig. 1.3(b)):

- *Wire medium*: the wire medium, also named rod medium, consists in a two- or three-dimensional rectangular lattice of resistive metallic wire grids [ROTM 62]. When the electric field is parallel to the wires, the medium behaves similar to a plasma, forbidding propagation below the resonance frequency. Moreover, it shows a strong spatial [BELOV 03], [DEME 08] and the homogenization process as effective medium is well defined in terms of the structural parameters [PEND 98], [SILV 05].
- *Complementary Split-Ring Resonator (CSRR)*: as its name indicates, the CSRR is a particle complementary to the SRR where the concentric rings are now subtracted from a metallic thin film. According to Babinet's principle [JACK 98] a dual behavior is obtained between the electric and magnetic field in the SRR and CSRR and hence, ε shows a strong resonance instead of μ [FALC 04], [FALC 04b].

Double-Negative Media (DNG)

A medium with simultaneous negative value of ε and μ was theoretically analyzed by V. G. Veselago in 1968 for the first time [VESE 68]. If $\varepsilon < 0$ and $\mu < 0$, then $\boldsymbol{E}$, $\boldsymbol{H}$ and $\boldsymbol{k}$ form a left-handed triplet and $\boldsymbol{S}$ and $\boldsymbol{k}$ point in opposite directions. Therefore, the energy flows in the opposite direction to the phase propagation. Moreover, the index of refraction is negative[7] which implies that a wave traveling from a right-handed to a left-handed medium (or vice versa) undergoes negative refraction. Then, according to Snell's law, the wave is negatively bent, as represented in Fig. 1.4. These media are also called left-handed media (LHM)[8], backward wave media or negative refractive index media (NRI) and no natural materials are known to have this characteristic. Furthermore, these media have other fascinating properties such as reversal of Doppler [VESE 68] and Goos-Hänchen effect [TSAK 07], reverse Cerenkov radiation [VESE 68], and reversed Casimir force from attraction to repulsion [LEON 07].

Lenses are probably the most benefited field of the negative refraction property. This property allows, for instance, interchanging the role of diverging concave and converging convex lenses. Moreover, unlimited resolution can potentially be achieved as a result of the enhancement of the evanescent components of the propagating waves

[7] This can be deduced from the definition of the index of refraction.
[8] Left-handed media will be the preferred name for this media from now on.

[PEND 00]. Pendry theoretically proposed this perfect lens that, although physically unrealizable due to limitations like losses, opened the door to new superlenses [PEND 06]. The concept of perfect focusing has triggered controversy since its inception [PEND 03].

The most typical structures that exhibit left-handed propagation are:

- *Wires and SRRs*: the combination of SRRs embedded in a wire medium was the first experimental demonstration of a synthesized artificial DNG medium [SMIT 00]. Smith and co-workers verified within a limited frequency range in the microwave region a simultaneous negative effective permittivity and permeability. Figure 1.3(c) shows a picture of the fabricated prototype.
- *Stacked Hole Array*: this structure consists of thin metallic layers periodically perforated with small holes and stacked with a subwavelength periodicity (Fig. 1.3(c)). Negative permittivity comes from transmission through a single subwavelength hole array, which is ascribed to ***extraordinary transmission*** phenomenon [EBBE 98], and negative permeability from the virtual current loop formed by the coupling between the layers [LIU 08]. The study of extraordinary transmission in stacked hole arrays and their applications is one of the aims of this thesis, so it is analyzed in depth in Chapter 2.

Apart from the previous classification of effective metamaterials according to the sign of the constitutive parameters, few subcategories have been proposed to highlight extreme cases with exciting properties such as, metamaterials exhibiting permittivity and/or permeability near zero (no matter the sign). They are called zero-index metamaterials because the index of refraction is, in absolute value, much smaller than unity when $\varepsilon \approx 0$ and/or $\mu \approx 0$. In steady state, the fields in a zero-index medium are quasistatic in character and zero phase variation is seen across the medium. Moreover, the entire medium is able to radiate coherently in phase. Such properties have derived in a large number of potential applications such as compact resonators, highly directive sources, delay lines or wave front transformers among others [ENGH 06]. A particular case of zero-index metamaterials is that with only $\varepsilon \approx 0$, the so-called ***epsilon-near-zero*** metamaterials. An important section within this thesis is dedicated to them. In Chapter 3, the most relevant properties of such materials, roughly similar to the zero-index ones, and inspiring applications in metallic lenses are presented.

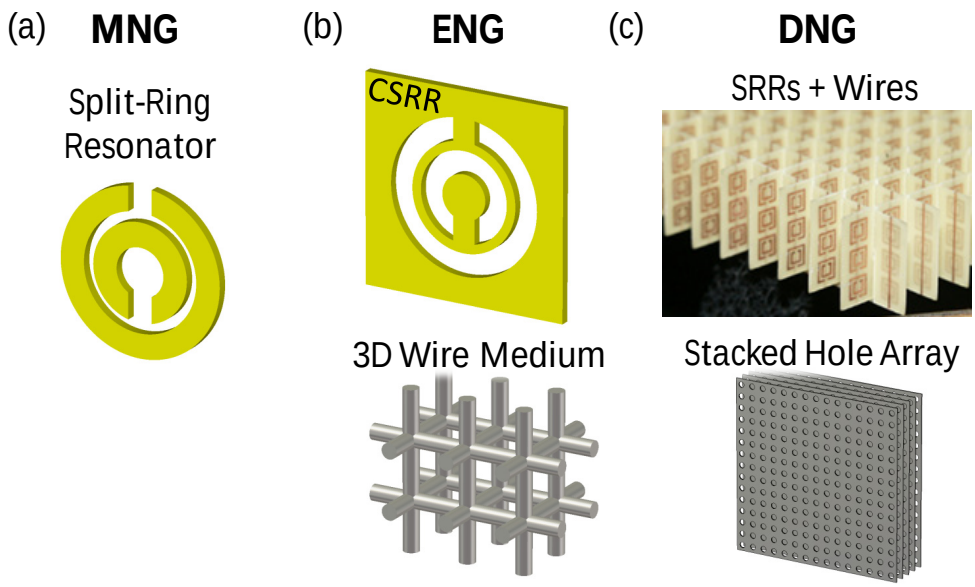

Figure 1.3. Representation of elementary particles or full structures which are able to produce (a) MNG, (b) ENG and (c) DNG media.

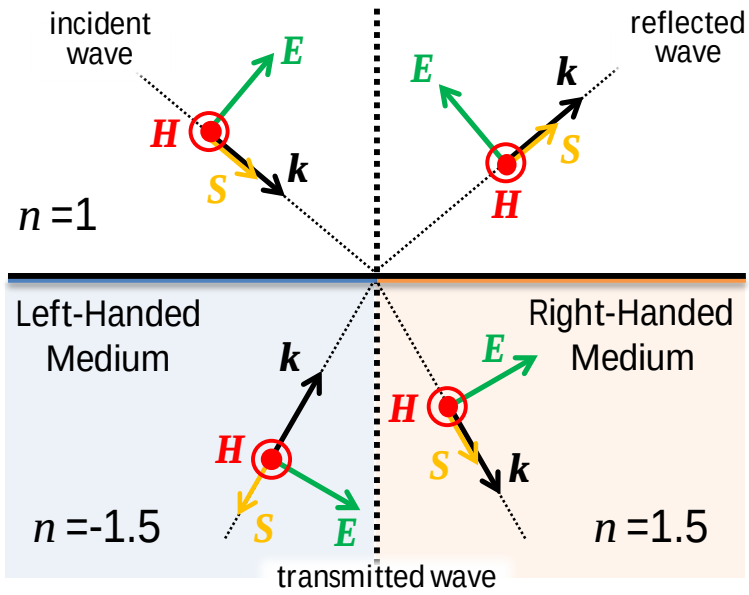

Figure 1.4. Wave obliquely impinging from air upon a LHM–RHM interface. Direction of electric ***E*** and magnetic ***H*** field, wave vector ***k*** and Poynting vector ***S*** are depicted in order to highlight left-handed and right-handed propagation.

1.3 The Terahertz gap Electromagnetic considerations

The THz band is the portion of the electromagnetic spectrum corresponding to frequencies between 0.1 THz and 10 THz. Accordingly, THz fields have wavelengths extending from 3 mm up to 30 mm. This wavelength interval ranges between the top edge of the microwave region to the bottom edge of the optical spectrum corresponding to the boundary of the far-infrared (FIR) with the mid-infrared (MIR) spectral region. Despite the fact that THz radiation is located between two highly developed technologies such as microwaves and optics, the technical difficulties involved in developing efficient and compact THz sources and detectors made this band the least explored region of the spectrum [LEE 09]. The historical lack of suitable technologies led to the THz band being called the "THz gap". In Fig. 1.5, the location of the THz band within the electromagnetic spectrum is depicted.

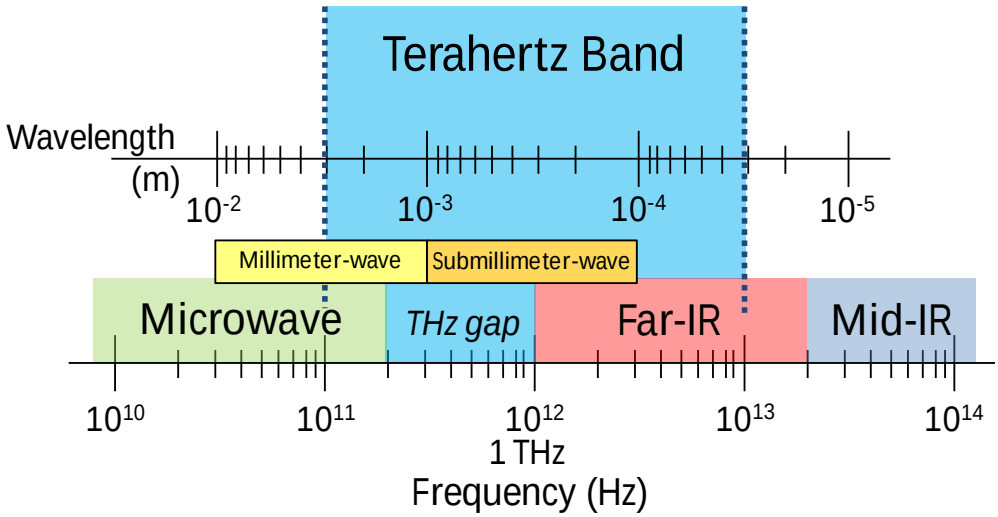

Figure 1.5. Terahertz band in the electromagnetic spectrum

The origin of THz science as we know it today started during the late 1960s and 1970s with the study of the response of materials to the excitation of ultrafast pulsed lasers [REDO 13]. However, it was during the 2000s when THz science experienced a boost thanks to the commercialization of user-friendly and reliable THz systems. The outstanding applications that THz can offer have precipitated the wide commercialization over the last decade. Next, a summary of features and applications of THz science is provided [REDO 13], [DRAG 04]:

- THz waves can penetrate most materials, like microwaves, but offer a much better spatial resolution that makes them very suitable for imaging applications. The see-through capability of THz waves makes them very suitable for explosive and related compounds detection and identification.
- The spectral energy distribution in observable galaxies shows that 50% of the total luminosity and 98% of photons emitted since Big-Bang are located in the THz band. Moreover, high-resolution THz spectroscopy is used to monitor the Earth atmosphere and observe molecules in the interstellar medium.
- Many organic molecules have unique absorption features in the THz band. Applications in the medical area have been proposed for skin, breast and liver cancer diagnosis and skin burn evaluation.
- THz spectroscopy is also proposed for detection of contaminants and pesticides in the food industry, pharmaceutical characterization and pill coating research.
- Small and miniaturized antenna arrays and circuits can be used in the THz range to send or receive a huge quantity of information encoded in ultra widebands.
- The interest to exploit THz has boosted the development of continuous wave systems such as quantum cascade laser, backward-wave oscillators or photo-mixers, and time-domain systems based on femto-second lasers.

Despite the effort during the last decade, THz technology has not yet reached maturity and a lot of work remains to be done. Specially, passive devices such as lenses, waveguides, beam-splitters and antennas are needed and the research conducted through this thesis pretends to help with this aim.

Models for metals

The THz band is also an intermediate spectral region for the electromagnetic properties of materials. While the Drude mechanism and Debye relaxation are dominant processes at the medium-low region of the THz band, at the mid-infrared, lattice vibrations (optical phonons) become important and should not be disregarded [LEE 09]. In general, the Drude model is able to explain accurately how media respond to external electromagnetic fields, specially the transport properties of electrons in materials. However, several approximations are usually done at low frequencies in order to simplify the analysis of the wave-matter interactions. The Drude model, proposed by Paul Drude in 1900 [DRUD 00], considers a medium consisting of a density n_e of free electrons per unit volume of mass m and charge e, in a background of fixed positive ions of the same density. This can model a conductor, semiconductor or plasma. It establishes a relation between the free current density $\boldsymbol{J}$ and the electric field $\boldsymbol{E}$:

$$\boldsymbol{J} = \frac{n_e e^2 \boldsymbol{E}}{m(v + j\omega)} \tag{1.11}$$

where v is the collision frequency. This can be inserted in Maxwell's equations resulting in a complex permittivity for the medium:

$$\varepsilon = \varepsilon' - j\varepsilon'' = \left(\varepsilon_1 - \frac{n_e e^2}{m(v^2 + \omega^2)} \right) - j\left(\frac{v}{\omega} \frac{n_e e^2}{m(v^2 + \omega^2)} \right) \tag{1.12}$$[9]

From the above expression is defined the plasma frequency

$$\omega_p = \sqrt{n_e e^2 / \varepsilon_0 m} \tag{1.13}$$

where the permittivity becomes zero[10]. Then, Eq. 1.12 can be rewritten, now in terms of the relative permittivity, as follows

$$\varepsilon_r = \varepsilon_\infty + \frac{\omega_p^2}{-\omega^2 + j\omega v} \tag{1.14}$$

which is the most common form of expressing the complex permittivity of the Drude model and where ε_∞ is the value of the permittivity at infinite frequency[11]. For instance, for noble metals such as gold or silver, the plasma frequency is located at ultraviolet frequencies [ORDA 85].

For microwave and millimeter-wave frequencies $\omega^2 << v^2$ and Eq. (1.14) becomes

$$\varepsilon_r = 1 - j\frac{\sigma}{\omega\varepsilon_0} \tag{1.15}$$

where $\sigma = n_e e^2 / mv$ is the low-frequency electric conductivity. This expression is usually applied to model metals as good conductors in such frequency ranges. It is also denominated as constant conductivity model since the conductivity is a frequency independent constant. From Maxwell's equations two important facts can be extrapolated that actually may be taken as a definition of a good conductor [RAMO 94]:

---

[9] ε_1 represents the effect of the bound electrons of the positive ion background. In an ideal free-electron medium $\varepsilon_1 = \varepsilon_0$.

[10] At the plasma frequency the collision frequency is negligible so we can take $\varepsilon_1 = \varepsilon_0$ and $\varepsilon'' = 0$.

[11] Usually $1 \le \varepsilon_\infty \le 10$.

- Conduction current is given by Ohm's law: $\boldsymbol{J} = \sigma \boldsymbol{E}$ and therefore, the net charge density is zero for homogeneous conductors.
- Displacement current $\boldsymbol{D}$ is negligible in comparison with conduction current $\boldsymbol{J}$.

An additional model for metals is very commonly used in electromagnetic theory: the perfect conductor model. A perfect conductor, also perfect electrical conductor (PEC), would be a conductor in which the collision frequency approaches zero and accordingly, the conductivity tends to infinite. Therefore, a steady current within a PEC will flow without dissipating energy and hence ohmic losses will not be present. Moreover, the electric field inside the perfect conductor is null and an instantaneous magnetic field is assumed [RAMO 94]. For frequencies well below the plasma frequency, these assumptions can be applied in metals with small error. PEC models are frequently used in computational electromagnetics since they allow saving simulation time.

Therefore, metals can be modeled as Drude media according to Eq. 1.14, as good conductors according to Eq. 1.15 or as perfect electrical conductors. Apart from the PEC model, which is clearly the less accurate one since losses are not considered, a question must be answered; *which model is preferable in the THz gap?* Or simply, *which model (if any) is correct?* In order to shed light on this question, a comparison between good and imperfect conductor is done for gold. In this example, gold is modeled with the following Drude parameters [ORDA 85]: $\varepsilon_\infty = 9.1$, $\omega_p = 1.38 \cdot 10^{16}$ rad/s and $\nu = 1.075 \cdot 10^{14}$ Hz. A finite conductivity equal to $4.1 \cdot 10^7$ S/m is assumed for the good conductor model [ORDA 85]. A comparison between the real and imaginary part of ε_r in both models as a function of the frequency is shown in Fig. 1.6. Moreover, a figure of merit is defined in order to clarify whether the real part dominates over the imaginary one or vice versa.

First of all, it is observed in Fig. 1.6(a) that at low frequency ε'_r does not match between both models. This is expected because of the non-dispersive nature in the good conductor model. However, the imaginary parts agree very well up to 10 THz (Fig. 1.6(b)). Secondly, by inspecting Fig. 1.6(c), we see that for frequencies below 10 THz (10^{13} Hz) $|\varepsilon''_r| > |\varepsilon'_r|$. So, we conclude:

- For f < 10 THz: $|\varepsilon''_r|$ dominates over $|\varepsilon'_r|$ and accordingly, the disagreement in $|\varepsilon'_r|$ is not crucial. In other words, the behavior of the metal depends mainly on $|\varepsilon''_r|$ and, as shown in Fig. 1.6(b), both models give similar results for this parameter. So both models can be applied in this frequency range without large difference.

· For f > 10 THz: $|e'_r|$ dominates over $|e''_r|$ and thus, the good conductor model must not be applied since it does not predict the dispersive behavior of metals.

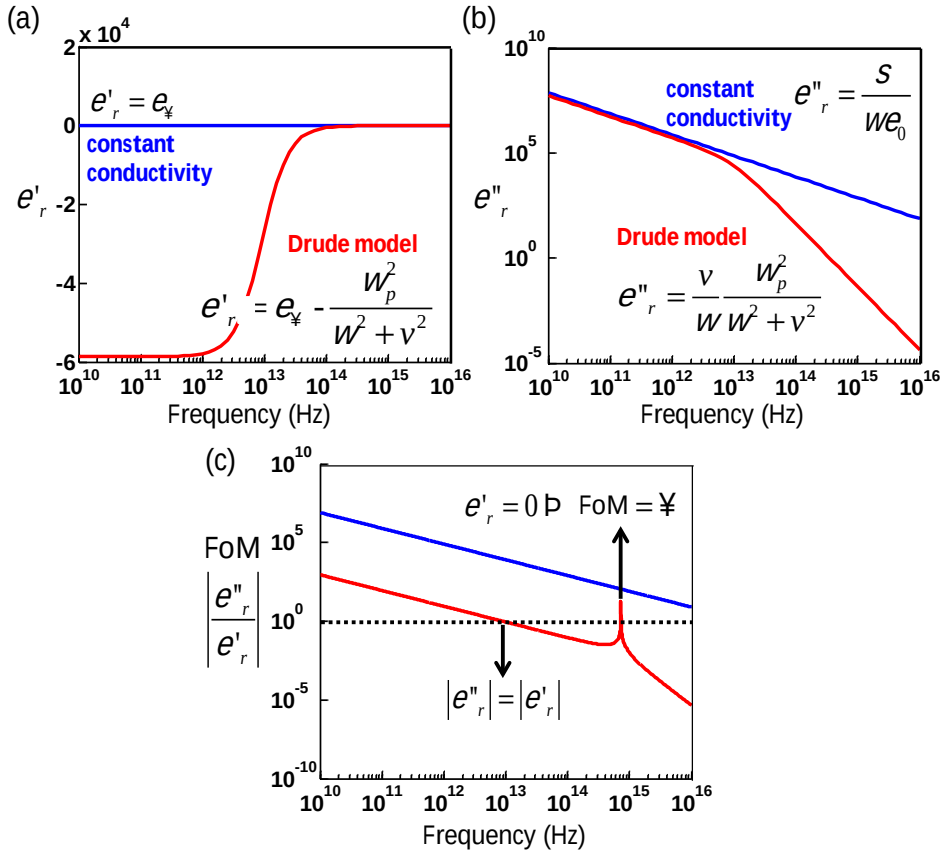

Figure 1.6. Comparison of gold permittivity obtained with constant conductivity (blue) and Drude model (red). a) Real part b) Imaginary part c) Figure of merit $|e''_r/e'_r|$.

Finally, the validity of the Drude model is corroborated by comparing the complex permittivity of the model with values obtained experimentally. There are two seminal works, one conducted by P. B. Johnson and R. W. Christy [JOHN 72] and other by Palik [PALI 85], where the permittivity of different metals is experimentally obtained for optical frequencies. Permittivity of gold (Au), silver (Ag) and copper (Cu) are compared in Fig. 1.7 where a very good agreement is observed in all cases for e'. However, the imaginary part is not well predicted for very high frequencies due to the occurrence of interband transitions, leading to an increment of e'' [MAIE 04]. Therefore, Drude model adequately describes the optical response of metals for frequencies below the threshold of transitions between electronic bands. Because of

that, it is one of the most used models at the THz and infrared region and of indubitable importance in this thesis.

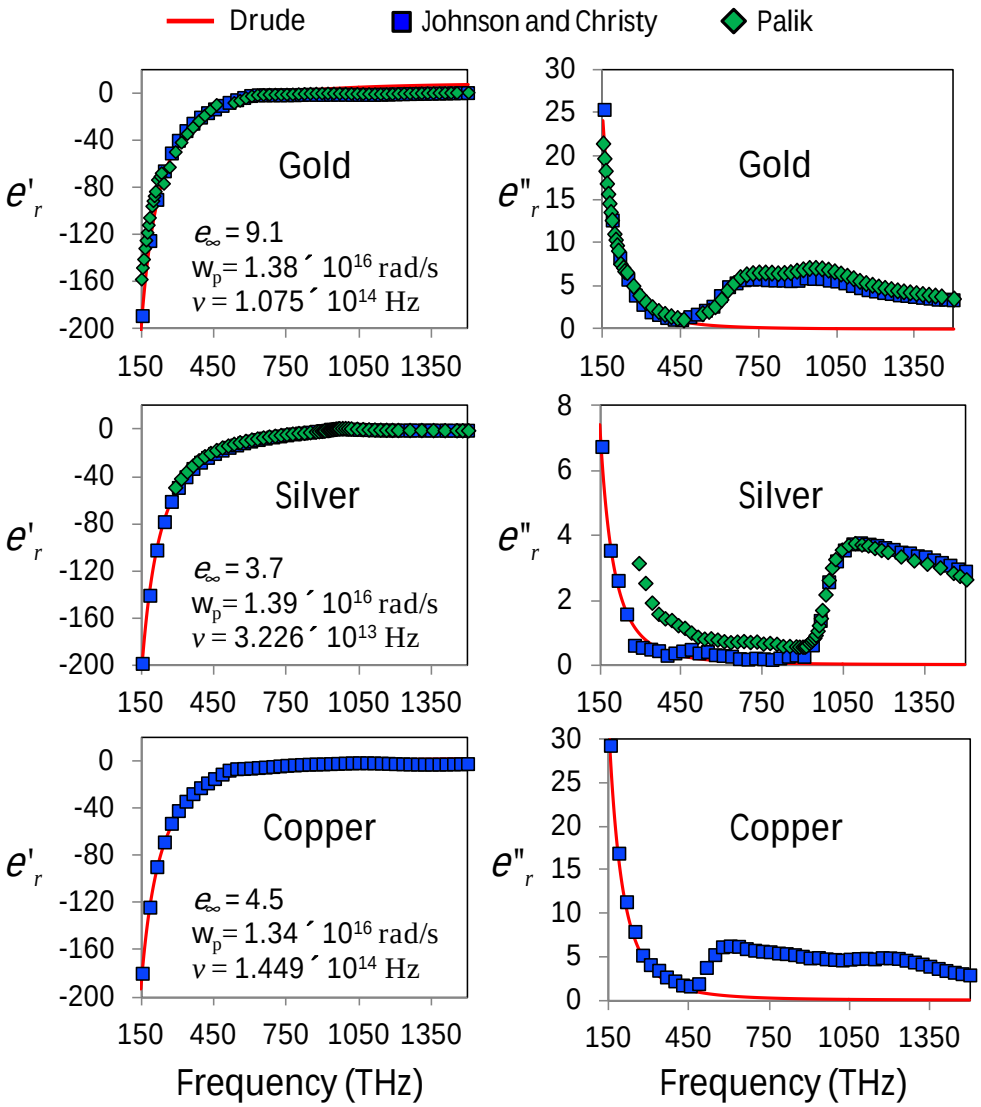

Figure 1.7. Validation of Drude model (continuous line) with respect to experimental values obtained by Johnson and Christy (blue squares) and Palik (green rhombus) for gold, silver and copper (Palik does not provide any value for copper).

1.4 Plasmonics and surface plasmons

Plasmonics describes the interaction process between electromagnetic radiation and conduction electrons at metals. It forms part of the field of nanophotonics, which explores the confinement of electromagnetic fields over dimensions on the order of or smaller than the wavelength of light. In the previous section, we have seen how for the THz band and below, metals behave as good conductors since electrons can follow easily the driving electromagnetic field. However, at higher frequencies, free electrons in metals can be excited to have collective oscillations and hence, more refined theories are needed. Plasmonics explains this phenomenon, for instance, with models such as the Drude approximation which characterizes with high accuracy the behavior of metals up to the visible. There are two main players in the field of plasmonics: surface plasmons polaritons and localized surface plasmons.

Surface plasmons polariton

Surface plasmons polaritons (SPPs) are electromagnetic excitations propagating at the interface between a dielectric and a conductor, evanescently confined in the perpendicular direction [MAIE 04]. At optical frequencies, the fields are able to slightly penetrate into the metal due to the rapid variation of the electromagnetic fields and, under certain conditions, a self-sustained excitation can be induced near the surface which may propagate closely confined to the metal. Research on SPPs dates back to 1899, when Sommerfeld studied propagation along the surface of conductors with finite conductivity in the context of radio waves over Earth's surface [SOMM 99].

The simplest geometry sustaining SPPs is a flat interface between a dielectric with real positive constant permittivity and a metal. In [ISHI 90], it is presented a straightforward explanation of how starting from Maxwell's equations through Helmholtz equation we arrive to the dispersion relation of SPPs[12]:

$$\beta_x = k_0 \sqrt{\frac{\varepsilon_d \varepsilon_m(\omega)}{\varepsilon_d + \varepsilon_m(\omega)}} \tag{1.16}$$

where β_x is the propagation constant which corresponds with the component of the wave vector in the direction of propagation, k_0 is the wave vector of the propagating wave in vacuum and ε_d and $\varepsilon_m(\omega)$ the permittivity of the dielectric and the metal, respectively. The dispersion relation is depicted in Fig. 1.8 together with the

[12] Certain boundary conditions are assumed at the interface to allow wave coupling and only transverse magnetic modes fulfill them.

representation of the geometry. From Eq. (1.16) and Fig. 1.8(b) the bound nature of the SPP can be deduced: b_x is larger than dielectric's wave vector $\boldsymbol{k}$ and therefore, the dispersion curve lies to the right side of the dielectric's light cone leading to evanescent decay on both sides of the interface, as represented in Fig. 1.8(a). Accordingly, a wave impinging with an angle θ to the interface will never excite a SPP since the projection of its wave vector $k_x = k\sin(\theta)$ is always smaller than b_x. So, in order to excite a SPP, phase-matching techniques should be applied to provide an additional momentum to the impinging light [MAIE 04]. The most common techniques for SPP excitations are: excitation upon charged particle impact, prism coupling, grating coupling, excitation using highly focused optical beams or near field excitations.

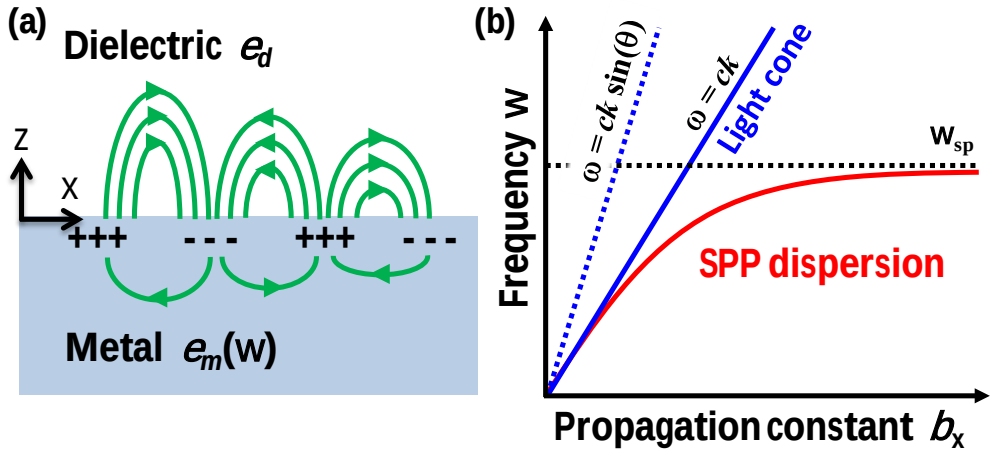

Figure 1.8. (a) Geometry and electric field for SPP propagation at a dielectric-metal interface. (b) Dispersion relation[13].

Localized surface plasmons

Localized surface plasmons (LSPs) are non-propagating excitations of the conduction electrons of metallic nanostructures coupled to the electromagnetic field. This resonance arises from effective restoring forces on the driven electrons thanks to the geometry of the nanostructure which allow the suitable scattering condition [JACK 98]. A major difference from SPP is that LSP can be excited by direct light illumination without the need of phase-matching techniques. Let us describe briefly the scattering problem.

For a particle of size much smaller than the wavelength of excitation in the surrounding medium, a quasi-static approximation can be done since over the volume

[13] A lossless Drude model is assumed in Fig. 1.8(b).

of the particle, the phase of the oscillating electromagnetic field is practically constant. For a small nanosphere, under this electrostatic approach and after some algebra [MAIE 04] we arrive to an expression for the dipole moment $\boldsymbol{p} = \varepsilon_0 \varepsilon_m \alpha \boldsymbol{E}$ with

$$\alpha = 4\pi a^3 \frac{\varepsilon - \varepsilon_m}{\varepsilon + 2\varepsilon_m} \tag{1.17}$$

where α is the electric polarizability of a small sphere of subwavelength diameter *a*, permittivity ε within a medium with ε_m under the excitation of an electric field $\boldsymbol{E}$. According to Eq. (1.17), the polarizability experiences a resonant enhancement under the condition that $|\varepsilon + 2\varepsilon_m|$ is a minimum. For the case of small or slowly-varying imaginary part of ε, the resonance takes place when $\mathrm{Re}[\varepsilon] = -2\varepsilon_m$, expression known as the Fröhlich condition. Notice that there is a strong dependence of the resonant frequency on the surrounding medium. Therefore, metal nanoparticles are ideal elements for optical sensing of changes in the index of refraction. This is shown in Fig. 1.9(a) where the polarizability of a gold sphere within two different media is depicted. A consequence of the resonantly polarization of the particle is an efficiency enhancement of the scattering and absorption features, much more interesting from the viewpoint of optics because they are measurable magnitudes. The corresponding cross section for scattering C_{sca}, absorption C_{abs} and extinction C_{ext} are calculated as [BOHR 98]:

$$C_{sca} = \frac{k^4}{6\pi}|\alpha|^2 \qquad C_{abs} = k\,\mathrm{Im}[\alpha] \qquad C_{ext} = C_{sca} + C_{abs} \tag{1.18}$$

where *k* is the wave number. The extinction cross section of the gold nanosphere is shown in Fig. 1.9(b) where the influence of the surrounding medium can be noticed as well.

We have seen that a nanoparticle behaves as an electric dipole, resonantly scattering and absorbing electromagnetic fields if the Fröhlich condition is fulfilled. However, this theory is only valid for a spherical or ellipsoidal small particle. For particles of larger dimensions, a more rigorous analysis is required. In 1908, Mie developed a complete theory (today known as Mie theory) of the scattering and absorption of electromagnetic radiation by a sphere [MIE 08] being the beginning of the localized surface plasmons theory. Nevertheless, Mie theory cannot be applied to complex geometries and thus, computational methods are needed. In Chapter 4, the modeling of nanoparticles working as plasmonic nanoantennas will be described.

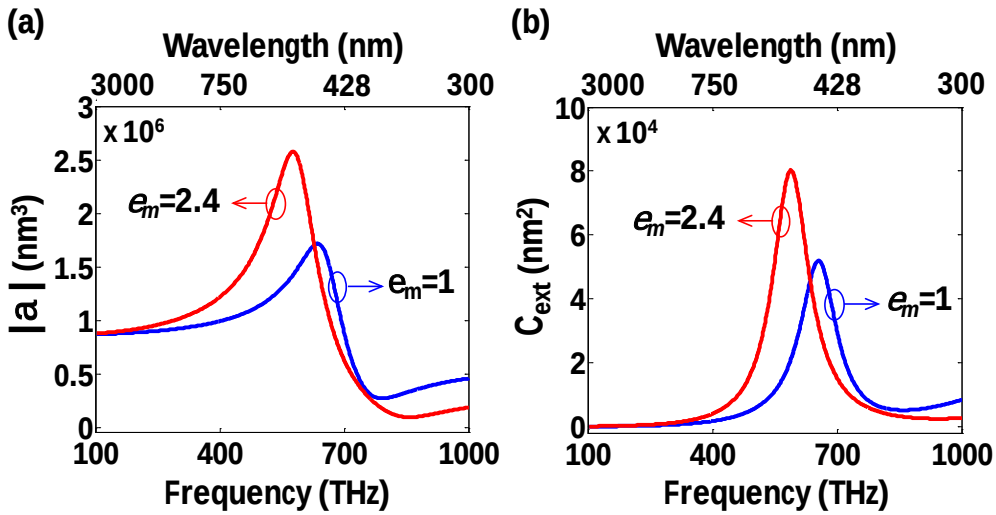

Figure 1.9. (a) Polarizability and (b) extinction cross section of a gold nanosphere of radius 50 nm in two media with two different permittivity e_m. Gold permittivity is taken from Drude model.

Implication of plasmonics in THz metamaterials

Strong electromagnetic field confinement in a dielectric-metal interface can occur over length scales smaller than the wavelength as long as the fields oscillate at frequencies close to the plasma frequency of the metal. Therefore, SPPs are limited to the visible and near-infrared range since noble metals find their plasma frequency close to that part of the spectrum. For lower frequencies, permittivity of metals is very large leading to negligible field penetration in the conductor and thus, SPPs are highly delocalized. In the limit of perfect electrical conductors, no field resides inside the metal forbidding the existence of SPPs.

So it seems that potential applications of SPP such as localized waveguiding and optical sensing cannot be achieved for the THz band and below. However, this limitation can be overcome with metamaterials[14] tailoring the effective permittivity and thus, the effective plasma frequency to lower frequencies by means of engineering the metal surface geometry. Pendry and coworkers demonstrated that metallic surfaces periodically corrugated are able to support bounded surface waves, even if the metal is a perfect conductor, mimicking the behavior of SPPs [PEND 04]. They coined these waves as spoof SPPs. However, this interpretation is just a useful equivalence for the optical community of a specific kind of complex waves: surface waves. Surface waves supported by corrugations have been used in antennas engineering for a long time

[14] Also with doped semiconductors.

[WALT 65]. Moreover, from a microwave engineering point of view, complex waves are also very well known [COLL 91], [ISHI 90] and they include backward/forward leaky waves, trapped surface waves or Zenneck waves among others. In [ISHI 90] a complete analysis of all types of complex waves can be found. Of special interest for this thesis are complex waves supported on the surface of metallic layers periodically perforated with subwavelength holes, intimately linked to extraordinary transmission phenomenon which is discussed next.

1.5 Extraordinary transmission phenomenon

Extraordinary transmission (ET) is a phenomenon referred to high transmittance peaks in the cutoff region of subwavelength hole/slit arrays or a single aperture surrounded by periodic corrugations. It was denominated "extraordinary" because a metal layer drilled with subwavelength holes is expected to behave like an opaque screen since the small size of the holes limits the transmission efficiency. According to Bethe's theory [BETH 44], under normal incidence, transmission through a single hole in a thin perfect conductor is proportional to $(r/\lambda)^4$, where r is the hole radius and λ the operation wavelength. Therefore, very low transmission efficiency would be expected in subwavelength apertures due to the poor coupling with radiative electromagnetic modes. However, in 1998, Ebbesen and coworkers reported experimentally high transmittance through a square array of subwavelength circular holes in a thin silver screen [EBBE 98]. They named this phenomenon extraordinary optical transmission since the discovery was carried out at optical frequencies. Since then, much attention has been paid on explanations and potential applications of ET which has finally become a milestone in metamaterials and plasmonics.

ET background: Dichroic filters

Antecedents of ET can be traced back to more than one century ago with the first studies of light transmission through holes or gratings. Probably, it was Lord Rayleigh who firstly analyzed transmission through subwavelength apertures [RAYL 07]. Others authors such as Wood [WOOD 02] or Synge [SYNG 28] also contributed to the topic at the beginning of the 20th century. Later, in 1940s, Bethe developed a deep analysis of the field scattered by a single aperture [BETH 44] and subsequently, analytical corrections were introduced by Bouwkamp [BOUW 54]. It was during the 50s, 60s and 70s when transmission through perforated plates acquired more relevance

in the context of dichroic filters in microwave engineering [BROW 53], [ROBI 60], [CHEN 71], [CHEN 73] and infrared [ULRI 67].

Dichroic filters are periodic structures fabricated from relatively closed-packed waveguides drilled in a metallic plate. Therefore, they might be understood as periodic hole arrays since a thin waveguide might be seen as a drilled hole. Dichroic filters are typically used as frequency selective surface since they exhibit a bandpass response: the lower cutoff frequency of the band is determined by the cutoff frequency of the propagating modes inside the waveguide whereas the higher cutoff frequency is due to the redistribution of energy caused by the periodic array when a new diffraction order becomes propagating [HESS 65], [MUNK 00]. Nevertheless, the principle of operation of ET through subwavelength hole arrays (SHAs) is inherently different since the hole sizes are considerable small for those wavelengths at which there is transmission, i.e. modes inside the holes are evanescent. Therefore, if the thickness increases, the transmission decreases due to the evanescent decay of the fields inside the aperture. In Fig. 1.10 several simulation results of transmission in PEC hole arrays for different hole sizes and different thickness are shown. Notice, in the small holes case (Fig. 1.10(b)), the narrower bandwidth of operation and the transmission decay when the thickness t increases, in comparison to larger holes (Fig. 1.10(a)) where practically total transmission is observed for any t in a wider bandpass.

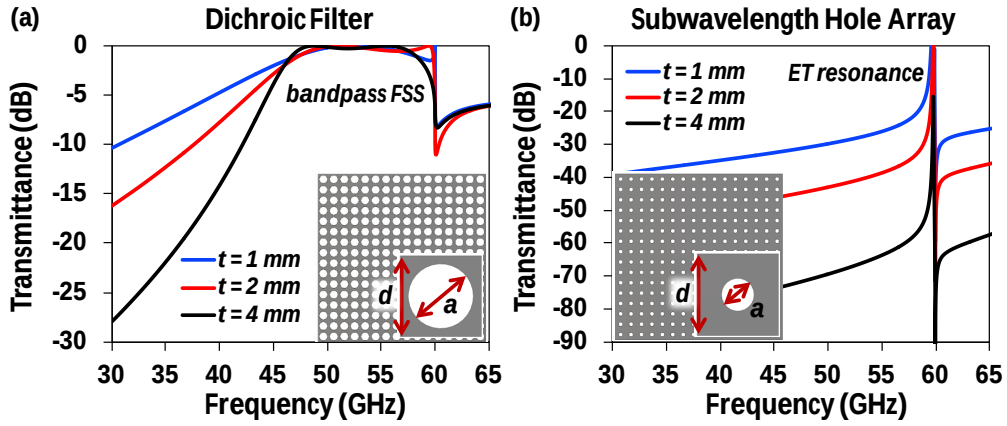

Figure 1.10. Frequency response of (a) a dichroic filter with hole diameter a = 4 mm and in-plane lattice constant d = 5 mm and (b) a subwavelength hole array with parameters a = 2 mm and d = 5 mm, for different plate thickness t.

Understanding ET: A walk through the history

Since Ebbesen *et al*. reported ET in 1998, many theories and models have been proposed in order to explain this fascinating phenomenon. Next, the most relevant works, according to this author's opinion, are presented, organized by date, where the contributions to the phenomenon are highlighted.

Precedents

The phenomenon of transmission above Bethe's prediction was observed by Betzig *et al*. in 1986 while working on the development of the near-field scanning optical microscopy [BETZ 86] but they did not elucidate its origin.

1998

In Ebbesen's seminal paper, the onset of the ET was firstly attributed to the coupling of SPPs on the metal surface and the light scattering on the periodic array [EBBE 98]. The same group reinforced this idea in [GHAE 98], where they claim that ET results specifically from a resonant excitation of surface plasmons.

1999

Ebbesen's group establishes the relation of the minimum in transmission with Wood's anomalies for the first time [KIM 99] and they also demonstrate enhancement of transmission through a single subwavelength hole surrounding by periodic corrugations [GRUP 99]. In parallel, different explanations for the ET are raised. In [TREA 99], Treacy explained ET in terms of Bloch waves where SPPs and diffracted beams are considered part of the same dynamical scattering process. Moreover, his theoretical analysis showed that efficient light transmission occurs also in one-dimensional arrays of slits where the underlying physics are essentially different[15] and thus, SPP theory may not be needed for explaining ET on SHA [PORT 99].

2000

During this year further theoretical models explaining ET appeared. Avrustsky *et al*. communicated the first model with quantitative results where ET is predicted even without the presences of holes. They showed that only periodic corrugations are needed [AVRU 00]. Popov *et al*. developed the first fully three-dimensional study of ET in hole arrays [POPO 00] ascribing ET to propagating modes appearing in the hole array as long as a non-PEC model of the permittivity is considered for the metal. Grupp *et al*. studied the importance of metals in ET linked to the inherent presence of SPPs in the phenomenon [GRUP 00].

2001

In contrast to Popov's model, Martín-Moreno *et al*. proposed another analytical three-dimensional minimal model connected to SPPs [MART 01]: ET is ascribed to coupling of the incident wave to a SPP which is transmitted through the hole by means of evanescent waveguide modes to the other interface where the wave is radiated. However, it would be proved later that an outstanding consequence of this model is that ET can occur at any frequency range, even where the metals can be considered as PEC and hence pure SPPs make no sense. The same group also studied the influence

[15] Slits always support transverse electric and magnetic (TEM) waves without cutoff frequency while in holes there is a cutoff frequency for the propagating waves.

of dielectrics on both interfaces [KRIS 01] and the transmission through a single aperture surrounded by periodic corrugations engineered at the input interface [THIO 01].

2002

Cao and Lalanne discussed that high transmittance through slit arrays is mainly due to waveguide modes and diffraction effects [CAO 02]. Furthermore, they observed a suppression of the transmission near the frequency of the SPP resonance, questioning, one more time, the inherent importance of SPPs. In the same line, Treacy extended his previous work for a unified explanation for ET where he claimed that SPPs do not play an independent causal role but, rather, they are an intrinsic component of the diffracted wave field [TREA 02]. In the context of SPP, Ebbesen's group studied the effects of hole depth [DEGI 02] and beamforming by means of ET in a single aperture with periodic corrugations at the exit interface [LEZE 02].

2003

Additional theoretical and experimental works were communicated during this year about beamforming through single apertures with corrugations based on SPP considerations [GARC 03], [MART 03]. Meanwhile, highly relevant was the work of Sarrazin *et al*. where they attributed ET to the coupling of the incident plane wave to any metal-dielectric interface loaded by a convenient grating [SARR 03], concluding that ET can occurs at any frequency.

2004

Pendry *et al*. tried to unify, under the concept of spoof SPPs [PEND 04], the two tendencies regarding the origin of ET: (i) interaction of apertures with SPPs and (ii) dynamical light diffraction and Wood's anomalies. The most relevant result of this work is the homogenization theory which allows achieving a desired effective permittivity and thus an effective plasma frequency in SHA (also slits arrays) by means of engineering the geometry of the holes or corrugations. In this year, Beruete *et al*. demonstrated experimentally for the first time ET in SHA at millimeter-waves [BERU 04] (where the finite size of the periodicity is also investigated[16]) and beamforming by means of corrugations [BERU 04b] in parallel to Ozbay's group in microwaves [AKAR 04]. Lomakin and coworkers provided a refined theoretical study based on leaky waves where the structure details are deeply analyzed [LOMA 04].

2005/2006/2007

Sarrazin *et al*. presented ET also as multiple-scattering of Brewster-Zenneck modes [SARR 05]. Lomakin *et al*. continued with the theoretical analysis of the structure [LOMA 05]. García de Abajo *et al*. found an alternative analysis of transmission

[16] It was demonstrated that the ET peak reaches maximum transmittance when 31 × 31 holes are illuminated.

through SHA comparing it with reflection on planar metallic disk arrays applying Babinet's principle [GARC 05]. Beruete *et al*. carried on with the experimental studies at millimeter-waves [BERU 05], [BERU 05b], [BERU 05c]. Moreover, further new theoretical works showed the excitation of LSPs in single apertures which produces resonant peaks that can overcome Bethe's prediction [GARC 05b], [CHAN 05], [WEBB 06] and additional ones which presented theoretically [BRAV 07] and experimentally [PRZY 06], [MATS 07] ET in non-periodical Penrose structures.

2008

We stop in this year because two new explanations emerged. Medina *et al*. proposed a new model founded on waveguides and impedance matching concepts [MEDI 08]. This new model is able to explain all details of the observed transmission spectra and easily gives predictions on many features of the phenomenon[17]. Meanwhile, Liu and Lalanne [LIU 08b] derived a microscopic theory by considering the elementary scattering process occurring in each hole. The coherent diffraction by all the individual holes acting as elementary scatters explains the physical origin of the surface wave (Bloch mode). Further works were also presented: Przybilla *et al*. [PRZY 08] demonstrated at optics the transmission saturation with the increment of the number or holes, Williams *et al*. [WILL 08] experimentally tested the subwavelength confinement in dimple arrays in the terahertz range and Li *et al*. [LI 08] present improve transmission with non-uniform and non-periodic corrugations.

2009 – Present

Therefore, more than fifteen years after the first demonstration and explanation of ET, many theories have been presented. However, in all of them, it is acceptable the coupling of the incident wave to a surface wave by means of a periodic (or quasi-periodic) structure which scatters the wave into an infinite number of diffraction modes (Bloch/Floquet). The energy is tunneled through the apertures via evanescent modes to the other interface where the process is inverted obtaining high transmittance. Many different works have been presented during the last years, some trying to explain finer details of the phenomenon and most of them focused in the applicability of the ET. They can be found together with additional bibliographic references in these two ET reviews [GARC 07], [GARC 10].

[17] In the next chapter, ET-based equivalent circuits, which are one of the cornerstones of this thesis, are presented together with novel applications.

Chapter 2

Modeling mono- and bi-layer subwavelength hole arrays

In this chapter we focus the attention on extraordinary transmission (ET) through mono- and bi-layer subwavelength hole arrays (SHAs). ET in SHA is analyzed from an equivalent circuit (EC) point of view, where the transmission line theory is presented in the first place. Built upon the equivalent circuit of the ET, the equivalent circuit of stacked SHAs is described. Three original contributions are presented at the end: (i) a plasmonic inductor for SHAs at 17 THz, (ii) an EC of the double-layer fishnet metamaterial and (iii) a double-band quarter-wave-plate ET metasurface.

2.1 Extraordinary transmission from an equivalent circuit perspective

Equivalent circuits (ECs) are powerful tools that allow simplifying complex electromagnetic problems by means of modeling the discontinuity effects with lumped circuit elements. The main reason for employing ECs is that it is usually much harder to solve Maxwell's equations than it is to apply the simple and intuitive ideas of circuit analysis for the same problem. Obviously, Maxwell's equations provide much more information, since the electric and magnetic field is calculated in every point of the space. However, we usually are interested in a few general quantities that can be obtained or approximated with ECs.

Equivalent circuits are based on transmission line (TL) theory and network analysis. Actually, TL theory bridges the gap between field analysis and low-

frequency circuit theory. At low frequencies, circuits can be treated as an interconnection of lumped passive or active components since dimensions are electrically small (relative to the wavelength) and thus phase changes from one point in the circuit to another is negligible. This leads to a quasi-static type of Maxwell's solution: the Kirchhoff voltage and current laws [RAMO 94]. On the contrary, TLs may be a fraction of a wavelength, or many wavelengths, in size. Hence, they can be seen as a distributed parameter network, where voltage and currents can vary in magnitude and phase over its length and thus, they cannot be modeled with lumped-element circuits. Therefore, in general, the useful set of techniques used for analyzing low-frequency circuits cannot be directly applied to TLs. However, some circuit and network concepts can be extended to handle many problems of practical interest, for instance, the use of lumped elements to model subwavelength discontinuities [POZA 05].

The impedance concept

The TL theory has been used in microwave engineering since the 1930's[18] to explain and model wave propagation in waveguides and coaxial lines [SCHE 38], [PACK 84], but it can also be applied to other media such as microstrip lines, optical fibers or free space, among others. In this theory, a wave propagating in any TL is defined by a set of transverse modes[19] which are the spatial distribution of the electric and magnetic field imposed by the boundary conditions and thus supported by that TL. Each mode has an associated wave impedance which can be modeled with a circuit element by means of the characteristic line impedance. There are three kind of transverse modes supported in conventional TLs:

- *Transverse electromagnetic (TEM) modes*: these modes have neither electric nor magnetic field in the propagation direction. The wave impedance of these modes is defined as $Z_{TEM} = \sqrt{m/e} = h$ where h is the intrinsic impedance of the medium.
- *Transverse electric (TE) modes*: the electric field is null in the propagation direction and the wave impedance is $Z_{TE} = kh/b$.
- *Transverse magnetic (TM) modes*: the magnetic field is null in the direction of propagation and the wave impedance is $Z_{TM} = bh/k$.

[18] Although, in 1897, Lord Rayleigh mathematically proved wave propagation in waveguides also noting the infinite set of TE and TM modes and the existence of a cutoff frequency, the waveguide was essentially forgotten until 1932.

[19] The transverse modes are calculated solving Maxwell's equations in a plane perpendicular to the propagation direction taking into account the boundary conditions.

In the above equations $k = \omega\sqrt{\mu\varepsilon} = 2\pi/\lambda$ is the wavenumber of the material filling the transmission line and $\beta = \sqrt{k^2 - k_c^2}$ is the propagation constant with k_c the cutoff wavenumber of the mode. Moreover, notice that three different impedances have been mentioned. Let us clarify the impedance concept which actually is the base in EC models.

- $\eta = \sqrt{\mu/\varepsilon}$ = *intrinsic impedance of the medium*. It is dependent only on the material parameters and is equal to the wave impedance for plane waves[20].
- $Z_w = E_t/H_t = 1/Y_w$ = *wave impedance*. It is the ratio of electric to magnetic field in the transverse plane of the propagation direction and thus, it is different for each type of wave (Z_{TEM}, Z_{TE}, Z_{TM}). It may depend on the type of waveguide, the material and the operating frequency.
- $Z_0 = 1/Y_0 = \sqrt{L/C}$ = *characteristic line impedance*. It is the ratio of voltage to current for a propagating wave on a TL and has associated an inductance *L* and a capacitance *C*. Since voltage and current are uniquely defined for TEM waves, for TE and TM waves the characteristic line impedance may be defined in various ways. In general, voltage and current are defined proportional to E_t and H_t,[21] respectively, so this impedance is usually selected as equal to the wave impedance [POZA 05].

In our case, the electromagnetic problem consists in an incoming wave propagating trough a homogeneous media (commonly free space) that interacts with a metamaterial structure. This problem can be modeled, applying certain boundary conditions, as a wave propagating in a guided media where the energy is carried by a set of electromagnetic modes defined by their characteristic line impedance. This wave will find one or several discontinuities, which are the metamaterial itself, giving rise to an interchange of electric and magnetic energy. The static or quasi-static interactions can be modeled by means of lumped elements and the distributed effects with circuit elements extracted from transmission line theory [RAMO 94]. Once the model is established, after classic network analysis, several magnitudes such as the scattering parameters can be calculated.

Modeling ET in SHA

The analysis of a plane wave impinging normally to the surface of a SHA can be reduced to the analysis of one rectangular waveguide containing a single unit cell

[20] A plane wave is actually a TEM mode.
[21] So their product gives the power flow of the mode.

provided that the unit cell is symmetric and certain boundary conditions are imposed. An artificial waveguide with electric and magnetic walls [BERU 07], [MEDI 08], is defined in order to replicate the electromagnetic fields in the transverse directions. So, the impinging wave propagating in free space will find a subwavelength discontinuity, which is the hole. The aim is to obtain the necessary lumped circuit elements that model this diffraction problem in order to obtain the transmission and reflection coefficients.

The problem of a transmission line with a discontinuity is very well known in microwave engineering since, in some cases, they are an unavoidable result of mechanical or electrical transitions from one medium to another (e.g. a junction between two waveguides of different sizes or a coax-to-microstrip transition). In other cases they are deliberately introduced to perform a certain function, for instance, impedance matching or filtering effects. In Figure 2.1 some discontinuities found in microwaves and their ECs are depicted. The basic procedure to obtain the circuit elements is to start with a field theory solution to a canonical discontinuity problem and develop a circuit model [MARC 51]. Regarding periodic structures, Goldsmith described the principle of operation of dichroic filters from transmission line formalism [GOLD 98]. Nevertheless, this approach ignores diffraction and therefore, the modeling must be refined for ET in SHA.

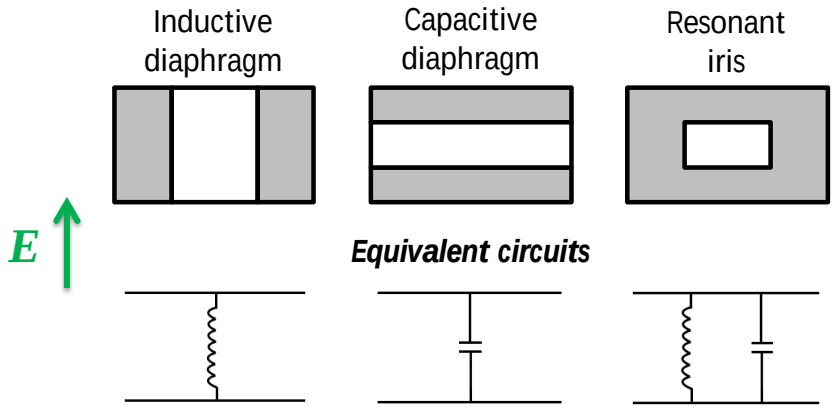

Figure 2.1. Some common transmission line discontinuities and their equivalent circuits.

Back to our problem, Medina and coworkers presented a truly illuminating work of ET through SHA from a circuit theory perspective [MEDI 08]. They use simple concepts from the theory of waveguides, transmission lines and frequency selective surface to explain ET for both thin and thick SHA made of PEC. They are able to obtain all transmission spectra details as well as give prediction of many features of the phenomenon. Here, we highlight the necessary points to understand their EC

model which is shown in Figure 2.2 together with the full 3D structure and the reduction to the unit cell analysis, and the transmission spectra for a thin SHA.

- The input transmission line, modeled as an artificial waveguide with characteristic line impedance Z_0 (Fig. 2.2(a)), supports TE_{2n2m} and TM_{2n2m} modes (n and m are integer numbers), as well as the fundamental TEM mode. Moreover, according to the structure dimensions and the polarization of the impinging wave, the frequency of the first Wood-Rayleigh anomaly (minimum in transmission) is given by $f_{WR} = c/d$ (c is the speed of light in vacuum) which is also the cutoff frequency of the TM_{02} and TE_{20}. Therefore, all TE and TM modes are in cutoff below f_{WR}, which is in fact our zone of interest, and the problem is reduced to the scattering of the incident TEM mode by a resonant iris.
- The EC for such discontinuity is an *LC* tank where *L* is related with the excess electric energy associated to all below-cutoff TE modes and *C* with the magnetic one associated to TM modes.
- The equivalent capacitance is obtained from the impedance of the TM_{02} and the higher order modes. Since the cutoff frequency of those higher order modes is located well above f_{WR}, they are weakly frequency dependent and only for the TM_{02} the frequency dispersion is considered. In conclusion, the equivalent capacitance is:

$$C(f) = C_0 + C_{TM_{02}}(f) = C_0 + \frac{A_{TM}}{2\pi f h_0 \sqrt{\left(\frac{f_c^{TM_{02}}}{f}\right)^2 - 1}} \tag{2.1}$$

  where C_0 is the constant capacitance associated to the TM higher order modes, A_{TM} is a coefficient accounting for the relative degree of excitation of the TM_{02} and $f_c^{TM_{02}}$ is its cutoff frequency.

- The surface currents generated along the hole are modeled as an inductance L_h. Moreover, since $C_{TM_{02}}(f) \to \infty$ when $f \to f_{WR}$, one resonance is always predicted for any value of L_h below f_{WR}. But L_h is very small due to its subwavelength size and therefore the resonance condition is only fulfilled for high values of $C(f)$ and, in consequence, the ET peak rises close to f_{WR}.

- Moreover, an inductance singularity would be also introduced at f_{WR} since $f_c^{TE_{20}} = f_c^{TM_{02}}$. However, further shunt inductances of high values[22] coming from the TE_{20} and higher order TE modes, will not affect the resonance condition and frequency response and may be disregarded. Therefore it is only the shunt capacitance which produces noticeable variations in the transmission coefficient.
- Since the hole is electrically small, its cutoff frequency is also located above f_{WR} and further resonant peaks due to slot resonances (Fabry-Perot resonances) are not present in the bandwidth of interest.
- The thickness of the plate is modeled with a series p-circuit L_p-L_s-L_p in order to account with the reactive energy stored inside the hole[23]. These new elements lead to a second peak in the spectrum (Fig. 2.2(b)). If the thickness increases, both peaks collapse and tend to disappear. For thickness comparable to the wavelength, the p-circuit is substituted by a transmission line characterized with the impedance of the TE_{10} mode which is the relevant evanescent mode inside the aperture.
- Losses have been neglected in the circuit of Fig. 2.2(c) since they are very small for good conductive metals (zero for PEC). However ohmic losses might become important, for example when the frequency increases, leading to lower transmission values. In the circuit model, losses would be modeled as a resistance connected in series with L_h.

Additional works have been presented in order to complete the EC modeling for ET in SHA. Beruete *et al*. presents in [BERU 11], [BERU 11b] EC for the so-called anomalous ET where the role of the TE_{20} cannot be neglected. Closed expressions for the lumped elements were given in [MARQ 09]. ET in slit arrays has also been modeled from an EC perspective in [MEDI 10], [YANG 11] and also in [RODR 10] where the circuit elements for dielectric slabs backing the structure are included.

Finally, it must be highlighted that, although initially proposed for microwaves, EC models have been extended to higher frequency bands such as infrared and optics [ENGH 07], [SCHW 08], [STAF 12] because they give accurate results and predictions as well as additional theoretical explanations to the physical phenomena. However, as the frequency increases, additional considerations must be taken into account and simple EC models might not completely catch the underlying physics.

---

[22] A very high inductance is practically an open circuit which in parallel to the $L_hC(f)$ tank will not affect the response.

[23] When the p-circuit is introduced, the $L_hC(f)$ tank is split in two $2L_hC(f)/2$ tanks, one for each metal interface.

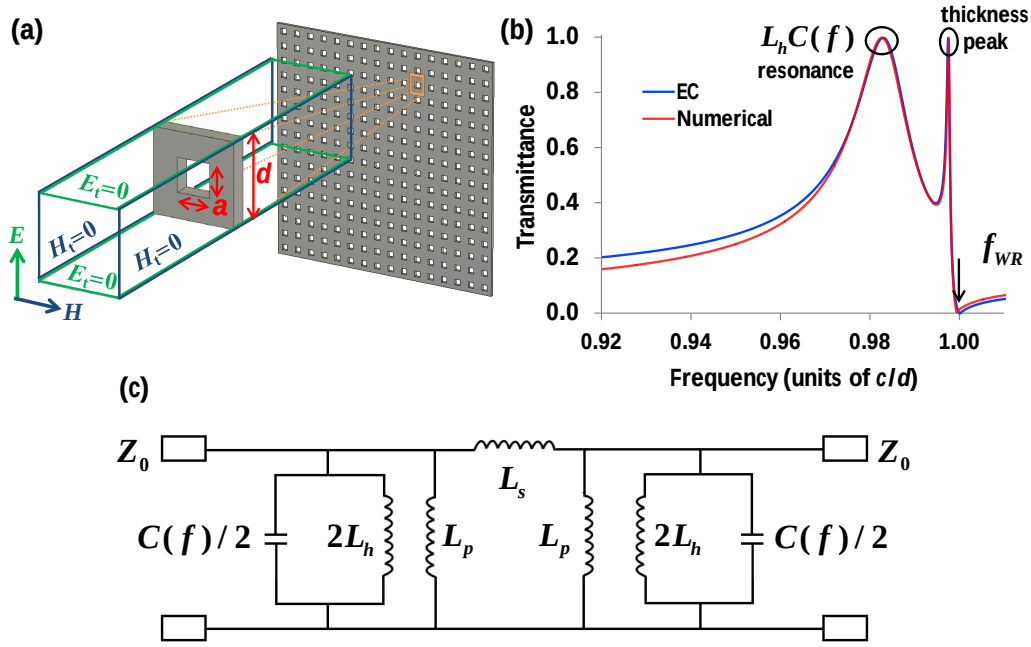

Figure 2.2. (a) SHA and unit cell inside the artificial waveguide. Hole size is $a = 0.4d$. (b) Transmission spectra obtained with numerical and EC simulation. (c) EC model.

2.2 Stacking subwavelength hole arrays

A single metallic layer of SHA is one of the most intriguing structures since it is able to exhibit ET in almost any frequency range, as it has been described in previous sections. However, a configuration based on several stacked layers of SHA is even more interesting, from a practical point of view, since it is able to support left-handed propagation and thus, negative index of refraction with low losses at high frequencies (infrared and optics) [ZHAN 05].

Other popular metamaterials, such as the SRRs+wires configuration, also behave as left-handed media [SMIT 00]. However, they usually have low transmission and, in the case of the SRR, its strong magnetic resonances vanish for high frequencies. This makes the implementation of such metamaterials not very suitable for practical applications, especially at higher frequencies where metal losses increase. Because of that, stacked subwavelength hole array (SSHA) is probably the most popular and used left-handed media. Actually, the first attempt of a low-loss left-handed metamaterial at optical frequencies was proposed by Zhang [ZHAN 05] using a double layer SSHA in a metal-dielectric-metal configuration. This structure, also known as ***fishnet***, or its

stacked configuration, was rapidly studied and used by other groups from microwave to optical frequencies [BERU 06], [BERU 07b], [ORTU 09], [DOLL 06], [CHET 07], [VALE 08], [GARC 09], [GARC 11].

Inverse TL interpretation

Most works devoted to the fishnet metamaterial have been focused on understanding its underlying physics. A typical procedure is to retrieve the electromagnetic effective parameters by means of a numerical calculation from the scattering parameters [SMIT 05], [CHEN 05]. Nevertheless, some controversies emerged regarding the consideration of SSHA as a homogeneous media since the size of the unit cell in the transversal direction is usually comparable to the wavelength and because of the appearance of unphysical artifacts in the retrieval. Other works use transmission line theory and EC concepts to explain the electromagnetic features [BERU 07], [BERU 06], [KAIP 10], [MARQ 09], [CARB 10], [KAFE 07]. Next, this approximation is briefly explained.

Similar to ET on single SHA, left-handed propagation on SSHA can be easily explained from an equivalent circuit point of view. In a simplified point of view, a SSHA might be seen as an inverse transmission line (Fig. 2.3(a)), which is well known to support left-handed propagation [RAMO 94]. The series capacitance is due to the electric coupling that exists between the layers and the shunt inductance is caused by the inductive behavior of the aperture. In [BERU 06] a more meticulous explanation can be read.

Furthermore, the importance of the separation between the layers must be underlined. The longitudinal periodicity plays a determinant role in the fishnet, since if the separation between layers increases, the electric coupling becomes weaker and eventually the left-handed feature is lost [BERU 07]. This is shown in Fig. 2.3(c) where the dispersion diagram, for the first propagating band, of SSHA with several longitudinal periods is numerically calculated. For separations below half the transversal periodicity, the band exhibits a negative slope, i.e. phase velocity antiparallel to the group velocity, and hence left-handed propagation. On the contrary, larger separations lead to positive slope and thus, right-handed propagation. Notice that the transition between these two propagation regimens shows zero-slope (zero group velocity) and a frozen mode appears inside the stacked structure, very interesting from a theoretical [BERU 13] and practical [NAVA 11] perspective. Moreover, the transmission band is shifted toward lower and upper frequencies for larger and lower separation distance, respectively. Therefore, the fishnet structure is a very versatile metamaterial structure able to easily modify its electromagnetic properties and thus, very useful in practical applications such as lenses, prisms, demultiplexers or polarizers [BERU 07c], [NAVA 08], [BERU 08], [NAVA 09], [PACH 13].

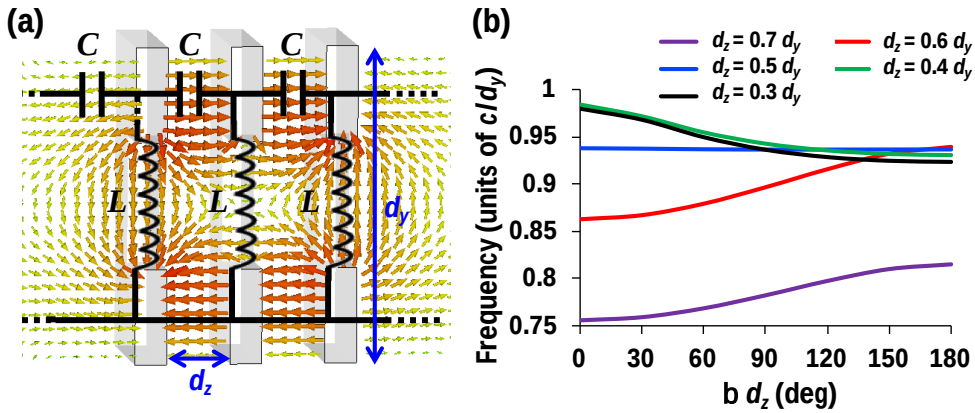

Figure 2.3. (a) Electric field in the middle cutting plane and superimposed the equivalent inverse transmission line (b) Dispersion diagram of SSHA for several longitudinal periods d_z.

2.3 [PAPER A] Mid-infrared plasmonics inductors: Enhancing inductance with meandering lines

As can be seen from previous sections, the inductance associated with subwavelength apertures is very small. This leads to very narrow ET resonance which is always located close to the onset of the first diffraction order of the periodic structure (the first Wood's anomaly). Our main motivation here is to increase the overall inductance of the structure in order to redshift the resonant frequency as well as to increase the bandwidth of operation. To do that, the regular hole array is modified by means of engineering meandering lines in the metal strips between adjacent holes. This way, the path followed the currents is increased as well as the inductance of the aperture [MARC 51]. An initial theoretical and experimental demonstration of the phenomenon is presented in [BERU 11c] at millimeter-waves. The inductance addition is corroborated with a simple version of the EC which is used to explain qualitatively the results observed theoretically.

In [PAPER A], the phenomenon is demonstrated theoretically and experimentally at the mid-infrared band, supported with a full EC model and numerical analysis, where a more complete description of the phenomenon is provided. The contribution of this paper in this field can be summarized as follows:

- We fabricate a mid-infrared inductor that when applied to an extraordinary transmission hole array produces a strong redshift of the resonant frequency and a remarkable increment in the operational bandwidth. Redshift and fractional bandwidth of 40% and 97% is achieved, respectively, with an infrared radiation efficiency of 47.5%.
- We perform experimental and theoretical studies of several SHA with different number of meander lines in order to quantify the inductance increment. The experimental results are corroborated with a new EC model of ET which includes plasmonics losses[24] for the first time, with very good agreement.
- Experimental and EC results also agree very well with those obtained with numerical simulation and classical electrodynamics. Therefore, we demonstrate the

[24] Lossy metals have been considered in [YANG 11] to model ET in slit arrays but under the assumption of good conductor. Here, we consider losses coming from the surface impedance obtained from the Drude model for the metal.

direct applicability of microwave concepts based on ECs at frequencies as high as 17 THz. Moreover, a closed expression for the bandwidth increment is given.

- Strong magnetic field localization is observed between the meander lines that can be very useful to improve infrared devices for sensing application.

PAPER A

Scientifics Reports ***4***, *3592 (2014)*

Mid-infrared plasmonic inductors: Enhancing inductance with meandering lines

Víctor Torres, Rubén Ortuño, Pablo Rodríguez-Ulibarri, Amadeu Griol, Alejandro Martínez, Miguel Navarro-Cía, Miguel Beruete, and Mario Sorolla

SCIENTIFIC REPORTS

OPEN

SUBJECT AREAS:
METAMATERIALS
ELECTRICAL AND ELECTRONIC ENGINEERING
ELECTRONIC PROPERTIES AND MATERIALS

Received
24 September 2013

Accepted
10 December 2013

Published
7 January 2014

Correspondence and requests for materials should be addressed to M.B. (miguel.beruete@unavarra.es)

Mid-infrared plasmonic inductors: Enhancing inductance with meandering lines

Víctor Torres[1], Rubén Ortuño[1], Pablo Rodríguez-Ulibarri[1], Amadeu Griol[2], Alejandro Martínez[2], Miguel Navarro-Cía[3], Miguel Beruete[1] & Mario Sorolla[1]

[1]TERALAB (MmW-THz – IR & Plasmonics Laboratory), Universidad Pública de Navarra, 31006, Pamplona, Spain, [2]Nanophotonics Technology Center, Universitat Politècnica de València, 46022, Valencia, Spain, [3]Optical and Semiconductor Devices Group, Department of Electrical and Electronic Engineering, Imperial College London, SW7 2BT, London, UK.

We present a mid-infrared inductor that when applied to an extraordinary transmission hole array produces a strong redshift of the resonant peak accompanied by an unprecedented enlargement of the operation bandwidth. The importance of the result is twofold: from a fundamental viewpoint, the direct applicability of equivalent circuit concepts borrowed from microwaves is demonstrated, in frequencies as high as 17 THz upholding unification of plasmonics and microwave concepts and allowing for a simplification of structure design and analysis; in practical terms, a broadband funnelling of infrared radiation with fractional bandwidth and efficiency as high as 97% and 48%, respectively, is achieved through an area less than one hundredth the squared wavelength, which leads to an impressive accessible strong field localization that may be of great interest in sensing applications.

Recently, a great interest on the potential of plasmonics to enhance mid-infrared sources, sensors and detectors for applications like chemical sensing, thermal imaging and heat scavenging has emerged[1]. Plasmonics took off by the end of the 20th century after the influential paper by Ebbesen *et al.*[2] where extraordinary transmission (ET) through small apertures was demonstrated, leading to the so-called "plasmonic resurrection"[3]. A full understanding of the physical mechanism underlying plasmonics is provided by the paradigm of complex waves[4], i.e. waves with mutually orthogonal amplitude and phase planes. This kind of waves permits to unify the interpretation of plasmonic-like phenomena in different frequency ranges: leaky-plasmons or surface-plasmons at optics[1] and classical leaky waves or surface-waves[5] (coined recently spoof plasmons[6]) at microwaves.

The complex waves paradigm opens immediately the application of the useful microwave toolbox at full, in particular, equivalent circuits. They were initially proposed for low frequency electronics[7] and were generalized after the seminal paper by Schelkunoff[8] to describe plane wave propagation as a transmission line problem, where discontinuities are lumped reactive elements[9], widening ultimately the applicability of equivalent circuits up to the far infrared[10]. Plasmonics[11] research, hence, benefits today from both solid state physics and circuit concepts. However, it was common practice to explain plasmonic phenomena initially in terms of dimmers, molecules, coupled resonant states, and so on, even though it is satisfactorily explained with classical electromagnetism theory. This tendency is nowadays evolving and, for instance, infrared circuits - dubbed metatronics[12–14] - are explained in terms of lumped elements and other plasmonic nanocircuits are designed making use of microwave circuit concepts such as characteristic impedance and transmission line theory[15,16]. Equivalent circuit analysis applied to plasmonic structures has served to put the limits for genuine plasmonics, giving additionally an electrical circuit description for bulk plasmons, single-surface plasmons, and parallel-plate plasmons[17]. Also, equivalent circuits have been employed to satisfactorily describe ET[18,19]. These analyses served to unify the different manifestations of ET resonance all along the electromagnetic spectrum, from millimetre-waves/tera-hertz[5,20] to visible[2] where metals admit very different models, either finite conductivity or classical Drude model[4] (as is customarily done in plasmonics), and allowed to engineer the ET resonance[21].

Here, expanding ideas from microwaves, such that an inductance exists wherever a current loop resides, we demonstrate experimentally a terahertz inductor in frequencies as high as 17 THz by using meander-lines in a canonical ET hole array. Furthermore, rather than simply modelling the response of the metallic mesh from a

circuital point of view, as it has been done before[10,18,19], we synthesize and engineer the response of ET hole arrays loaded with inductors of different turns from a metatronics perspective[12]. We demonstrate that a strong frequency shift and a wider bandwidth appear even for a 1-turn inductor. This approach also allows us to quantify straightforwardly the inductance of the meander-line. The proposed inductance could be used as a building block for sophisticated devices in the THz and mid-infrared regimes, finding potential application in imaging or sensing among others[1].

Results

Three ET hole arrays loaded with 3-, 1- and 0-turn meander-lines were fabricated in order to experimentally validate the prospects of extending microwave theory to infrared frequencies. The samples were etched on a silicon (Si) wafer following the fabrication steps, detailed in Methods, covering an area of 5 × 5 mm^2. The scanning electron microscopy (SEM) photograph of Fig. 1a shows the fabricated 3-turn meandering line hole array. The lower insets from left to right present the patterns unit cell of the 0-, 1-, and 3-turn meanders, where all prototypes were milled with the same hole and meander's width dimensions. The relevant structural dimensions and the different material layers that form the samples are given in the right upper inset. A 5 nm-thick chromium layer was deposited just for gold bonding purposes. The reason for choosing rectangular lattice arrays with a dense periodicity in one of the directions is due to their efficiency in the experimental verification of ET compared to square arrays[22].

Experimental measurements were performed in the vacuum chamber of a Fourier-transform infrared spectrometer (FTIR) equipped with an optical bench and a He-cooled bolometer detector. A linear polarizer is used to excite the structure with vertical polarization. Horizontal polarization is neglected because the main aim of this work is to evaluate the influence of the meander lines on the spectral response. Vertical polarization is the one that allows the meanders to get excited by the induced current running along them. If the polarization is rotated, marginal currents will flow through the meander but this is out of the scope of this paper. Experimental results normalized with respect to the transmission through a bare silicon wafer can be seen in Fig. 1b for all prototypes. The resonance frequency corresponds to that at which the impinging light couples to a symmetric leaky mode thanks to the additional momentum provided by the lattice[20,21,23]. This peak of transmission undergoes a significant redshift (around 21.57% and 39.65% for 1- and 3-turns with respect to 0-turn, respectively) along with a broadening of the operation bandwidth as the number of meander turns increases. Specifically, the fractional bandwidth defined as FBW = $(\omega_H - \omega_L)/\omega_C$ (where $\omega_H - \omega_L$ is the frequency range within which the spectral density is above half its maximum value and ω_C is the center operation frequency) is 3.85%, 40.45% and 96.62% for 0-, 1- and 3-turn meander-lines. This behavior is related to the effective inductance introduced by the meander-lines as it will be discussed next. A maximum infrared radiation efficiency of 47.56% is obtained for the 3-turns design through an area as small as $(\lambda_0/12.83)^2$ where λ_0 corresponds to the wavelength of the resonance frequency. Numerical results corresponding to best fits based on estimated dimensions from SEM pictures of the samples are also shown in Fig. 1b. Gold (chromium) was modeled following a Drude model with plasma frequency, $\omega_p = 1.196 \times 10^{16}$ (6.6942×10^{15}) rad/s and collision frequency $\omega_r = 8.0519 \times 10^{13}$ (7.1408×10^{13}) rad/s[24]. The slight disagreement between experiment and numerical calculations can be attributed to the fact that metal properties are altered by nanocarves, since it is well known that nanostructured metals behave differently than in bulk[25].

Discussion

The physical mechanism underlying the meandering line hole array operation can be easily understood by means of circuit theory where

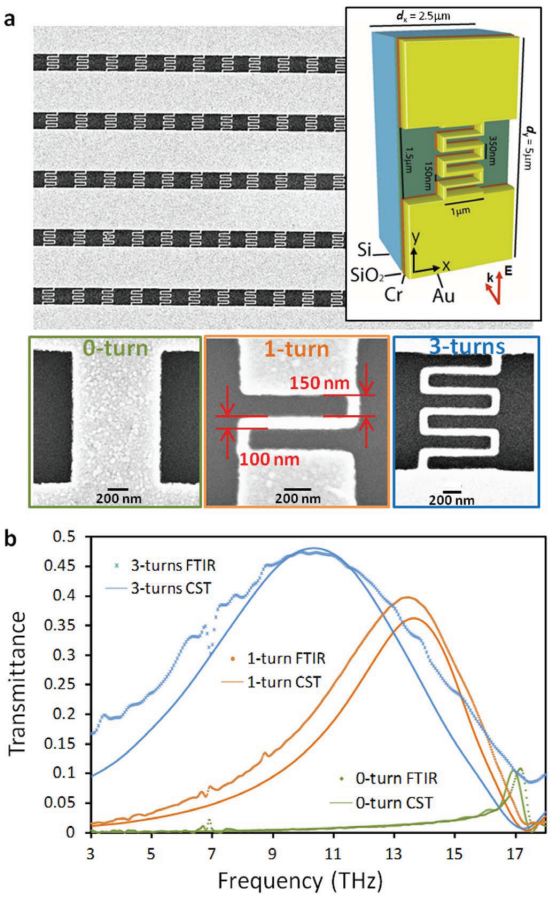

Figure 1 | SEM photographs of the prototypes and numerical vs. experimental results. (a), SEM photograph of the fabricated 3-turns meandered hole array. Lower insets from left to right show detailed photographs of the pattern unit cell of the 0-, 1-, and 3-turn meanders. Right upper inset depicts the structural dimensions and the different material layers that form the samples. (b), Numerical (CST) vs. experimental (FTIR) results of the field transmission for the 0-, 1-, and 3-turn designs.

the circuit elements are extracted from a straight physical interpretation of the hole array electrodynamics. To extract rigorously the inductance of the aperture, the induced-surface current that flows on the metal and the magnetic flux generated by this current are calculated numerically (see Methods). As illustrated in Fig. 2a for the 0-turn design, each aperture behaves as a pair of virtual current loops (VCLs): the total induced surface-current (I_T) divides in two identical branches, each one carrying $I_B = I_T/2$ and flowing on the metal around each side of the aperture, which produce a magnetic flux through the aperture plane; the surface current is closed by a displacement current through the aperture (due to symmetry considerations, exactly in the middle of the aperture the magnetic field is null). Thus, the inductive nature of the aperture is modelled as two inductances L_B in parallel, leading to a total aperture inductance of $L_B/2$. Applying directly classical electrodynamics[26], the magnetic flux is defined as[7,27]:

$$\Phi_B = \mu_0 \iint_S \vec{H} d\vec{S} \quad (1)$$

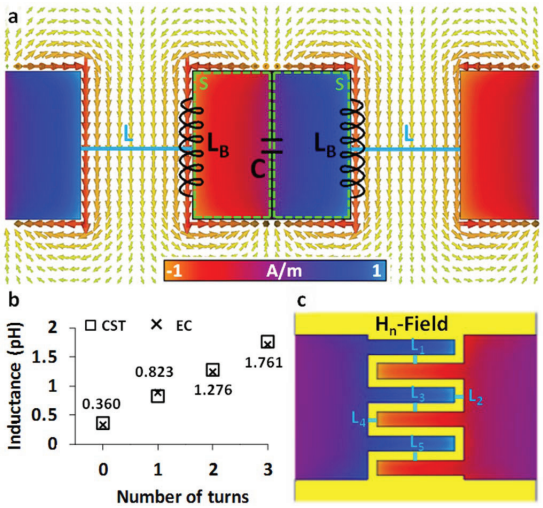

Figure 2 | Inductance extraction by means of the magnetic field and induced surface currents. (a), Normal component of the magnetic field (in color) and induced surface currents (arrows) when the structure is excited with a normal incident plane wave with the electric field oriented vertically. The interpretation of the inductances is shown explicitly. L_B models the inductance of each current branch around the aperture and C the admittance of the below-cutoff TM modes excited at the discontinuity plane. S (dashed green) depicts the surface taken for the integration of the magnetic flux of each VCL and L (solid blue) the closed line to compute the total induced surface current. (b), Inductance values obtained numerically (squares) and after optimization with the equivalent circuit model (crosses). (c), Normal component of the magnetic field (H_n-Field) for the 3-turns design where the magnetic field concentration in the meander's interstices is shown. For the meander-turns, several lines are evaluated to compute the total induced current. For the 3-turns design the lines are depicted as L_1 to L_5. (a, c) share the same color bar.

calculated over the surface enclosed by one VCL, i.e. half the aperture area, represented as a green dashed line in Fig. 2(a); μ_0 is the permeability of free space and $\vec{H}$ is the magnetic field. The surface current on the metal for one branch, by Ampère-Maxwell's law, is:

$$I_B = \frac{I_T}{2} = \frac{1}{2}\oint_L \vec{H}\, d\vec{l} \tag{2}$$

where L is a closed line orthogonal to the current path rounding the metallization (represented as blue in the figure). Thus, the total aperture inductance is:

$$L_{ap} = \frac{L_B}{2} = \frac{\Phi_B}{2I_B} \tag{3}$$

To extract the inductance, the calculations are done at very low frequency where the lumped elements from classical circuit theory are defined. Moreover, at such frequencies, the structural dimensions are much smaller than the wavelength, so propagation effects can be neglected. Thus, an instantaneous magnetic field can be assumed[27] and therefore Ampère-Maxwell's law is applied with small error.

The total inductance for 0-, 1-, 2- and 3-turns meandering line hole array is shown in Fig. 2b, where the increment of the total inductance with the number of turns is observed. This trend stems from the two main effects brought by the meander's turns: from one side, an enhancement of the magnetic field at the meander's interstices (Fig. 2c), as expected from Faraday's law, and from the other side, a rise of the area enclosed by the VCL. Both effects boost the magnetic flux, and so L_{ap}, as the induced-surface current keeps constant despite the meander's turns increase. Approximately, each turn adds 0.45 pH. This increment is roughly linear since each additional meander turn can be seen as a new inductance in series with the previous one. Displacement currents appear at the meander's interstices, although in a first order approximation they can be neglected because, in the frequency range of interest, the inductive behavior dominates over the capacitance associated to them. However, the displacement current grows with frequency, and hence, one must consider the capacitance C related to the electrical energy in excess associated with below-cutoff TM modes excited at the discontinuity planes[18,19]. For TM polarization and under normal incidence the relevant higher order Floquet-mode that takes part in ET resonance is the TM_{01}, whose capacitance is:

$$C^{(i)}(\omega) = \frac{A_{TM}k^{(i)}}{\omega Z^{(i)}\sqrt{\left(\frac{2\pi}{d_y}\right)^2 - \left(k^{(i)}\right)^2}} \tag{4}$$

where $Z^{(i)} = \sqrt{\mu_0 \Big/ \left(\varepsilon_0 \varepsilon_r^{(i)}\right)}$ is the background material characteristic impedance and $k^{(i)} = \omega\sqrt{\mu_0 \varepsilon_0 \varepsilon_r^{(i)}}$ is the propagation constant of the incoming wave; ε_0 is the permittivity of free space and $\varepsilon_r^{(i)}$ is the relative permittivity of the medium (i = *air* or *Si*); d_y is the length of the unit cell in the direction of the incident electric field and A_{TM} accounts for the degree of excitation of the TM_{01} mode at the interfaces. The losses owing to the interaction of the electromagnetic fields on the metal surface are modelled as a dispersive complex impedance $Z_c(\omega) = R_c(\omega) + j\omega L_c(\omega)$ defined as[28]:

$$Z_c(\omega) = R_c(\omega) + j\omega L_c(\omega) = \eta_0(1-j)\sqrt{\left(\frac{\omega\omega_r}{2\omega_p^2}\right)\left(1 - j\frac{\omega}{\omega_r}\right)} \tag{5}$$

where $\eta_0 = 377\ \Omega$ is the intrinsic impedance of vacuum. For the finite area of the unit cell, this surface impedance is multiplied by d_y/d_x. Finally, in order to take into account the thickness of the metal and thus, the reactive energy stored inside the aperture, the resulting meander's equivalent circuit (Fig. 3a) is refined by adding a π-network of inductances[18] $L_p - L_s - L_p$. Hence, the total inductance L_{ap} and the complex impedance Z_c split in two, one for each face of the metal.

Once the final model is established, the numerically found inductance values are introduced in the circuit and an optimization process is launched subsequently. The inductance obtained with the optimizer agrees well with that obtained with the numerical simulation, see Fig. 2b. The accuracy of the equivalent circuit is validated in Fig. 3b, where the transmission is shown, by comparing it against the numerical simulation. It is evident the good agreement between both results demonstrating the physical meaningful circuit representation. Therefore the frequency shift can be explained in terms of an increment of the total inductance: approximating equation (4) as a constant capacitance and assuming zero-thickness for simplicity (so the equivalent circuit is a simple *RLC* tank), the ET resonance happens at the *RLC* tank resonance frequency $\omega_0 = \sqrt{\frac{1}{LC} - \left(\frac{R_c}{L}\right)^2}$, where the imaginary admittance component vanishes, with L the serial sum of the aperture inductance L_{ap} and the internal surface impedance L_c. With the same approximation, the fractional bandwidth can be easily calculated:

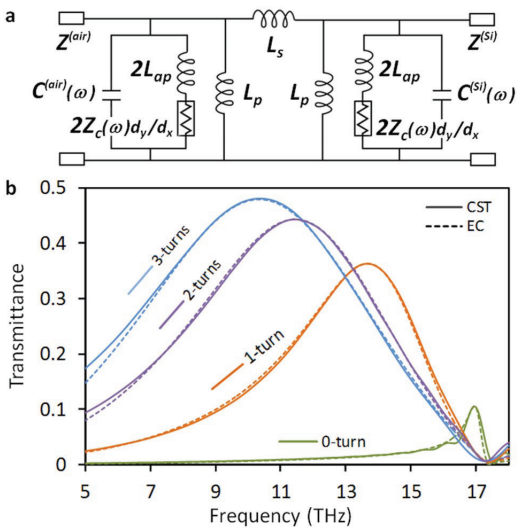

Figure 3 | Squematic and results of the equivalent circuit model. (a), Physical meaningful equivalent circuit model. $Z^{(air)}$ and $Z^{(Si)}$ are the background material characteristic impedance. L_{ap} models the aperture inductance, $Z_c(\omega)$ the losses in the metal and $C^{(air)}(\omega)$ and $C^{(Si)}(\omega)$ the admittance of the below-cutoff TM_{01} mode excited at the air-metal and metal-silicon interface, respectively. The π-network of inductances $L_p - L_s - L_p$ accounts for the thickness of the structure. (b), Field transmission results computed numerically (CST - solid lines) and via the equivalent circuit (EC - dotted lines).

$$FBW = \frac{R_c + \frac{\left(1+\sqrt{\varepsilon^{(Si)}}\right)}{Z^{(air)}}\frac{L}{C}}{\sqrt{\frac{L}{C} - R_c^2}} \qquad (6)$$

where the bandwidth increment with $\sqrt{L}$ is easily inferred.

It is worth remarking that total transmission is not obtained due to the impedance mismatch between air and silicon interfaces[7]. As a final remark, notice that despite the fundamental aperture mode depends on the number of meander turns, we checked numerically using the mode calculator of CST Microwave Studio that it remains at cutoff for all designs, and thus within the realm of ET. Hence, the transmission showed by the subwavelength apertures is surely ascribed to ET phenomena.

In conclusion, we demonstrate experimentally the synthesis of a meander-line inductor working at 17 THz borrowing ideas from microwave theory. The inductance increment with the number of meander-turns is due to an increment of the magnetic field at the meander's interstices. This increment is proved numerically following classical electrodynamics and validated by means of an equivalent circuit analysis, demonstrating the physical meaningful circuit representation at the mid-infrared frequency band. Therefore, this technique may suggest new ways of understanding circuits at infrared, although all electromagnetic considerations should be carefully taken in each design. These results can bring exciting prospects in new infrared devices based on classic designs at lower frequencies opening new application possibilities and merging the gap between microwave and infrared frequencies. Specifically, here we obtain experimentally an unprecedented mid-infrared redshift of 39.65% and a fractional bandwidth of 96.62% for the ET peak with a 3-meander-turns design. Furthermore, an infrared radiation efficiency of 47.56% is obtained together with strong magnetic field localization that can be very useful to improve infrared devices for sensing or imaging application.

Table I | Initial/final values of the optimized elements

N	L_{ap} (pH)	L_p (pH)	L_s (pH)	$A_{TM}^{(air)}$	$A_{TM}^{(Si)}$
0	0.360/0.330	0.5/0.160	0.1/0.097	1/1.36	1/0.65
1	0.823/0.886	0.5/0.395	0.1/0.084	1/1.91	1/1.23
2	1.276/1.241	0.5/1.035	0.1/0.096	1/2.18	1/1.41
3	1.761/1.710	0.5/1.392	0.1/0.106	1/2.40	1/1.43

Methods

Numerical simulation. Full-wave Floquet-modes simulations were performed with the commercial software CST Microwave Studio™. Unit Cell (Floquet) boundaries conditions were set and ten Floquet-modes were considered. The system solver accuracy chosen, in terms of the relative residual norm, was $1e^{-12}$. An adaptive tetrahedral mesh was used with convergence criteria of 0.01 over the zero-order transmission coefficient parameter. The meander turns were meshed further than the rest of the unit cell with a mesh step of $\lambda_{max}/100$ in order to obtain accurate results where λ_{max} corresponds to the wavelength of the maximum simulated frequency (18 THz).

Equivalent circuit analysis. The equivalent circuit results were obtained with the software Agilent Advanced Design System™. The extraction of the equivalent circuit parameters was done with an optimization process from a few frequency points of the numerical simulations: three points from around the peak frequency and two points from low frequency. The optimizer parameters were set to use a Least-Square error-function and a random search method, where the inductance L_{ap} obtained with the numerical analysis was used as the seed for the optimization. L_s, L_p and A_{TM} are also optimized where the initial values are derived from our previous experience in equivalent circuits. Table I shows the initial/final values of the optimized elements.

Sample fabrication. The fabrication process was based on an optimised electron beam lithography step combined with a lift-off process. The first step consisted in the deposition of three consecutive PMMA950K positive resist layers to achieve a 270 nm resist height coating a silicon wafer. This resist was then exposed by means of a Raith150 e-beam system at 10 KeV with an aperture of 30 μm. After optimization, the resist doses were 85 μQ/cm^2 for areas and 735 pQ/cm for open paths forming the meanders structures. Then, the exposed pattern was transferred into the resist. The next step consisted in the evaporation of 100 nm of gold prior to lift-off process carried out with N-Methylpyrrolidone (NMP) as solvent at a pressure of 100 bars. After the lift-off process the gold meander patterns were obtained on the silicon substrates. Meander patterns with different unit cells were obtained as can be seen in Fig. 1a.

Measurement procedure. The measurement equipment used in the experiment was a Bruker Optics Vertex 80 v FTIR spectrometer. This spectrometer covers a wide bandwidth from the far infrared up to the ultraviolet. It is based on Fourier Transform of the infrared time signal. The interferogram is obtained by directing the infrared light emitted from the source (Globar in this case) to an interferometer that modulates the light. Afterwards, the signal passes through the sample under test placed in an additional optical bench attached to the instrument, eventually focusing the transmitted beam on the He-cooled bolometer detector. These measurements have been done in vacuum in order to avoid spurious absorption peaks due to air (water vapour, carbon dioxide among other gases). A resolution of 4 cm^{-1} was considered, with 16 scans per measurements to get the averaged spectrum and a scanning velocity of the interferometer moving mirror set to 2.5 kHz.

1. Stanley, R. Plasmonics in the mid-infrared. *Nature Photon.* **6**, 409–411 (2012).
2. Ebbesen, T. W., Lezec, H. J., Ghaemi, H., Thio, T. & Wolf, P. A. Extraordinary optical transmission through sub-wavelength hole arrays. *Nature* **391**, 667–669 (1998).
3. Editorial, Surface Plasmon Resurrection, *Nature Photon.* **6**, 707 (2012). (doi:10.1038/nphoton.2012.276).
4. Ishimaru, A. *Electromagnetic Wave Propagation, Radiation, and Scattering* (Prentice Hall, New Jersey, 1991).
5. Beruete, M. *et al.* Enhanced millimeter-wave transmission through subwavelength hole arrays. *Opt. Lett.* **29**, 2500–2502 (2004).
6. Pendry, J. B., Martín-Moreno, L. & García-Vidal, F. J. Mimicking Surface Plasmons with Structured Surfaces. *Science* **305**, 847 (2004).
7. Ramo, S., Whinnery, J. R. & Van Duzer, T. *Fields and Waves in Communication Electronics* (Wiley, New York, 1994).
8. Schelkunoff, S. A. The Impedance Concept and its Application to Problems of Reflection, Refraction, Shielding, and Power Absorption. *Bell Syst. Tech. J.* **17**, 17–48 (1938).
9. Marcuvitz, N. *Waveguide Handbook* (McGraw-Hill, London, 1986).

10. Ulrich, R. Far-infrared properties of metallic mesh and its complementary structure. *Infrared Phys.* **7**, 37–55 (1967).
11. Maier, S. A. *Plasmonics: Fundamentals and Applications* (Springer, New York, 2007).
12. Engheta, N. Circuits with light at nanoscales: optical nanocircuits inspired by metamaterials. *Science* **317**, 1698–1702 (2007).
13. Sun, Y., Edwards, B., Alù, A. & Engheta, N. Experimental realization of optical lumped nanocircuits at infrared wavelengths. *Nature Mater.* **11**, 208–212 (2012).
14. Monticone, F., Estakhri, N. M. & Alù, A. Full Control of Nanoscale Optical Transmission with a Composite Metascreen. *Phys. Rev. Lett.* **110**, 203903 (2013).
15. Veronis, G. & Fan, S. Bends and splitters in subwavelength metal-dielectric-metal plasmonic waveguides. *Appl. Phys. Lett.* **87**, 131102 (2005).
16. Kocabas, S. E., Veronis, G., Miller, D. A. B. & Fan, S. Transmission line and equivalent circuit models for plasmonic waveguide components. *IEEE J Sel. Top. Quant.* **14**, 1462 (2008).
17. Staffaroni, M., Conway, J., Vedantam, S., Tang, J. & Yablonovitch, E. Circuit analysis in metal-optics. *Phot. Nano. Fund. Appl.* **10**, 166–176 (2012).
18. Medina, F., Mesa, F. & Marqués, R. Extraordinary transmission through arrays of electrically small holes from a circuit theory perspective. *IEEE T. Microw. Theory* **56**, 3108–3120 (2008).
19. Beruete, M., Navarro-Cía, M., Kuznetsov, S. A. & Sorolla, M. Circuit approach to the minimal configuration of terahertz anomalous extraordinary transmission. *Appl. Phys. Lett.* **98**, 014106 (2011).
20. Kuznetsov, S. A. *et al*. Regular and anomalous extraordinary optical transmission at the THz-gap. *Opt. Express* **17**, 11730–11738 (2009).
21. Beruete, M., Navarro-Cía, M., Torres, V. & Sorolla, M. Redshifting extraordinary transmission by simple inductance addition. *Phys. Rev. B* **84**, 075140 (2011).
22. Beruete, M. *et al.* Extraordinary transmission and left-handed propagation in miniaturized stacks of doubly periodic subwavelength hole arrays. *Opt. Express* **15**, 1107–1014 (2007).
23. Ulrich, R. Modes of propagation on an open periodic wave-guide for the far infrared. *Proceedings of the Symposium on Optical and Acoustical Micro-Electronics*, 359–376 (Polytechnic Press, New York, 1974).
24. Rakić, A. D., Djurišić, A. B., Elazar, J. M. & Majewski, M. L. Optical properties of metallic films for vertical-cavity optoelectronic devices. *App. Optics* **37**, 5271–5283 (1998).
25. Lloyd-Hughes, J. & Jeon, T.-I. A Review of the Terahertz Conductivity of Bulk and Nano-Materials. *J. Infrared Millim. Waves* **33**, 871–925 (2012).
26. J. Jackson, J. D. *Classical Electrodynamics* (Wiley, New York, 1999).
27. Rosa, E. B. The self and mutual inductances of linear conductors. *Nat. Bur. Stand.* **4**, 301–344 (1908).
28. Ordal, M. A., Bell, R. J., Alexander, R. W., Long, L. L. Jr. & Querry, M. R. Optical properties of fourteen metals in the infrared and far infrared: Al, Co, Cu, Au, Fe, Pb, Mo, Ni, Pd, Pt, Ag, Ti, V, and W. *App. Optics* **24**, 4493–4499 (1985).

Acknowledgments

In memoriam Prof. Mario Sorolla. Effort sponsored by Spanish Government under contracts Consolider "Engineering Metamaterials" CSD2008-00066, TEC2011-28664-C01 and TEC2011-28664-C02. V.T. acknowledges funding from Universidad Pública de Navarra. P.R.-U. is sponsored by the Government of Navarra under funding program "Formación de tecnólogos" 055/01/11. M.N.-C. is supported by the Imperial College Junior Research Fellowship. M.B. acknowledges funding by the Spanish Government under the research contract program Ramón y Cajal RYC-2011-08221.

Author contributions

M.B. and M.S. conceived the idea and supervised the study. V.T., R.O. and P.R.-U. performed the experiment and data analysis. A.G. fabricated the samples. V.T. and R.O. contributed to the numerical results. V.T., R.O. and P.R.-U. contributed to the equivalent circuit analysis. V.T., R.O., P.R.-U., A.M., M.N.-C. and M.B. contributed to the discussion. V.T., R.O., M.N.-C. and M.B. wrote the paper.

Additional information

Competing financial interests: The authors declare no competing financial interests.

How to cite this article: Torres, V. *et al.* Mid-infrared plasmonic inductors: Enhancing inductance with meandering lines. *Sci. Rep.* **4**, 3592; DOI:10.1038/srep03592 (2014).

2.4 [PAPER B] Fishnet metamaterial from an equivalent circuit perspective

The importance of left-handed media mainly resides in the wide variety of their potential applications [ENGH 06]. SSHA, i.e. fishnet metamaterial, is one of the most suitable realizations of left-handed metamaterials, as it has already been highlighted in the previous sections. Because of that, many theoretical works have been already presented to explain the fishnet features, the most instructive based on EC concepts [BERU 06], [BERU 07], [KAFE 07], [MARQ 09b], [KAIP 10], [CARB 10]. However, none of them provide a full EC model for a finite number of stacked layers with subwavelength holes which can be more helpful in practical applications.

Our motivation with this work is to develop a complete EC model for the double-layer fishnet metamaterial. The complete model will be a useful tool from the design and optimization point of view, and will facilitate the realization of new applications. The main points of this work are:

- The lumped elements of the circuits are inferred from the interpretation of the electric and magnetic fields as well as the surface currents generated when the structure is excited with a normally incident plane wave.
- Therefore, the proposed EC provides a physical meaningful circuit representation of the electromagnetic response and a very good agreement between EC and numerical results is obtained.
- Moreover, the EC is able to predict with high accuracy the effective index of refraction and thus, the left-handed regime of operation, consequence of the physical interpretation of the fields, demonstrating the utility of the model.
- Closed expressions as well as frequency limits for the impedances/admittances of all relevant modes are provided.

PAPER B

Applied Physics Letters ***101***, *244101 (2012)*

Fishnet metamaterial from an equivalent circuit perspective

Víctor Torres, Pablo Rodríguez-Ulibarri,
Miguel Navarro-Cía, and Miguel Beruete

2.5 [PAPER C]
Compact dual-band terahertz quarter-wave plate metasurface

The discovery of the ET phenomenon boosted metamaterial research due to the theoretical implications besides the potential applications. For the past decade, two topics have been greatly benefited [GARC 10]: (i) since the electromagnetic fields can be strongly enhanced at the apertures in the metal films, ET has been extensively explored for molecular absorption, fluorescence and vibrational spectroscopy (infrared and Raman); (ii) the ability of periodic structures of tailoring the electromagnetic properties by simply tuning the geometrical parameters, makes them very suitable for developing passive devices such as filters, polarizers, beam splitters, demultiplexers or lenses.

However, despite the fact that ET (and metamaterials in general) has been reported in almost any frequency band, the THz gap still suffers a lack of efficient devices, especially those able to work wideband or multiband to be used along with broadband or tuning THz sources and detectors. Our motivation here is to develop a metasurface for terahertz frequencies based on a modification of classical SHAs which acts as a dual-band quarter-wave plate (QWP). The main features of this contribution can be summarized as follows:

- We fabricate a single layer metasurface that works as QWP at two different frequencies, 1 THz and 2.2 THz with a wide and narrow measured fractional bandwidth of 16.77% and 2.90% and total thickness of only $0.13\lambda_0$ and $0.29\lambda_0$, respectively.
- Numerical analysis shows that, overcoming fabrication and experimental limitations, better performance can be achieved up to unprecedented fractional bandwidth for the THz band of 53.85% and 3.78%.
- The form birefringence is achieved by means of complementary inductive and capacitive response: for one polarization, the wave effectively sees a SHA loaded with meander-lines, and for the orthogonal one, the structure effectively works as a subwavelength slit array.
- The wide and narrow band response is accomplished operating off-resonance and at Fabry-Perot resonance, respectively.

PAPER C

IEEE Photonics Technology Letters

(under review)

Compact dual-band terahertz quarter-wave plate metasurface

Víctor Torres, Nuria Sánchez, David Etayo, Rubén Ortuño,
Miguel Navarro-Cía, Alejandro Martínez,
and Miguel Beruete

Chapter 3

Epsilon-near-zero lenses based on the energy squeezing principle

In this chapter, the main features of ϵ-near-zero (ENZ) media are presented together with real applications and experimental realizations for different frequency bands. Special emphasis is put on the energy squeezing principle in narrow channels and its application in focusing and tailoring radiation. Two original contributions are presented: (i) the first experimental demonstration of an ENZ metamaterial lens made of a metallic rectangular waveguide array working at 140 GHz, (ii) the analysis and design of an ENZ graded-index lens for the THz band which shows promising results in terms of free space matching and energy enhancement.

3.1 Epsilon-near-zero metamaterials

Metamaterial research offers the possibility of synthesizing a material with almost any desired values of permittivity (ϵ) and permeability (μ) leading to unique properties that can be successfully employed to either improve the performance of the existing components or even conceive new devices. Particularly, metamaterials characterized by low-positive (i.e. between 0 and 0.1) or low-negative values (i.e. between −0.1 and 0) of the real part of the relative permittivity, the so-called epsilon-near-zero (ENZ) metamaterials, have become subject of extensive investigation during the last decade.

The high interest in ENZ metamaterials resides in their unusual and exciting properties and hence, in their potential applications. If $e = 0$ in a given material (in a source-free region), from Maxwell's equations

$$\tilde{N}' \boldsymbol{H} = 0 \qquad \tilde{N}' \boldsymbol{E} = - j w \eta_0 \boldsymbol{H} \tag{3.1}$$

Equation 3.1 implies that the magnetic field is a curl-free vector and that wave propagation in this material can happen only with phase velocity being infinitely large, satisfying the static-like equation $\tilde{N}^2 \boldsymbol{E} = 0$ [JACK 98]. Therefore, values of permittivity near zero make the wave propagate with almost no phase variation over a physically long distance since the phase velocity becomes near-infinite. Moreover, $e \to 0$ ensures local negative electric polarizability and therefore, the scattered fields dominated by the dipolar field will flip their phase. Also, in the interface of a regular material and an ENZ one, the normal component of the electric field should be remarkably high in order to match the required boundary condition. This property reveals the potential of ENZ materials in field confinement, localization and supporting highly directive leaky waves. Due to such properties and additional ones [ZIOL 04], [ALU 07], ENZ materials have found interesting applications in radiation patterning and tailoring the phase-front of light [ALU 07b], tunneling and squeezing energy [SILV 06], [EDWA 08], [LIU 08c], confinement and enhancement of electromagnetic fields [SILV 07], [ALU 08], angular filters [SILV 07], design of directive electromagnetic beams [ZIOL 04], [LOVA 06], [ENOC 08], optical nanocircuits [ENGH 07], [SUN 12], enhanced transmission in subwavelength apertures [ALU 06], cloaking devices based on the scattering cancellation approach [SILV 07b], [ALU 05], [ALU 09], [EDWA 09], [BILO 10], innovative lenses with enhanced focusing properties [NAVA 11b], [NAVA 12] or electric levitation [RODR 14].

Several solutions have been proposed to implement ENZ metamaterials at different frequency bands. At microwave frequencies, its realization is rather straightforward by using the wire-medium [SILV 05], [LOVA 06], or a parallel-plate waveguide [ROTM 62], [MARQ 02]. At higher frequencies, alternative solutions are presented based on creating an effective medium mixing plasmonics materials and regular dielectrics in such a way to shift the plasma frequency towards the desired frequency [MONT 12], [MONT 13], [YANG 13]. Notice that close to the plasma frequency, the real part of the permittivity is close to zero and thus, natural materials may also exhibits the ENZ properties. This behavior is usually found at mid infrared frequencies for polar dielectrics and lightly-doped semiconductors [GOME 05] and in the visible and ultraviolet for noble metals [JOHN 72]. Therefore, as we are limited by the dispersion

of the materials, metamaterials are one possible solution in order to choose the operation frequency.

Squeezing energy through metallic channels

One of the most interesting properties of ENZ materials is the ability of tunneling and squeezing energy trough very narrow channels. In [SILV 06], Silveirinha and Engheta theoretically demonstrated that if a channel is filled with an ENZ material, an incoming wave is able to tunnel through the channel with almost no reflection if at least one of the physical dimensions of the channel is electrically small. In the lossless limit, the reflection from an arbitrarily shaped channel filled with an ENZ material is proportional to its longitudinal cross-sectional area [SILV 06], [SILV 07]. Moreover, since the guided wavelength inside the ENZ material is extremely large, abrupt bends or junctions will not affect to the propagation and no relevant reflection losses would be expected. This exciting result was experimentally probed at microwaves, almost simultaneously, in [LIU 08c], where the ENZ channel was synthesized using a screen patterned with complementary split-ring resonators, and in [EDWA 08], where the intrinsic dispersion characteristic of a metallic waveguide near cutoff was exploited.

It is well known that the intrinsic dispersion of a waveguide mode is electromagnetically analogous to the propagation in artificial materials and metamaterials [JACK 98]. For instance, plasma-like materials at microwaves frequencies have been realized using arrays of parallel-plate waveguides [ROTM 62] or the intrinsic dispersion of the TE_{10} mode in a rectangular metallic waveguide has been employed to realize an effective Drude-like negative permittivity media [MARQ 02]. Therefore, a rectangular metallic waveguide working at the cutoff frequency of the TE_{10} mode might emulate an ENZ media and be used to squeeze energy [EDWA 08]. An illustrative transmission line explanation of this fact is provided in [ALU 08b] where the squeezing phenomenon is achieved by means of making the height of one section of the waveguide electrically much smaller than the rest and matching the characteristic line impedance of all sections. This demonstration suggests that it would be also possible to squeeze an incoming plane wave propagating in free space into a rectangular waveguide [NAVA 12] by following the rules presented in [SILV 06], [SILV 07], [ALU 08b].

Figure 3.1(a) shows a rectangular waveguide of transversal dimensions $h_x \times h_y$ and length L caved in PEC block of dimension $d_x \times d_y \times L$ which is illuminated by a plane wave. According to the polarization of the impinging wave and assuming the waveguide is air-filled, the cutoff frequency of the TE_{10} mode inside the narrow channel is $f_c^{TE_{10}} = c/2h_x = 75$ GHz (c is the speed of light in free space). The

impedance mismatch between free space and the ENZ channel is reduced by the choice of very small cross-sectional area of the channel: $h_y/d_y = 0.1$. Moreover, the structure is assumed to be periodic in the transverse directions in order to avoid edge effects. The squeezing phenomenon is analyzed for different values of the channel length *L*.

The energy squeezing is expected to happen close to, but not exactly at $f_c^{TE_{10}}$ due to the finite value of h_y/d_y. This is corroborated in Fig. 3.1(b) where the transmittance is shown. Almost total transmission is observed at frequencies very close and above to $f_c^{TE_{10}}$. The slight variation in the squeezing frequency is due to weakly evanescent impinging and reflected modes inside the channel produced by reactive fields at the discontinuities. Notice that further peaks rise at higher frequencies corresponding to Fabry-Perot resonances[25]. Observing the electric field at the squeezing frequencies (Fig. 3.1(c)), it is clearly noticed the energy squeezing through the channel and the static-like behavior, since the phase of the field is practically constant along the waveguide. clearly noticed the energy squeezing through the channel and the static-like behavior, since the phase of the field is practically constant along the waveguide. The magnitude and phase in the middle of the channel are depicted in (Fig. 3.1(d)). The magnitude of the electric field is highly enhanced and is also practically constant inside the ENZ channel, as expected. Moreover, the phase propagates very slow as the change in the slope inside the waveguide indicates. The phase delay is not exactly zero because the waveguide works in a regime where $\varepsilon \gg 0^+$. Actually, it is possible to estimate the effective (relative) epsilon ε_{r_eff} of the ENZ channel from the phase delay $\Delta\varphi$. Assuming a homogenization for the waveguide, the phase delay is

$$\Delta\varphi = \beta_{eff} L = \frac{2\pi f}{c}\sqrt{\varepsilon_{r\_eff}}\,L \tag{3.2}$$

where β_{eff} is the effective propagation constant. Then, from Eq. 3.1, $\varepsilon_{r\_eff} = 0.0052$, 0.0046 and 0.0044 for $L = 5$, 7.5 and 10 mm, respectively.

[25] The Fabry-Perot resonances depend on the channel length, hence the larger the channel, the lower the resonant frequency.

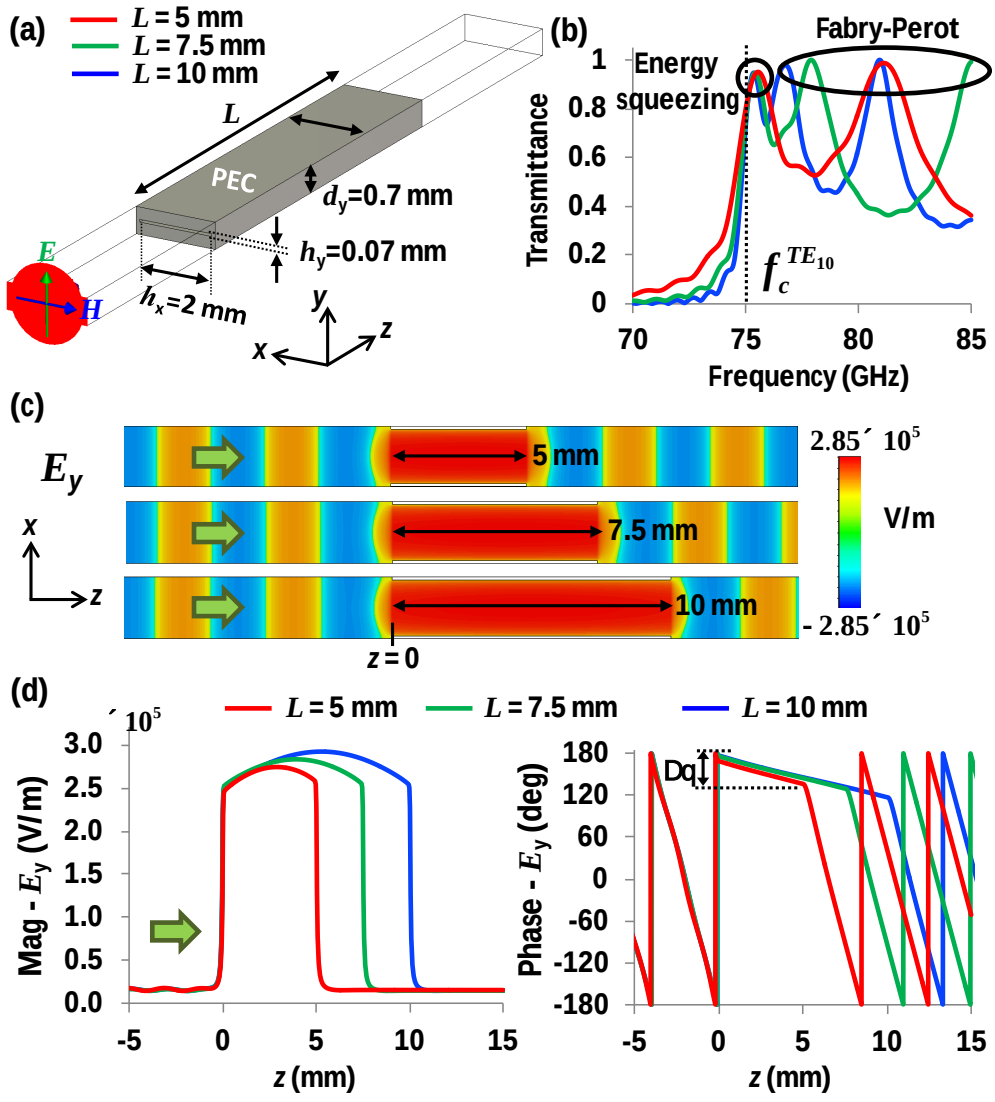

Figure 3.1. (a) Unit cell of a plane wave impinging on a narrow rectangular waveguide array. (b) Transmittance for different values of length L. (c) Electric field distribution E_y in the middle cutting plane xz at the energy squeezing frequencies. (d) Magnitude and phase of E_y along z.

It must be highlighted that propagation using the squeezing phenomenon is different from classic wave tunneling which relies on Fabry-Perot resonances[26] [HUPE 68], [CRAV 66]. As it has been proved above, the transmission enhancement due to the squeezing phenomenon is independent of the channel length (also of the geometry and shape) and always occurs around the same frequency, where $\varepsilon \approx 0^{+}$. Moreover, the field magnitude and phase variation across the channel is interestingly uniform, which might be very useful for beamforming and focusing applications.

Tailoring the radiation pattern

Exploiting the static-like behavior of ENZ media, the manipulation of the phase fronts of electromagnetic sources seems very interesting for obtaining anomalous imaging, lensing and radiation effects [ALU 07b]. With the use of ENZ media, an impinging phase front can be manipulated in order to transform its phase distribution into a desired shape by properly tailoring the exit face of the ENZ media. The wave front should conform to the exit face since very low phase variation is expected in the wave propagating inside the material.

In [NAVA 12], the possibility of using ENZ metamaterials for lensing and Fourier transforming is theoretically discussed. An array of waveguides working near cutoff, similar to that presented in the previous section, is used to mimic the electromagnetic response of an ENZ lens. The waveguide array has a plano-concave profile which allows concentrating an incoming plane wave impinging on the flat face, in a focus at the exit (and vice versa), by means of conforming the outgoing phase front to the concave exit face. The Fourier transform capabilities are studied as well, obtaining very promising results. The work presented by Navarro *et al.* serves as a starting point for the two original contributions presented in the next sections.

[26] Strictly speaking, the propagation at the squeezing frequency in a rectangular wave guide can be seen as the 0th-order Fabry-Perot resonance but classic solution does not exploit this regime.

3.2 [PAPER D] Experimental demonstration of a THz metallic ENZ lens based on the energy squeezing principle

Lens research and development has been greatly benefited with the advent of metamaterials, specially thanks to those engineered with a permittivity and/or permeability close to zero [ALU 07], [NAVA 11b]. Specifically, ENZ metamaterials seems to be very suitable for focusing applications thanks to the ability of tailoring the radiation pattern exploiting the energy squeezing principle [ALU 07b], [NAVA 12]. Nevertheless, at low frequencies such as microwaves and millimeter-wave, just a few experimental realizations of this phenomenon have been performed [EDWA 08], [LIU 08c].

In [PAPER D], we present an experimental demonstration of a plano-concave ENZ metamaterial lens synthesized with an arrangement of very narrow metallic waveguides working at 144 GHz. The relevance of this communication can be summarized as follows:

- We experimentally demonstrate, for the first time, the performance of an ENZ lens comprised of an array of narrow metallic waveguides working near cutoff at THz.
- Taking advantage of the squeezing phenomenon, the lens shows great performance in terms of free space matching and a transmission enhancement of 15.9 dB is measured in both E- and H-planes.
- We also demonstrate the capabilities of improving the radiation properties of a system formed by a feeder antenna and the ENZ lens: a directivity and cross-polar component of 37.3 dBi and -34 dB have been measured, respectively.
- The lens has been made after a challenging fabrication and assembling process where high accuracy in the final dimensions and tolerances has been achieved.

PAPER D

IEEE Transactions on Antennas and Propagation

(under review)

Experimental demonstration of a millimeter-wave metallic ENZ lens based on the energy squeezing principle

Víctor Torres, Bakhtiyar Orazbayev, Víctor Pacheco-Peña, Miguel Beruete, Miguel Navarro-Cía, and Nader Engheta

3.3 [PAPER E] Terahertz epsilon-near-zero graded-index lens

Metallic lenses have been used since the 1940's as a thinner alternative to conventional dielectric lenses because they usually exhibit a positive but less than unity refractive index, allowing the use of concave profiles instead of convex ones [KOCK 48], [NAVA 11b]. Other techniques, such as those used in zoned or graded-index lenses also help to reduce the total volume [MINI 08], [LUNE 66], a desired circumstance in most practical applications. Therefore, metamaterials and their ability of tailoring the refractive index play a major role in this field.

As it has been theoretically demonstrated before, the use of an arrangement of metallic waveguides working near their cutoff frequencies can act as an ENZ metamaterial lens [NAVA 12]. Our aim here is to individually control the propagation inside each waveguide in order to perform a graded-index converging lens operating at terahertz frequencies. The main features of this work are:

- The cross section of each waveguide is individually design. One dimension controls the cutoff frequency of the fundamental mode and therefore the propagation constant and the phase delay at the operation frequency. The other is chosen in order to match the characteristic line impedance of free space and the channel.
- Several designs to achieve cylindrical and spherical phase fronts are presented. Low reflection coefficient equal to 0.3 is predicted and an acceptable focusing performance achieved in a very compact lens of wide and thickness equal to $6l_0$ and $2l_0$, respectively.
- The analysis of the chromatic aberration and numerical aperture shows that this lens may works as a frequency and spatial filter as well.
- The guidelines presented in this paper may be very useful for optimizing further devices such as beam steerers or beam splitters among others.

PAPER E

Optics Express ***21***, *9156 (2013)*

Terahertz epsilon-near-zero graded-index lens

Víctor Torres, Víctor Pacheco-Peña, Pablo Rodríguez-Ulibarri, Miguel Navarro-Cía, Miguel Beruete, Mario Sorolla, and Nader Engheta

Terahertz epsilon-near-zero graded-index lens

Víctor Torres,[1,2,*] Víctor Pacheco-Peña,[1] Pablo Rodríguez-Ulibarri,[1] Miguel Navarro-Cía,[3,4,5] Miguel Beruete,[1] Mario Sorolla,[1] and Nader Engheta[2]

[1]*TERALAB (MmW – THz – IR & Plasmonics Laboratory), Universidad Pública de Navarra, Pamplona 31006, Spain*
[2]*Department of Electrical and Systems Engineering, University of Pennsylvania, Philadelphia 19104, USA*
[3]*Optical and Semiconductor Devices Group, Department of Electrical and Electronic Engineering, Imperial College London, London SW7 2BT, UK*
[4]*Centre for Plasmonics and Metamaterials, Imperial College London, London SW7 2AZ, UK*
[5]*Centre for Terahertz Science and Engineering, Imperial College London, London SW7 2AZ, UK*
[*]*victor.torres@unavarra.es*

Abstract: An epsilon-near-zero graded-index converging lens with planar faces is proposed and analyzed. Each perfectly-electric conducting (PEC) waveguide comprising the lens operates slightly above its cut-off frequency and has the same length but different cross-sectional dimensions. This allows controlling individually the propagation constant and the normalized characteristic impedance of each waveguide for the desired phase front at the lens output while Fresnel reflection losses are minimized. A complete theoretical analysis based on the waveguide theory and Fermat's principle is provided. This is complemented with numerical simulation results of two-dimensional and three-dimensional lenses, made of PEC and aluminum, respectively, and working in the terahertz regime, which show good agreement with the analytical work.

OCIS codes: (080.3630) Lenses; (070.0070) Fourier optics and signal processing; (160.1245) Artificially engineered materials; (160.3918) Metamaterials.

References and links

1. L. Solymar and E. Shamonina, *Waves in Metamaterials* (Oxford, 2009).
2. N. Engheta and R. W. Ziolkowski, *Metamaterials: Physics and Engineering Explorations* (Wiley, 2006).
3. D. R. Smith, W. J. Padilla, D. C. Vier, S. C. Nemat-Nasser, and S. Schultz, "Composite medium with simultaneously negative permeability and permittivity," Phys. Rev. Lett. **84**(18), 4184–4187 (2000).
4. R. W. Ziolkowski, "Propagation in and scattering from a matched metamaterial having a zero index of refraction," Phys. Rev. E Stat. Nonlin. Soft Matter Phys. **70**(4), 046608 (2004).
5. M. G. Silveirinha and N. Engheta, "Tunneling of electromagnetic energy through subwavelength channels and bends using ε-near-zero materials," Phys. Rev. Lett. **97**(15), 157403 (2006).
6. A. Alù, M. G. Silveirinha, A. Salandrino, and N. Engheta, "Epsilon-near-zero metamaterials and electromagnetic sources: tailoring the radiation phase pattern," Phys. Rev. B **75**(15), 155410 (2007).
7. C. Bohren and D. Huffmann, *Absorption and Scattering of Light by Small Particles* (Wiley, 1983).
8. J. D. Jackson, *Classical Electrodynamics* (Wiley, 1999).
9. J. Gómez Rivas, C. Janke, P. Bolivar, and H. Kurz, "Transmission of THz radiation through InSb gratings of subwavelength apertures," Opt. Express **13**(3), 847–859 (2005).
10. P. B. Johnson and R. W. Christy, "Optical constants of the noble metals," Phys. Rev. B **6**(12), 4370–4379 (1972).
11. A. Alù, M. G. Silveirinha, and N. Engheta, "Transmission-line analysis of ε -near-zero-filled narrow channels," Phys. Rev. E Stat. Nonlin. Soft Matter Phys. **78**(1), 016604 (2008).
12. H. Shi, C. Wang, C. Du, X. Luo, X. Dong, and H. Gao, "Beam manipulating by metallic nano-slits with variant widths," Opt. Express **13**(18), 6815–6820 (2005).
13. L. Verslegers, P. B. Catrysse, Z. Yu, J. S. White, E. S. Barnard, M. L. Brongersma, and S. Fan, "Planar lenses Based on Nanoscale Slit Arrays in a metallic film," Nano Lett. **9**(1), 235–238 (2009).
14. Z. Sun and H. K. Kim, "Refractive transmission of light and beam shaping with metallic nano-optic lenses," Appl. Phys. Lett. **85**(4), 642–644 (2004).
15. C. Ma, M. Escobar, and Z. Liu, "Extraordinary light focusing and Fourier transform properties of gradient-index metalenses," Phys. Rev. B **84**(19), 195142 (2011).
16. C. Ma and Z. Liu, "A super resolution metalens with phase compensation mechanism," Appl. Phys. Lett. **96**(18), 183103 (2010).
17. L. Verslegers, P. B. Catrysse, Z. Yu, and S. Fan, "Deep-subwavelength focusing and steering of light in an aperiodic metallic waveguide array," Phys. Rev. Lett. **103**(3), 033902 (2009).

#183764 - $15.00 USD Received 22 Jan 2013; revised 7 Mar 2013; accepted 7 Mar 2013; published 5 Apr 2013

18. S. Ishii, A. V. Kildishev, V. M. Shalaev, K. P. Chen, and V. P. Drachev, "Metal nanoslit lenses with polarization-selective design," Opt. Lett. **36**(4), 451–453 (2011).
19. S. Ishii, A. V. Kildishev, V. M. Shalaev, and V. P. Drachev, "Controlling the wave focal structure of metallic nanoslit lenses with liquid crystals," Laser Phys. Lett. **8**(11), 828–832 (2011).
20. S. Ishii, V. M. Shalaev, and A. V. Kildishev, "Holey-metal lenses: sieving single modes with proper phases," Nano Lett. **13**(1), 159–163 (2013).
21. D. M. Pozar, *Microwave Engineering* (Wiley, 2005).
22. B. Edwards, A. Alù, M. E. Young, M. Silveirinha, and N. Engheta, "Experimental verification of epsilon-near-zero metamaterial coupling and energy squeezing using a microwave waveguide," Phys. Rev. Lett. **100**(3), 033903 (2008).
23. M. G. Silveirinha and N. Engheta, "Theory of supercoupling, squeezing wave energy, and field confinement in narrow channels and tight bends using ε near-zero metamaterials," Phys. Rev. B **76**(24), 245109 (2007).
24. R. E. Collin, *Foundations for Microwave Engineering* (Wiley, 2000).
25. M. Beruete, I. Campillo, M. Navarro-Cia, F. Falcone, and M. Sorolla Ayza, "Molding left- or right-handed metamaterials by stacked cutoff metallic hole arrays," IEEE Trans. Antenn. Propag. **55**(6), 1514–1521 (2007).
26. M. Navarro-Cía, M. Beruete, M. Sorolla, and N. Engheta, "Lensing system and Fourier transformation using epsilon-near-zero metamaterials," Phys. Rev. B **86**(16), 165130 (2012).
27. D. Filipovic, S. Gearhart, and G. Rebeiz, "Double-slot antennas on extended hemispherical and elliptical silicon dielectric lenses," IEEE T. Microw. Theory **41**(10), 1738–1749 (1993).
28. N. Llombart, G. Chattopadhyay, A. Skalare, and I. Mehdi, "Novel terahertz antenna based on a silicon lens fed by a leaky wave enhanced waveguide," IEEE Trans. Antenn. Propag. **59**(6), 2160–2168 (2011).
29. Microtech Instruments Inc, *http://mtinstruments.com*
30. Thorlabs Inc, *http://www.thorlabs.com*
31. J. W. Goodman, *Introduction to Fourier Optics* (Roberts & Company Publishers, 2004).
32. W. Kock, "Metal-lens antennas," Proceedings of the IRE **34**(11), 828–836 (1946).
33. J. Ruze, "Wide-angle metal-plate optics," Proceedings of the IRE **38**(1), 853–855 (1950).
34. M. Navarro-Cía, M. Beruete, I. Campillo, and M. Sorolla Ayza, "Beamforming by left-handed extraordinary transmission metamaterial bi- and plano-concave lens at millimeter-waves," IEEE Trans. Antenn. Propag. **59**(6), 2141–2151 (2011).
35. H. D. Hristov, *Fresnel Zones in Wireless Links, Zone Plate Lenses and Antennas* (Artech House, 2000).
36. M. Navarro-Cía, M. Beruete, I. Campillo, and M. Sorolla, "Enhanced lens by ε and μ near-zero metamaterial boosted by extraordinary optical transmission," Phys. Rev. B **83**(11), 115112 (2011).

1. Introduction

The challenge of engineering and controlling the electromagnetic properties of materials is on the forefront of basic materials science and engineering. Electromagnetic metamaterials have followed this trail, focusing on the control of electromagnetic fields [1,2]. In order to surpass the limits available in natural materials, metamaterials with unconventional values of permittivity (ε) or permeability (μ) have been extensively studied during the last decades. The realization of a double negative medium [3] was one of the most relevant advances in material science. Afterwards, metamaterials with an effective index of refraction near zero ($n \rightarrow 0$) [4] and, more recently, metamaterials with low permittivity, so called ε-near-zero (ENZ) [5,6], have become subject of extensive investigation.

Extreme values of the permittivity (i.e. near-zero or very large) can be found in dispersive natural materials. In these materials, permittivity is dispersive due to internal molecular resonances where their frequency response can be approximated by Drude-Lorentz models [7,8]. By definition, at the plasma frequency of a Drude medium the real part of the permittivity effectively goes to zero and at the resonance of a Lorentzian medium, the permittivity may become very large. However, this behavior is usually found at mid infrared frequencies for polar dielectrics and lightly-doped semiconductors [9], and in the visible and ultraviolet for noble metals [10]. Therefore engineered materials, i.e. metamaterials, are needed to obtain such electromagnetic singularities at the lower frequency bands such as microwaves or terahertz waves.

A typical procedure to obtain ENZ metamaterials is to employ an arrangement of perfectly-electric conducting (PEC) metallic waveguides working near their cut-off frequencies [11]. By tuning the dimensions of the waveguides it is possible to have good impedance matching at the frequency where the effective permittivity tends to zero. In this work, we theoretically study and numerically confirm the realization of a graded index ENZ lens based on these waveguide configurations [11]. The dimensions of each waveguide is designed independently in order to have the desired propagation constant and thus phase

#183764 - $15.00 USD Received 22 Jan 2013; revised 7 Mar 2013; accepted 7 Mar 2013; published 5 Apr 2013

delay inside each waveguide for achieving a flat convergent lens while each waveguide remains approximately impedance matched to free-space. With this approach Fresnel reflection is significantly reduced. Several realizations of planar graded-index lenses composed of slit arrays with non-uniform width have been proposed and demonstrated in the past by other groups [12–20]. Although most of these lenses manipulate the phase delay inside each slit in an analogous fashion as we do here, they do so using the modes in waveguides with plasmonic walls, and they do not address the issue of the mismatch between the guided mode and the incident illumination. Some of them are also suitable for focusing in one plane, not two. As we will discuss below, here we use one dimension of the cross section of the hollow waveguide made of PEC walls to adapt the phase delay and the other one to effectively match our lens to the incoming plane-wave propagating in free-space.

2. Analytical formulation

Attending to the classical waveguide theory, we know that hollow rectangular waveguides made of PEC walls can propagate TM and TE modes above the cut-off frequency, whereas below the cut-off frequency the modes are evanescent [21]. The mode with the lowest cut-off frequency is called the dominant mode, and depending on the dimensions of the waveguide cross section and the orientation of the fields, this mode is unique. For a rectangular waveguide of dimensions h_x and h_y with $h_y > h_x$ and E-field oriented in the x-direction, the fundamental mode is the TE_{01} whose cut-off frequency is $f_c^{TE_{01}} = c/2h_y$, where c is the velocity of light in free space and it is assumed that the guide is filled with free space (or air). The propagation constant of this mode can be written as

$$\beta = k_0\sqrt{1-\left(\frac{f_c^{TE_{01}}}{f}\right)^2} = k_0\sqrt{1-\left(\frac{\pi}{k_0 h_y}\right)^2}, \qquad (1)$$

where $k_0 = 2\pi f\sqrt{\mu_0\varepsilon_0}$ is the wave number in free space. It was theoretically demonstrated in [11] and experimentally verified in [22] that working slightly above the cut-off frequency, a microwave metallic waveguide may behave as an ENZ metamaterial. Near the cut-off frequency the propagation constant is very small, as shown by Eq. (1). Thus the relative effective permittivity of the waveguide ε_{w_eff} is very close to zero, since:

$$\varepsilon_{w\_eff} = 1-\left(\frac{f_c^{TE_{01}}}{f}\right)^2 = 1-\left(\frac{\pi}{k_0 h_y}\right)^2, \qquad (2)$$

where it has been assumed that the effective permeability of the waveguide is μ_0. From here we can obtain an expression for the accumulated phase variation within the ENZ in terms of the waveguide dimensions:

$$\Delta\theta_w = \beta L = \left(k_0\sqrt{1-\left(\frac{\pi}{k_0 h_y}\right)^2}\right)L, \qquad (3)$$

where L is the waveguide length. Due to the low propagation constant of the guided mode (β), a small phase variation occurs even over a physically long distance. Moreover, with slight variations in the h_y dimension, we are able to control with high accuracy the propagation constant and consequently the phase of the mode. Thus, we have the basic ingredients for a graded-index lens, where the phase variation of each waveguide is carefully tuned to transform an incident plane wave into a spherical wave. Figure 1(a) illustrates this idea.

#183764 - $15.00 USD Received 22 Jan 2013; revised 7 Mar 2013; accepted 7 Mar 2013; published 5 Apr 2013

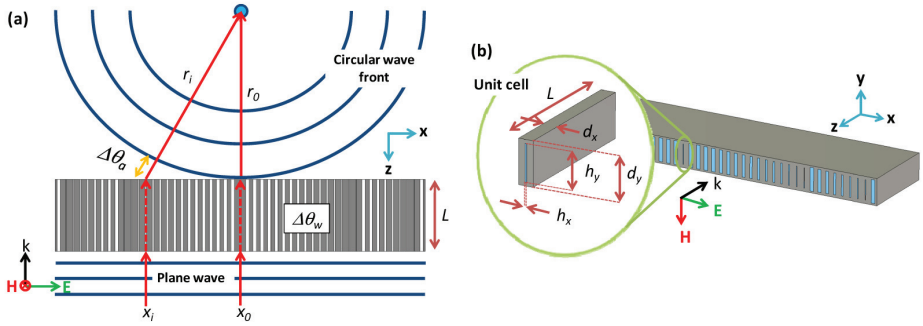

Fig. 1. (a) Schematic of a plane wave with TM-polarization impinging on an arrangement of metallic waveguides of constant length L. For each waveguide, width (h_x) and height (h_y) are determined in order to achieve the required circular wave front with focal length r_0. The values $\Delta\theta_w$ and $\Delta\theta_a$ are the phase delay inside the waveguide and the phase delay in the air, respectively. (b) Perspective view and unit cell detail of dimensions d_x and d_y.

For the central waveguide, choosing the height of the waveguide to work at $f = f_c$, leads to the effective permittivity is near zero, $\varepsilon_{w\_eff} \approx 0$. Therefore, theoretically, the wave propagates with no phase delay because the phase velocity is effectively infinite. Then, in order to obtain the desired phase at the output of each of the remaining channels, each waveguide should introduce a phase variation equal to

$$\Delta\theta_w(x_i) = 2\pi i - \Delta\theta_a(x_i) - \Delta\theta_w(x_i = 0) = 2\pi i - k_0(r_i - r_0) - \Delta\theta_w(x_i = 0), \quad (4)$$

where i is an integer number i = 1,2,…; $\Delta\theta_a(x_i)$ is the phase delay in the air due to the difference in distance from the exit of each waveguide to the focus, with respect to the central waveguide (r_i - r_0), and $x_i = i \cdot d_x$ represents the x-coordinate of the center of each aperture. It is worth mentioning that $\varepsilon_{w\_eff} = 0$ is an ideal condition that in practice may never be achieved, partly because of absorption and partly due to the imperfection in the waveguide geometry. Also, note that this condition implies an unphysical infinite phase velocity. In practice, the frequency of operation will be close to - but not exactly at - the cut-off frequency, so the phase velocity will be very large but finite and, therefore, there will be a certain phase delay. This small phase delay at the central waveguide is taken into account in Eq. (4) by $\Delta\theta_w(x_i = 0)$. Finally, calculating all $\Delta\theta_w(x_i)$ we immediately obtain from Eq. (3) the height values of each aperture:

$$h_y(x_i) = \frac{\pi}{\sqrt{k_0^2 - \left(\frac{\Delta\theta_w(x_i)}{L}\right)^2}}. \quad (5)$$

At first glance, it might seem that the structure is completely mismatched to the free-space because of the apparent impedance contrast between air and the ENZ waveguides. However, the wave is able to tunnel through the structure coupling most of the energy, if at least one of the physical dimensions of the channel is electrically small, phenomenon that is known as supercoupling and energy squeezing, described in [5,23]. The ideal value for h_x can be obtained by analyzing the structure from a transmission line perspective [24] and matching the normalized characteristic line impedance of free space η_{air} and the waveguide η_w. Reducing the problem to the single unit cell detailed in the Fig. 1(b), η_{air} is defined in the air volume surrounding an artificial waveguide of dimensions d_x and d_y with electric and magnetic walls in x-direction and y-direction, respectively [25]; and η_w in the narrow channel of the ENZ waveguide of dimensions h_x and h_y. Thus, matching the impedances, we obtain:

#183764 - $15.00 USD Received 22 Jan 2013; revised 7 Mar 2013; accepted 7 Mar 2013; published 5 Apr 2013

$$\frac{d_x}{d_y}\sqrt{\frac{\mu_0}{\varepsilon_0}} = \eta_{air} = \eta_w = \frac{h_x(x_i)}{h_y(x_i)}\sqrt{\frac{\mu_0}{\varepsilon_0\varepsilon_{w\_eff}}}. \quad (6)$$

Thereby, the width for each aperture needs to be

$$h_x(x_i) = \frac{\Delta\theta_w(x_i)}{k_0 \cdot L}\frac{d_x}{d_y}h_y(x_i). \quad (7)$$

3. Two-dimensional lens

To begin with, let us analyze the ENZ waveguide array lens shown in Fig. 1(b) where the structure is considered infinite in the *y*-direction and is excited by an incident plane wave that propagates in the *z* direction and whose electric field vector is polarized along the *x* axis. For a design frequency f_0 equal to 1 THz (λ_0 = 300 μm), the thickness of the lens is assumed to be $L = 2\lambda_0$, the total width in the *x*-direction is equal to $10.2\lambda_0$ and the dimensions of the unit cell are d_x = 60 μm and d_y = 180 μm. The dimensions of the narrow channels have been chosen to have the focus at r_0 = 1.5 mm = $5\lambda_0$ from the exit face. The material of the lens is assumed to be PEC and the boundary conditions have been fixed as open (perfectly matched layer) in the *x*-direction and magnetic walls in the upper and lower faces in order to make the structure infinitely periodic in the *y*-direction. For the numerical simulation the structure is meshed with accuracy equal to $\lambda_0/20$. For all the numerical results, we have used the finite-integration-technique software CST Microwave Studio™.

A set of 51 waveguides is then designed with specific heights and widths determined from Eqs. (5) and (7). Figure 2(a) shows the design values for both dimensions of each of the 51 waveguides together with their corresponding phase variation, identified by the position in the *x*-direction. The abrupt changes in the dimensions of adjacent waveguides correspond to phase changes equal to 2π. Note in the figure that the values for $\Delta\theta_w$ have been calculated taking into account the fact that we really work at a frequency slightly above 1 THz, exactly at 1.0035 THz. The relative effective permittivity ε_{w_eff} of all waveguides retrieved from the numerical results is compared with the theoretical values in Fig. 2(b). We achieve good agreement between the simulated values and those calculated with the analytical formulation. Moreover, it is clearly seen that all waveguides are working around the ENZ region (i.e., low-epsilon region), obtaining the value closest to zero for the central waveguide, as it has been initially designed.

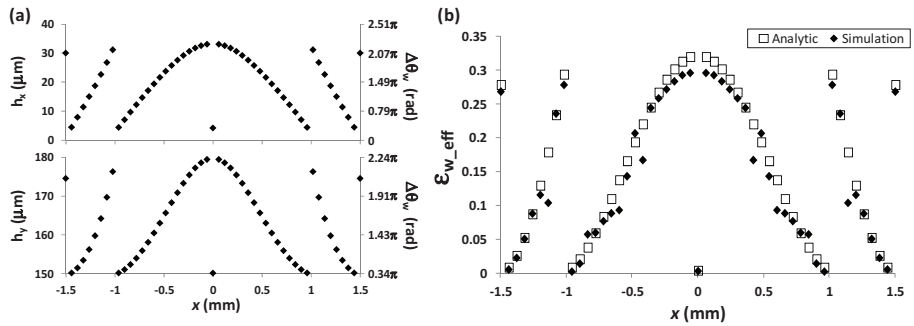

Fig. 2. (a) Dimensions of the waveguide width h_x, and height h_y and phase variation $\Delta\theta_w$ of each waveguide for a 2D graded-index lens of total width 3.06 mm and focal length 1.5 mm. (b) Comparison between the relative effective permittivity of each ENZ waveguide obtained with simulation (open square) and analytical formulation (solid rhombus).

In Fig. 3(a), the numerically-computed magnetic field distribution along the *xz*-plane is shown. It can be observed that the planar phase front at the input is converted into a

#183764 - $15.00 USD Received 22 Jan 2013; revised 7 Mar 2013; accepted 7 Mar 2013; published 5 Apr 2013

cylindrical phase front at the exit of the lens. It is also evident from the figure the slight differences in the phase of the magnetic field inside each waveguide. Figure 3(b) shows the magnitude of the *y*-component of the magnetic field (H_y) and the *x*-component of the electric field (E_x) along *z* axis for the central waveguide. A focus is clearly observed for both fields, less evident in the E-field because it is hidden due to an enhancement of the electric field inside the lens. This enhancement of the E-field in the waveguides is not the same in all waveguides because the E_x magnitude is higher when the effective permittivity is closer to zero [5]. The same fields are represented along *x* at the focal plane in Fig. 3(c) showing the focus and a *sinc*-like spatial distribution for H_y and E_x, demonstrating that the epsilon-near-zero graded-index structure behaves indeed as a lens acting as a Fourier transform operator [26]. It is also worth noting that a standing wave appears at the lens input, which is caused by some reflections coming from the finite size in the *x*-direction. Therefore, edge effects are unavoidable and the value for the free space characteristic line impedance deviates slightly from the theoretical value obtained for an infinitely replicated single waveguide. The approximate reflection coefficient $|\Gamma| = 0.3$ is obtained using the expression $\frac{A_{\max}}{A_{\min}} = \frac{1+|\Gamma|}{1-|\Gamma|}$, with A_{max} and A_{min} as the maximum and minimum values of the field amplitude [21]. The impedance matching is quite good compared with typical dielectric lenses at terahertz frequencies [27,28], generally made of silicon whose relative permittivity (ε_r) is 11.9, leading to a reflection coefficient of 0.55. It is also possible to find commercial dielectric lenses for terahertz applications [29,30] made of Teflon (ε_r = 1.9) or Tsurupica (ε_r = 2.31) whose reflection coefficient would be lower than 0.3, assuming lossless dielectrics. However, lenses made from the latter dielectrics have thicknesses around $10\lambda_0$, five times greater than our design.

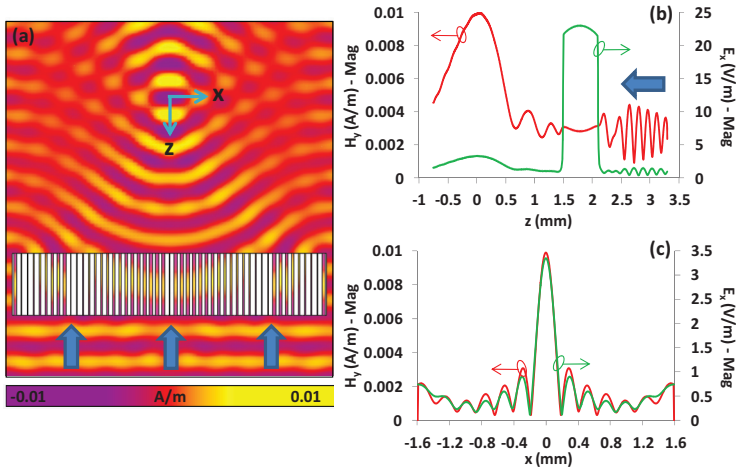

Fig. 3. (a) Top view (*xz*-plane) of the magnetic field distribution H_y on a system composed of a flat metallic lens made of arrangement of ENZ waveguides illuminated by a normally incident plane wave. (b) Magnetic field distribution H_y and electric field distribution E_x along the optical axis, *z*-direction; and (c) along the *x*-direction at the focal length.

The main features obtained for our lens are the enhancement factor (i.e. focus to incident intensity ratio) of 12.84, a depth of focus in the optical axis (*z*-direction) equal to 861.37 μm = $2.87\lambda_0$ and a full-width at half-maximum (FWHM) at the focal plane (*x*-direction) of 174.86 μm = $0.58\lambda_0$. It must be highlighted that with this completely flat graded-index ENZ lens, a reduction of 36.51% of the total volume of the lens is achieved with respect to an ENZ waveguide lens with a convex profile and same dimensions [26]. Notice that in this

#183764 - $15.00 USD Received 22 Jan 2013; revised 7 Mar 2013; accepted 7 Mar 2013; published 5 Apr 2013

comparison, the volume of the convex ENZ lens is computed by considering a rectangular cuboid with length equals to the length of the lateral waveguides

Table 1 shows a comparison of several designs with different sizes of the lens aperture, in order to evaluate the penalty in the performance of the lens when its aperture is reduced. As the total width is shortened, the enhancement factor is lowered because the number of waveguides that collects the impinging energy is reduced. Also, the greater values of depth of focus and FHWM show that the energy concentration is less effective. Attending to the focal length, the numerically-computed focus is just slightly shifted compared to the design. This is a direct consequence of working out of the ideal condition of effective permittivity of the central waveguide equal to zero. The number of apertures is also relevant for this parameter, as can be deduced from Table 1, since if there are not enough waveguides the phase front is no longer circular. Moreover, the diffraction caused by edge effects are more notable and further affect the focus. Under our design conditions, we have found the minimum of the total width with acceptable performance to be around $6\lambda_0$.

Table 1. Feature summary for a two-dimensional lens with different total widths

Number of Apertures (Width)	Focal Length (μm)	Enhancement Factor	Depth of Focus (μm)	FWHM (μm)
51 ($10.2\lambda_0$)	1475.31	12.84	861.37	174.86
41 ($8.2\lambda_0$)	1337.13	9.59	997.19	189.10
31 ($6.2\lambda_0$)	1337.20	7.24	1432.80	216.39

The behaviour of the lens under an obliquely incident plane wave illumination has also been analyzed. Figure 4 shows the cross section of the power along the focus plane when the angle of incidence is varied from 0 to 20 degrees. The focus shifts as expected according to Fourier analysis [26,31]. A reduction of the transmitted power is noticeable as the angle of incidence increases. For instance, the enhancement factor falls from 12.84 to 8.74 for 20 degrees angle of incidence. The numerical aperture calculated as $n \cdot sin\theta$ where n is the index of refraction of the medium surrounding the lens, air in this case; and θ the half-angle of the maximum cone of incident wave that can enter or exit the lens, is equal to 0.472. The angle of the maximum cone of incidence is calculated as the angle for which the transmitted power at the focus is half the transmitted power at the focus under normal incident.

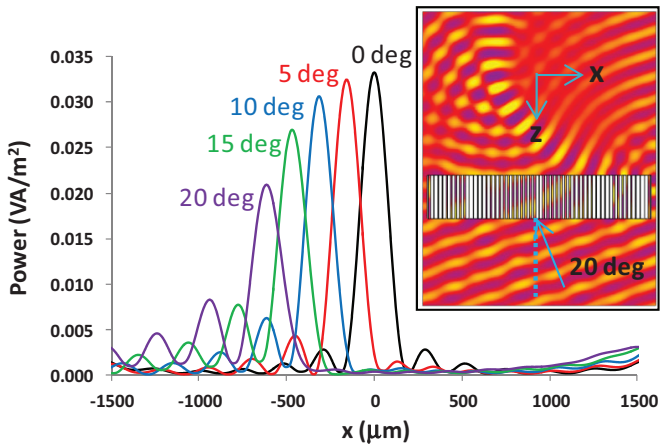

Fig. 4. Cross section of the power along x-direction at the focal plane when the input signal is an obliquely incident plane wave. It is represented from 0 to 20 degrees of angle of incidence in steps of 5 degrees. (inset) Top view (xz-plane) of the magnetic field distribution H_y along the focal plane for an input wave with an angle of incidence of 20 degrees.

#183764 - $15.00 USD Received 22 Jan 2013; revised 7 Mar 2013; accepted 7 Mar 2013; published 5 Apr 2013

Finally, Table 2 shows the behaviour of the lens for different operation frequencies in order to evaluate the chromatic dispersion/aberration of the lens. We observe that the focus moves further away as the frequency increases. This follows from Eq. (4). As the frequency increases, so does ε_{w_eff}, and thus, also the accumulated phase variations $\Delta\theta_w(x_i)$ and $\Delta\theta_w(x_i = 0)$. Therefore, $(r_i - r_0)$ is enforced to be reduced, which happens when the focal length increases. The table also shows a general degradation of the performance of the lens compared to the optimal frequency 1.0035 THz (highlighted in bold in Table 2). This degradation is more severe for frequencies below the optimal frequency because the waveguides with lower values of h_y start to operate at cut-off. The bandwidth of operation, estimated as a −3 dB from the optimum enhancement factor, is 0.27 THz, corresponding to a fractional bandwidth of 26.9%. Moreover, the reflection coefficient increases as the frequency of operation deviates from the optimal frequency: we obtain $|\Gamma| = 0.48$ at 0.98 THz and $|\Gamma| = 0.65$ at 1.2 THz. Therefore, this lens works in a narrow band, which is limited by the frequency dispersion of the effective permittivity and the impedance matching.

Table 2. Feature Summary for a Two-dimensional Lens at Different Operation Frequencies

Operation Frequency (THz)	Focal Length (μm)	Enhancement Factor	Depth of Focus (μm)	FWHM (μm)
0.98	1311.90	6.16	1356.61	209.43
0.99	1436.82	8.20	943.77	183.21
1.0035	**1475.31**	**12.84**	**861.37**	**174.86**
1.10	1825.33	10.37	907.19	229.05
1.20	1937.90	7.64	963.35	554.76

4. Three-dimensional lens

Unlike some of the graded-index lenses based on slit arrays [12–20], the ENZ lens proposed here has the potential to achieve spherical phase fronts, i.e., convergence in two orthogonal planes. This is investigated next with the ENZ lens shown in Fig. 5(a). The design frequency is again $f_0 = 1$ THz so the dimensions of the unit cell are the same: $d_x = 60$ μm and $d_y = 180$ μm. The total dimensions of the full structure are $L_x = L_y = 10.2\lambda_0 = 3.06$ mm and the thickness $L_z = 600$ μm. Moreover, in order to take into account metal losses, the structure is made of aluminium, with conductivity equal to 3.56×10^7 S/m. Figure 5(b) depicts the simulation results for the power distribution in the *xz* and *yz*-planes when the lens is excited with a plane wave with TM polarization, i.e. electric field polarized along *x*. It can be seen in both planes that the energy is focused demonstrating the performance of the lens. The enhancement factor is 62.3, and the focal length and depth of focus are equal to 1312.50 μm = $4.38\lambda_0$ and 614.04 μm = $2.05\lambda_0$ respectively. The cross section of the power along the focal plane in the *x*-direction and *y*-direction is shown in the inset of the Fig. 5(b). The FWHM is 184.04 μm, resulting in a resolution of $1.23\lambda_0/2$, very close to half wavelength. Along the *y*-direction, the FWHM obtained is 190.60 μm equal to $1.27\lambda_0/2$. It is important to note that this design has been done to get the focus at $5\lambda_0$. It is worth mentioning that the flexibility of tailoring the phase difference between waveguides allows us to modify the focal length and/or to get different phase fronts at the output such as plane waves radiating in other directions or convex phase patterns, by just properly changing the dimensions of the individual waveguide cross section. Finally, the simulation results for the extinction ratio between copolar and crosspolar polarization at the focal distance is 51.32 dB allowing us to use this lens as a polarization analyzer as well.

#183764 - $15.00 USD Received 22 Jan 2013; revised 7 Mar 2013; accepted 7 Mar 2013; published 5 Apr 2013

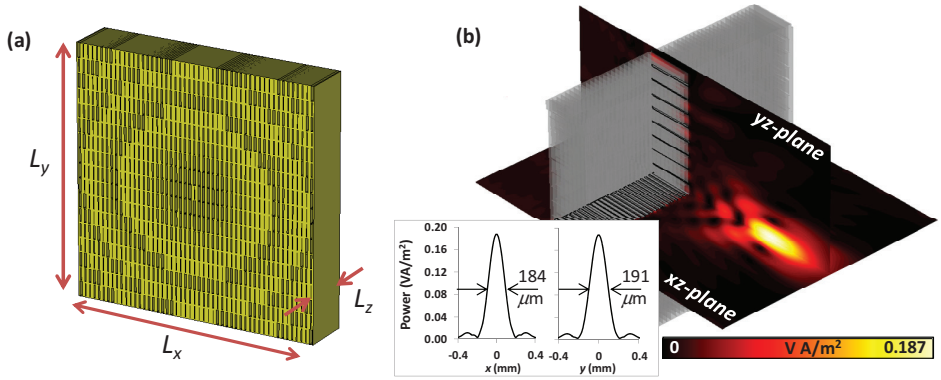

Fig. 5. (a) Sketch of the proposed 3D planar graded index lens, made of arrangement of ENZ waveguides, of total dimensions L_x and L_y and thickness L_z. (b) Power distribution along the *xz*- and *yz*-planes, and (inset) along the *x*-direction and *y*-direction when the structure is excited with a plane wave

A plane wave excitation is, in general, an ideal case that cannot be performed in most of the real experimental setups. For that reason and in order to emulate a realistic incident wave, the plane wave is replaced by a Gaussian beam [31]. The minimum beam radius is equal to 1496.95 μm and the excitation is defined to have the beam focus (that is, where the minimum beam radius is located) at 1.5 mm far from the lens face. This new system, Gaussian beam and lens, may emulate in a reliable way a real system composed by a horn antenna working at 1THz that illuminates the lens. Figures 6(a) and 6(b) show the magnetic field distribution H_y for *xz* and *yz*-planes, respectively. The focus is clearly observed in both planes but more interesting is that the intensity of the field on the edges is lower than in the middle of the structure thanks to the Gaussian beam excitation, and thus spurious diffraction effects are reduced. This can be observed in further detail in Figs. 6(c) and 6(d), where the power distribution is shown on the *xz*- and *yz*-plane. With this new excitation the enhancement factor (now calculated with respect to the beam maximum value) is 24.3. The obtained value of depth of focus is 700.41 μm = $2.33\lambda_0/2$ and the values of FWHM along *x* and *y*-direction are 210.8 μm = $1.41\lambda_0/2$ and 218.4 μm = $1.46\lambda_0/2$, respectively. Note that the performance of the focus is slightly worse than that of the plane wave excitation, as expected, since the contribution of the external waveguides is less effective.

The design of this lens may resemble classical metallic lenses such as constrained lenses [32–34] or Fresnel zone plates [35]. However, there are major differences arisen from their underlying physics. While classical lenses are based on an arrangement of waveguides working with fundamental modes well above their cut-off frequencies, the ENZ lenses use waveguides near cut-off. From an effective constitutive parameters point of view both lenses exhibit a permeability equal to one but the permittivity for constrained lenses is $0 < \varepsilon < 1$ and for ENZ ones is obviously $\varepsilon \to 0^+$. Consequently, attending to Fermat's principle [1], classical lenses always have ellipsoidal profiles and ENZ lenses cylindrical profiles if the graded-index techniques are not used. Furthermore, constrained lenses tend to display undesired grating lobes given the large in-plane periodicities, whereas the lens analyzed here prevents them in both planes, due to the subwavelength periodicity along the direction of the incident E-field and approximately $\lambda_0/2$ periodicity along the other in-plane direction. In addition, classical metallic lenses display Fresnel reflection losses given the mismatch between the normalized characteristic line impedance of free space and the waveguides. However, as we have shown here, ENZ lens based on near cut-off waveguides can be designed to be approximately impedance-matched. On the other hand, it exists other kind of

#183764 - $15.00 USD Received 22 Jan 2013; revised 7 Mar 2013; accepted 7 Mar 2013; published 5 Apr 2013

metallic lenses based on stacked subwavelength hole arrays, called extraordinary transmission lenses [34,36], that potentially solve this impedance matching as well. Nevertheless, they achieve it by manipulating the effective permeability of the metamaterial through electrically-coupled cut-off artificial waveguides such that $\varepsilon = \mu$ ($-\infty < \varepsilon < +\infty$, $-\infty < \mu < +\infty$). In terms of electromagnetic modes, these metamaterial lenses support a mixture of TEM and cut-off TE_{20} or TM_{02} (depending on the unit cell dimensions) modes, whereas the lens proposed here supports only a TE_{01}.

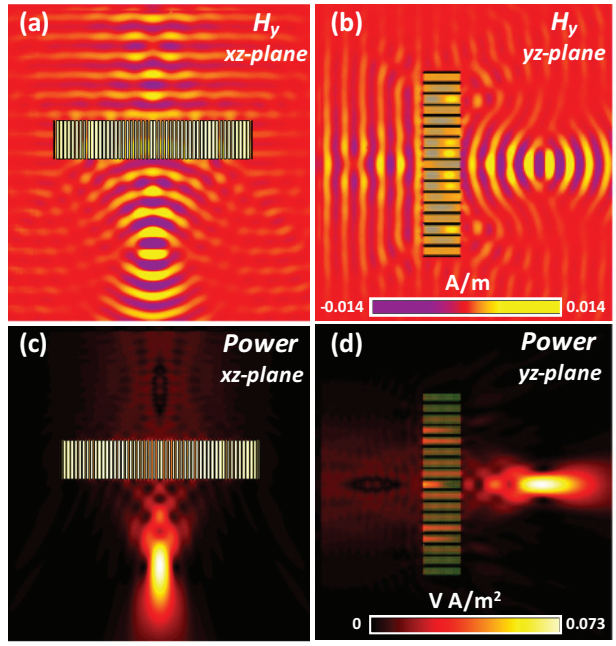

Fig. 6. (a) Top view (*xz*-plane) and (b) side view (*yz*-plane) of the magnetic field distribution H_y on a system composed of a three dimensional ENZ lens illuminated by a Gaussian beam. (c) *xz*-plane and (d) *yz*-plane of the power distribution on the same system. Scale on panel (b) and (d) is also valid in (a) and (c) respectively.

5. Conclusions

In this article, an arrangement of metallic ENZ waveguides is proposed as a method for planar graded-index lenses. Applying the standard theory of waveguides we are able to match the structure to free-space and individually control the propagation constant inside each waveguide comprising the ENZ metamaterial, tailoring the radiation phase pattern at the exit of the structure to emulate a flat graded-index converging lens. A two-dimensional design of this flat lens working at 1 THz and assuming perfect electrical conductor material is shown, obtaining a good match to the free-space with a reflection coefficient equal to 0.3 and where the importance of the number of waveguides is studied, resulting in a minimum width around $6\lambda_0$ to obtain an acceptable performance. In addition, the chromatic dispersion is studied showing a narrow bandwidth of operation equal to 0.27 THz (26.9% fractional bandwidth). Also a full three-dimensional prototype made of aluminum, in order to consider losses as well, is simulated obtaining a clear focus spot with an enhancement factor of 62.3, a FWHM equal to $1.23\lambda_0/2$ and a depth of focus of $2.05\lambda_0$. This technique may be applied to develop devices that require precise phase control, with low losses, good robustness and small size.

#183764 - $15.00 USD Received 22 Jan 2013; revised 7 Mar 2013; accepted 7 Mar 2013; published 5 Apr 2013

Acknowledgments

In memoriam Prof. Mario Sorolla.

Effort sponsored by Spanish Government under contracts Consolider "Engineering Metamaterials" CSD2008-00066 and TEC2011-28664-C02-01. P.R.-U. is sponsored by the Government of Navarra under funding program "Formación de tecnólogos" 055/01/11. M.N.-C. is supported by the Imperial College Junior Research Fellowship. M. B. acknowledges funding by the Spanish Government under the research contract program Ramon y Cajal RYC-2011-08221. N.E. acknowledges the support from the US Office of Naval Research (ONR) Multidisciplinary University Research Initiatives (MURI) grant number N00014-10-1-0942.

#183764 - $15.00 USD Received 22 Jan 2013; revised 7 Mar 2013; accepted 7 Mar 2013; published 5 Apr 2013

Chapter 4

Nanoantennas modeling

This chapter introduces optical antennas in the context of plasmonic devices able to enhance efficiently the light-matter interactions putting emphasis in their modeling. Optical antennas are presented as metallic nanoparticles whose designs can be inspired by classic antenna geometries but where high-frequency plasmonic effects must be taken into account. One original contribution is included in this chapter: (i) the modeling of a log-periodic plasmonic nanoantenna which exhibits polarization independence and broadband response for simultaneous surface-enhanced fluorescence, Raman, and infrared absorption spectroscopy.

4.1 Optical antennas

Antennas are devices traditionally used either to emit electromagnetic waves which can then travel over large distance or to receive them from a remote source without a guiding medium. Antennas provide then an interface between localized electric signals and the free space wireless transmission. Analogously, optical antennas can be defined as devices designed to efficiently convert free-propagation optical radiation to localized energy, and vice versa [BHAR 09].

Optical antennas were devised in the context of microscopy. Already in 1928, Synge described to Einstein a method in which the field scattered from a tiny particle could be used as a light source [NOVO 07]. However, it was not until 1985 when Wessel mentioned explicitly the analogy of local microscopy light sources to classical antennas [WESS 85]. Despite all precedents, optical antennas are relatively new devices in the field of physical optics. Since antennas have characteristic dimensions

of the order of the operation wavelength, optical antennas need fabrication accuracies of the order of a few nanometers. Therefore, until the advent of nanotechnology and the use of novel nanofabrication processes (e.g. electron-beam lithography, focused ion-beam milling, nano-imprint lithography) it was not possible to achieve these demands.

In optical science and engineering, lenses, mirror and other diffractive elements have been used to control light by means of redirecting the propagating wave fronts, manipulating the wave nature of the electromagnetic fields. However, all these elements are diffraction limited. Therefore, controlling fields on the subwavelength scale is not amenable with these devices. Optical antennas help to surpass the diffraction limit, making it possible to manipulate, control, and visualize optical fields on the nanometer scale. There are basically three distinct processes that can be enhanced with optical antennas (Fig. 4.1) [BHAR 09]. In light-emitting devices (LEDs) an electron-hole pair combines to emit a photon and optical antennas make the transfer of energy more efficient. The same occurs in photovoltaics, where incoming light causes a charge separation in a material. In spectroscopy, outgoing radiation is generated when incident light polarizes the material of interest. In this case, the antenna serves to make both the excitation and the emission more efficient.

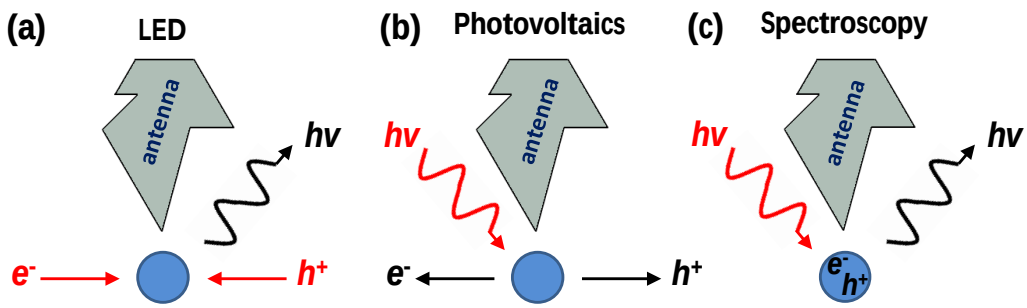

Figure 4.1. Antenna-based optical interactions

Metallic nanoparticles

The simplest realization of a nanoantenna is a single metallic nanoparticle and the most basic form is a sphere or a rod. Both geometries exhibit a resonance spectrum that shifts with the particle's aspect ratio. As we saw in Chapter 1, the resonances of a nanoparticle at optics can be related to localized surface plasmons which are accompanied by resonantly enhanced polarizabilities and accordingly enhanced scattering and absorption as well as enhanced near-field intensities.

Two end-to-end aligned particles separated by a small gap is a more interesting configuration since the coupling between the particles can create highly localized and strongly enhanced optical near fields inside the gap, beating the diffraction limit. The

smaller the gap, the higher the coupling and thus, the intensity enhancement [BIAG 12]. Moreover, when the nanoantenna is excited with an external field, oscillating surface charges are created in each particle. If they oscillate in phase (i.e. dipole-like charge oscillation) the nanoantenna couples strongly with the radiation fields via dipole radiation. On the contrary, if the charge distribution exhibits mirror symmetry, the nanoantenna does not efficiently emit into the far field since the two individual dipoles oscillate out of phase and therefore cancel each other[27].

There are several models such as the Mie theory, the mass-and-spring model or the Fabry-Perot model that are able to predict these resonances [BIAG 12]. However, complex antenna geometries (e.g. sharp corners, multiple gaps, multiple elements) lead to strong near fields enhancement and coupling not easy to predict, and the use of electromagnetic simulation software is almost compulsory.

Inspiration in radiofrequency antennas

Most advanced geometries in optical antennas are inspired in classical antenna designs. In fact, optical antennas are strongly analogous to their radiofrequency and microwave counterparts. Almost all antenna parameters such as the directivity, gain or radiation efficiency have their equivalency in both regimes [ALU 13]. However, there are crucial differences, most of them arising because metals are not perfect conductors at optical frequencies. Next, a few of the most important differences are described:

- Classical antenna engineering strongly benefits from the fact that metals at radio frequencies can be considered nearly lossless whereas above the millimeter-wave band losses become a constraint that antenna and circuit engineers have to deal with (see Chapter 1, section 1.3).
- Due to the variable dispersive behavior of different metals, the choice of the best material for a given application is a critical decision. Mainly gold, silver, aluminum and copper have been considered so far the most suitable according to their spectral features [WEST 10].
- Wavelength scaling must be performed taking into account that treating metal as strongly coupled plasma leads to a reduced effective wavelength seen by the antenna [NOVO 07b]. It is roughly a factor of 2–6 shorter than the free space wavelength for typical metals. This means, for instance, that the length of a $l_{au}/2$ dipole nanoantenna is surprisingly small, about $l_0/10.6$ in the case of gold.
- Moreover, the large mismatch between the wavelength of plasmonics resonances and of free-space waves implies reduced radiation efficiency, lower quality factor of the resonances and deviations in the radiation patterns.

[27] The out-of-phase resonance is denominated as a “dark mode” since it cannot be excited as long as the illumination path remains fully symmetric.

Despite all the differences, classical designs have demonstrated that, in general, the overall properties are independent of the frequency band. In [BHAR 09], [BIAG 12] a complete description of the analogies (and differences) between optical and radiofrequency antennas is provided. At infrared, antenna engineering has expanded considerably in the past decades by means of importing antennas configurations such as dipole, bowtie, spiral or log-periodic antennas among others [GONZ 05]. At optical frequencies, Yagi-Uda [CURT 10], bowtie [FROM 04], monopole [TAMI 07] or patch [ESTE 10] nanoantennas have demonstrated similar capabilities than their microwave counterparts.

Applications

Optical antennas hold promise for a variety of potential applications, especially those based on enhanced light-matter interactions taking advantage of high field enhancement, strong field localization and large absorption cross sections. For instance, the ability of optical antennas to influence light on the nanometer scale leads to microscopy and nanoimaging applications where the nanoantenna is used as a near-field optical probe [NOVO 06]. Also, the enhancement of the localized fields has been used for spectroscopy in fluorescence emission [KINK 09], infrared absorption [NEUB 08] and Raman scattering [BROL 04]. Optical antennas have also demonstrated the improvements in photovoltaic processes by means of increasing the efficiency of collecting and scattering photons into the far field as well as increasing the light absorption [ATWA 10]. The increment in the efficiency of light emission helps also to improve inherently low-efficiency lighting schemes like organic LEDs, silicon-based lighting, and solid-state lighting in the yellow and green spectral region [LIU 05], [WEDG 04]. Furthermore, optical antennas are able to exploit the nonlinear response of noble metals for applications such as harmonic generation [KIM 08], [NAVA 12b], two-photon excited luminescence [BOUH 03] or four-wave mixing [DANC 07]. Further applications can be found in the following review [NOVO 11].

Numerical modeling

Plasmonics nanoantennas offer uncountable possibilities and their features play a major role for a given application. As we have seen, importing radiofrequency designs is a common practice in order to achieve the desired properties. Principally, the properties of a nanoantenna are defined by its geometry and materials and, as commented above, numerical simulations are needed to devise and analyze complex geometries. Since the contribution to this thesis is related to nanoantennas modeling, the most important points to be taken into account in the numerical modeling of nanoantennas are listed:

- The dispersive behavior of the materials that composed the antenna is commonly strong at optics. A proper fitting between the simulated material parameters and those obtained in the literature must be set for the frequency range of interest.
- Small gaps and sharp edges highly enhance the fields in the surrounding areas, creating the denominated hot-spots. Furthermore, for proper estimation of the fields at such points, a very fine mesh, usually of a few nanometers, must be set. Converging tests where the mesh is gradually increased may help to find the most suitable mesh and save simulation time.
- For accurate calculation of the scattering properties, the distance between the structure and the perfectly matched layers defining the simulation volume has to be at least half-wavelength size.
- The stability factor, which defines together with the mesh the time step, and the simulation time must be properly chosen to let all field components decay enough within the simulation box for the CW information obtained by Fourier transformation to be valid.

For the modeling work presented in this thesis, the used simulation software is Lumerical FDTD Solutions, a high performance three dimensional FDTD-method Maxwell solver for the design, analysis and optimization of nanophotonic devices, processes and materials [LUM 14]. This software is expressly oriented to analyze the interaction of ultraviolet, visible and infrared radiation with complicated structures employing wavelength scale features. It includes a wide library of materials characterized at high frequencies as well as specific modules for the most common optics problems that makes this software very suitable for nanoatennas modeling.

As a final remark, it must be highlighted that after fabrication process and because of tolerances, the initial design may differ from the real sample. Therefore, structural parameters of fabricated structures should be measured in order to adjust the simulation parameters and obtain more accurate numerical results.

4.2 [PAPER F] Plasmonic nanoantennas for multispectral surface-enhanced spectroscopies

Plasmonic nanoantennas, the counterpart of classical radiofrequency antennas at the optical frequency band [NOVO 11], provide new ways to enhance light-matter interactions taking advantage of the resonant capabilities and field concentration of localized surface plasmons. In consequence, a wide catalogue of applications, such as molecular sensing, light-emitting devices or photovoltaics among others, has been benefited from nanoantennas recently.

However, the dipolar nature of most nanoantenna configurations leads to narrow-band response as well as limited polarization [BHAR 09]. This is a drawback for applications which are intrinsically multiwavelength or broadband in nature (e.g. spontaneous two-photon emission, multispectral biosensing or second and third order nonlinear process) as well as those where it is necessary to enhance the fields without perturbing its polarization state (e.g. polarimetry, chiral molecule mapping or optical data storage). Therefore, some optical antennas operating in a broad range of frequencies have been proposed recently [HARU 12], [NAVA 12b], [THYA 12], [AOUA 12], [AOUA 13] although much more research is needed in this field.

Our aim with this work is to provide a plasmonics nanoantenna able to work in a wide operation bandwidth in order to be applied in multispectral spectroscopy. The main features of this publication are:

- We design, fabricate and measure a broadband log-periodic nanoantenna which generates significant electromagnetic intensity enhancement from the visible to the mid-IR wavelength region.
- The nanoantenna is comprised of three different arms in order to achieve polarization independence. Each arm design is inspired by log-periodic radiofrequency antenna geometries, which are very well known to exhibit broadband response [BALA 05]
- We demonstrate simultaneously surface-enhanced fluorescence, Raman, and infrared absorption, with relevant enhancement factors.

PAPER F

The Journal of Physical Chemistry C ***117***, *18620 (2013)*

Plasmonic nanoantennas for multispectral surface-enhanced spectroscopies

Heykel Aouani, Mohsen Rahmani, Hana Šípová, Víctor Torres, Kate ina Hegnerová, Miguel Beruete, Ji í Homola, Minghui Hong, Miguel Navarro-Cía, and Stefan A. Maier

General discussion of results and future lines

The results presented in this thesis cover a wide variety of applications with a common background: metamaterials and plasmonics. Both fields are partially unexplored, principally at the THz band, and thus, they still offer extensive research possibilities. This work contributes to both areas with novel metamaterials and plasmonics devices such as quarter-wave plates, lenses or nanoantennas as well as refined analysis techniques based mainly on equivalent circuits. A summary of the main results are described subsequently.

We have proposed three original contributions under the framework of extraordinary transmission metamaterials:

- We investigated the possibility of extending classic microwave techniques such as inductance addition with meandering lines to the mid-infrared band with successful results. To this end, we fabricated and measured several subwavelength hole arrays (SHAs) with different plasmonics inductors based on meandering lines. We achieved an unprecedented redshift and bandwidth enlargement of the extraordinary transmission band at frequencies as high as 17 THz. Moreover, a lossy equivalent circuit model able to predict the underlying physics of the problem was proposed. The experimental and circuital results were supported by numerical simulations with very good agreement.
- Taking advantage of the properties observed in the previous work, we designed a very compact dual-band quarter wave plate exploiting the birefringence of a modified SHA. Besides adding meandering lines to increment the inductance for vertical polarization, vertical slits connect adjacent holes to provide the necessary capacitive behavior for horizontal polarization. Thanks to the frequency redshift and bandwidth increment, at 1 THz the structure operates out of resonance exhibiting a wideband response, whereas at 2.2 THz a narrower operation

bandwidth is obtain since it works in a Fabry-Perot resonance regime. The structure was fabricated and very promising experimental results were obtained.

- We obtained a lossless equivalent circuit model for the double-layer fishnet metamaterial (i.e. two stacked SHAs) analyzing the underlying physics by means of studying the electromagnetic fields. Almost perfect agreement in the magnitude and phase of the transmission and reflection coefficient was obtained between numerical and equivalent circuit results. Accordingly, the model also predicts the frequency bands with negative index of refraction. The fishnet is a very relevant structure since it is one of the most effective metamaterials to obtain negative refraction. Therefore, this model will help to analyze and design future structures based on it.

Another kind of metamaterials have been also investigated, those with near-zero permittivity. Especially we have focused on arrays of metallic rectangular waveguides which exhibit e-near-zero (ENZ) behavior when working near their cutoff frequency. Since one of the most interesting properties of ENZ metamaterials is the ability of tailoring the radiation pattern with remarkable impedance matching, they seems very suitable for lens applications.

- We demonstrated the performance of a plano-concave metallic lens comprised of ENZ waveguides being the first experimental demonstration of such structure at the THz band. Very good impedance matching was obtained exploiting the energy squeezing principle as well as great performance in focusing energy and improving the radiation properties of antennas. A maximum transmittance enhancement and directivity equal to 15.9 dB and 37.3 dBi were measured, respectively.
- We provided the guidelines for smart designs of planar graded-index lenses also based on ENZ waveguide arrays. We presented several designs for the THz band that show, after thorough analysis of the main features, excellent capabilities in the context of THz lenses. For instance, a reflection coefficient of only 0.3 was achieved in a lens as thin as $2\lambda_0$.

Finally, the first results in the modeling of optical nanoantennas were presented. Following design criterions of radiofrequency antennas but taking into account the plasmonics interactions, we designed a broadband and polarization independent nanoantenna based on its microwave counterpart log-periodic antenna. The nanoantenna is able to generate significant electromagnetic intensity enhancement from the visible to the mid-IR wavelength region. Moreover, it was tested by means of surface-enhanced fluorescence, Raman and infrared absorption experiments.

Concluding remarks

After an overview of the results obtained through these years, it can be concluded that the initial objectives of designing, fabricating and measuring new metamaterials and plasmonics devices for field manipulation and concentration have been accomplished.

Exploiting the inductance addition in SHAs, we proved an effective way to tailor the extraordinary transmission phenomenon at the THz band that can be used for real components such as quarter-wave plates. All our work in extraordinary transmission is mainly supported by equivalent circuits since they provide a straightforward and efficient technique to understand and analyze complex electromagnetic problems.

We also demonstrated the high efficiency of tunneling energy through narrow waveguides, exploiting the energy squeezing principle, and the potential possibilities in the context of metallic lenses.

Plasmonic nanoantennas are an emerging field which is being rapidly developed because of the wide number of applications. We showed the utility of applying the experience acquired in antennas engineering at low frequencies for novel plasmonic nanoantennas of high performance.

Future lines

Many of the research lines in the thesis assure future works and further results:

- Regarding extraordinary transmission metamaterials, new compact metasurfaces based on modified SHAs are being devised for other THz quasioptical devices such as filters, absorbers or demultiplexers.
- In the context of equivalent circuits, we are working on developing models for fishnet metamaterials of several layers (more than two), with different longitudinal periodicities and defects introduced intentionally.
- We have experimentally and theoretically demonstrated the high efficiency of squeezing energy through metallic waveguides and enormous possibilities to tailor the wave fronts. Therefore, these techniques may be applied to develop further devices that require precise phase control, with low losses, good robustness and small size (e.g. beam steerers or beam splitters).
- Plasmonic nanoantennas are probably the topic which holds more promising future applications. We are currently working in two exciting concepts: (i) third harmonic generation in the ultraviolet with fractal nanoantennas, (ii) thermoplasmonic effects linked to broadband nanoantennas for accurate control of the local heat. Both topics are currently in the fabrication and measure stage, after showing the desired performance in the theoretical analysis and numerical simulations.

Discusión general de los resultados y líneas de futuro

Los resultados presentados en esta tesis cubren una amplia variedad de aplicaciones con un fondo común: metamateriales y plasmónica. Ambos campos están parcialmente inexplorados, especialmente en la banda de THz, y por lo tanto, aun ofrecen extensas posibilidades de investigación. Este trabajo contribuye en ambas áreas con novedosos metamateriales y dispositivos plasmónicos como retardadores de cuarto de onda, lentes o nanoantennas así como con técnicas refinadas de análisis basada principalmente en circuitos equivalentes. Se describe a continuación un resumen de los resultados principales:

Hemos propuesto tres contribuciones originales bajo el marco de los metamateriales de trasmisión extraordinaria:

- Investigamos la posibilidad de extender técnicas clásicas de microondas, como el incremento de inductancia con líneas de meandro, a la banda del infrarrojo medio con exitosos resultados. Con este fin, fabricamos y medimos varias agrupaciones de agujeros sublambda (SHAs) con diferentes inductores plasmónicos basados en líneas de meandros. Conseguimos un corrimiento al rojo y un ensanchamiento del ancho de banda de la banda de transmisión extraordinaria, sin precedentes, a frecuencias tan altas como 17 THz. Además, se propuso un modelo de circuito equivalente con pérdidas capaz de predecir la física subyacente del problema. Los resultados experimentales y circuitales se apoyaron en simulaciones numéricas con muy buen acuerdo.
- Aprovechando las propiedades observadas en el trabajo anterior, diseñamos un retardador de cuarto de onda my compacto y de doble banda explotando la birrefringencia de SHAs modificados. Además de añadir líneas de meandro para incrementar la inductancia para polarización vertical, aberturas estrechas verticales que conectan agujeros adyacentes, proporcionan el comportamiento capacitivo necesario para polarización horizontal. Gracias al corrimiento al rojo en frecuencia

y el incremento del ancho de banda, a 1THz la estructura opera fuera de resonancia exhibiendo una respuesta de banda ancha, mientras que a 2.2 THz se obtienen un ancho de banda de operación más estrecho ya que se trabaja en un régimen de resonancia Fabry-Perot. La estructura fue fabricada y se obtuvieron resultados experimentales muy prometedores.

- Obtuvimos un modelo de circuito equivalente sin pérdidas para el metamaterial *fishnet* de doble capa (dos SHAs apilados) analizando la física subyacente mediante el estudio de los campos electromagnéticos. Se obtuvo un acuerdo casi perfecto para la magnitud y fase del coeficiente de transmisión y reflexión entre los resultados numéricos y de circuito equivalente. Por consiguiente, el modelo también predice la banda de frecuencia de índice de refracción negativo. El *fishnet* es una estructura muy relevante, ya que es uno de los metamateriales más efectivos para obtener refracción negativa. Por lo tanto, este modelo ayudará a analizar y diseñar futuras estructuras basadas en él.

Otro tipo de metamateriales que han sido investigados son aquellos con permitividad cercana a cero. Especialmente nos hemos centrado en agrupaciones de guías de onda metálicas rectangulares que exhiben un comportamiento épsilon cercano a cero (ENZ) cuando se trabaja cerca de su frecuencia de corte. Ya que una de las propiedades más interesantes de los metamateriales ENZ es la habilidad de adaptar los frentes de onda, éstos parecen muy adecuados para aplicaciones de lentes:

- Demostramos el rendimiento de una lente metálica plana cóncava que se compone de guías de onda ENZ siendo la primera demostración experimental de esta estructura en la banda de THz. Se obtuvo una muy buena adaptación de impedancias explotando el principio de *energy squeezing* así como grandes prestaciones en el enfoque de energía y en la mejora de las propiedades de radiación en antenas. Un incremento de la transmisión máxima y una directividad igual a 15.9 dB y 37.3 dBi fueron medidas, respectivamente.
- Proporcionamos las directrices para diseños avanzados de lentes planas de índice gradual basadas en agrupaciones de guías ENZ. Presentamos varios diseños para la banda de THz que muestran, tras un exhaustivo análisis de las principales características, excelentes capacidades en el contexto de lentes en el THz. Por ejemplo, un coeficiente de reflexión de solo 0.3 fue conseguido en una lente tan delgada como $2l_0$.

Finalmente, los primeros resultados en el modelado de nanoantenas ópticas fueron presentados. Siguiendo criterios de diseño de antenas de radiofrecuencia, pero teniendo en cuenta las interacciones plasmónicas, diseñamos una nanoantenna de gran ancho de banda e independiente de la polarización basada en la antena log-periódica de microondas. La nanoantenna es capaz de generar altos valores de intensidad de campo electromagnético desde el visible hasta la región del infrarrojo medio. Además,

se testeó mediante experimentos de fluorescencia y absorción de tipo Raman e infrarroja.

Observaciones finales

Después de una visión de conjunto de todos los resultados obtenidos durante estos años, se puede concluir que los objetivos iniciales de diseño, fabricación y medida de nuevos metamateriales y dispositivos plasmónicos para la manipulación y concentración de ondas electromagnéticas se han cumplido.

Explotando el incremento de inductancia en SHAs, probamos una manera efectiva de controlar el fenómeno de transmisión extraordinaria en la banda de THZ que se puede usar en componentes reales como retardadores de cuarto de onda. Todo nuestro trabajo de trasmisión extraordinaria está principalmente sustentado con circuitos equivalentes ya que proporcionan una técnica sencilla y eficiente de entender y analizar problemas electromagnéticos complejos.

También demostramos la alta eficiencia en la transmisión de energía a través de guías de onda estrechas, explotando el principio de *energy squeezing*, y las posibilidades potenciales en el contexto de lentes metálicas.

Nanoantenas plasmónicas son un campo emergente que está siendo desarrollado rápidamente por su amplio número de aplicaciones. Mostramos la utilidad de aplicar la experiencia adquirida en ingeniería de antenas de microondas en novedosas nanoantennas plasmónicas de altas prestaciones.

Líneas futuras

Muchas de las líneas de investigación de esta tesis aseguran trabajos futuros y más resultados:

- Respecto a metamateriales de transmisión extraordinaria, nuevas metasuperficies basadas en SHAs se están ideando para otros dispositivos quasiópticos en el THz como filtros, absorbentes o demultiplexores.
- En el contexto de circuitos equivalentes, estamos trabajando en desarrollar modelos para el metamaterial *fishnet* de múltiples capas (más de dos), con diferentes periodicidades longitudinales y con precisos defectos introducidos intencionadamente.
- Hemos demostrado experimental y teóricamente la alta eficiencia de exprimir energía a través de guías de onda metálicas y las enormes posibilidades en ajustar los frentes de onda. Por lo tanto, estas técnicas puede ser aplicado para desarrollar dispositivos que requieran un control preciso de la fase, con bajas pérdidas, alta robustez y pequeño tamaño (ej. direccionadores de haz o separadores de haz).
- Nanoantenas plasmónicas es probablemente el tema que promete más aplicaciones futuras. Actualmente estamos trabajando en dos excitantes conceptos: (i)

generación de tercer harmónico en el ultravioleta con nanoantenas fractales, (ii) efectos termoplasmónicos ligados a nanoantenas de banda ancha para un control preciso del calor generado por efecto Joule localmente. Ambos temas están en la fase de fabricación y medida después de mostrar el rendimiento deseado en los análisis teóricos y las simulaciones numéricas.

References

A

[AKAR 04] S. S. Akarca-Biyikli, I. Bulu, and E. Ozbay, “Enhanced transmission of microwave radiation in one-dimensional metallic gratings with subwavelength aperture,” *Appl. Phys. Lett.* **85**, 1098 (2004).

[ALU 05] A. Alù and N. Engheta, “Achieving transparency with plasmonic and metamaterial coatings,” *Phys. Rev. E* **72**, 016623 (2005).

[ALU 06] A. Alù, F. Bilotti, N. Engheta, and L. Vegni, “Metamaterial Covers Over a Small Aperture,” *IEEE Trans. Antennas Propag.* **54**, 1632 (2006).

[ALU 07] A. Alù, N. Engheta, A. Erentok, and R. Ziolkowski, “Single-Negative, Double-Negative, and Low-index Metamaterials and their Electromagnetic Applications,” *IEEE Antennas Propag. Mag.* **49**, 23 (2007).

[ALU 07b] A. Alù, M. Silveirinha, A. Salandrino, and N. Engheta, “Epsilon-near-zero metamaterials and electromagnetic sources: Tailoring the radiation phase pattern,” *Phys. Rev. B* **75**, 1 (2007).

[ALU 08] A. Alù and N. Engheta, “Dielectric sensing in ε-near-zero narrow waveguide channels,” *Phys. Rev. B* **78**, 045102 (2008).

[ALU 08b] A. Alù, M. Silveirinha, and N. Engheta, “Transmission-line analysis of ε-near-zero–filled narrow channels,” *Phys. Rev. E* **78**, 016604 (2008).

[ALU 09] A. Alù and N. Engheta, “Cloaking a Sensor,” *Phys. Rev. Lett.* **102**, 233901 (2009).

[ALU 13] A. Alù and N. Engheta, “Theory, Modeling and Features of Optical Nanoantennas,” *IEEE Trans. Antennas Propag.* **61**, 1508 (2013).

[AOUA 12] H. Aouani, M. Navarro-Cía, M. Rahmani, T. P. H. Sidiropoulos, M. Hong, R. F. Oulton, and S. A. Maier, “Multiresonant broadband optical antennas as efficient tunable nanosources of second harmonic light,” *Nano Lett.* **12**, 4997 (2012).

[AOUA 13] H. Aouani, H. Šípová, M. Rahmani, M. Navarro-Cía, K. Hegnerová, J. Homola, M. Hong, and S. A. Maier, “Ultrasensitive broadband probing of molecular vibrational modes with multifrequency optical antennas,” *ACS Nano* **7**, 669 (2013).

[ATWA 10] H. A. Atwater and A. Polman, “Plasmonics for improved photovoltaic devices,” *Nat. Mater.* **9**, 205 (2010).

[AVRU 00] I. Avrutsky, Y. Zhao, and V. Kochergin, “Surface-plasmon-assisted resonant tunneling of light through a periodically corrugated thin metal film,” *Opt. Lett.* **25**, 595 (2000).

B

[BALA 05] C. A. Balanis, *Antenna Theory Analysis and Design* (Wiley, 2005).

[BELOV 03] P. A. Belov, R. Marqués, S. I. Maslovski, I. S. Nefedov, M. Silveirinha, C. R. Simovski, and S. A. Tretyakov, “Strong spatial dispersion in wire media in the very large wavelength limit,” *Phys. Rev. B* **67**, 113103 (2003).

[BERU 04] M. Beruete, M. Sorolla, I. Campillo, J. S. Dolado, L. Martín-Moreno, J. Bravo-Abad, and F. J. García-Vidal, “Enhanced millimeter-wave transmission through subwavelength hole arrays,” *Opt. Lett.* **29**, 2500 (2004).

[BERU 04b] M. Beruete, I. Campillo, J. S. Dolado, J. E. Rodríguez-Seco, E. Perea, and M. Sorolla, “Enhanced microwave transmission and beaming using a subwavelength slot in corrugated plate,” *IEEE Antennas Wirel. Propag. Lett.* **3**, 328 (2004).

[BERU 05] M. Beruete, M. Sorolla, I. Campillo, and J. S. Dolado, “Increase of the transmission in cut-off metallic hole arrays,” *IEEE Microw. Wirel. Components Lett.* **15**, 116 (2005).

[BERU 05b] M. Beruete, M. Sorolla, I. Campillo, and J. S. Dolado, “Subwavelength slotted corrugated plate with enhanced quasioptical

millimeter wave transmission," *IEEE Microw. Wirel. Components Lett.* **15**, 286 (2005).

[BERU 05c] M. Beruete, M. Sorolla, I. Campillo, J. S. Dolado, L. Martín-Moreno, J. Bravo-Abad, and F. J. García-Vidal, "Enhanced millimeter wave transmission through quasioptical subwavelength perforated plates," *IEEE Trans. Antennas Propag.* **53**, 1897 (2005).

[BERU 06] M. Beruete, M. Sorolla, and I. Campillo, "Left-handed extraordinary optical transmission through a photonic crystal of subwavelength hole arrays," *Opt. Express* **14**, 5445 (2006).

[BERU 07] M. Beruete, I. Campillo, M. Navarro-Cía, F. Falcone, and M. S. Ayza, "Molding left-or right-handed metamaterials by stacked cutoff metallic hole arrays," *Antennas Propagation, IEEE Trans.* **55**, 1514 (2007).

[BERU 07b] M. Beruete, M. Sorolla, M. Navarro-Cía, F. Falcone, I. Campillo, and V. Lomakin, "Extraordinary transmission and left-handed propagation in miniaturized stacks of doubly periodic subwavelength hole arrays," *Opt. Express* **15**, 1107 (2007).

[BERU 07c] M. Beruete, M. Navarro-Cía, M. Sorolla, and I. Campillo, "Polarized left-handed extraordinary optical transmission of subterahertz waves," *Opt. Express* **15**, 8125 (2007).

[BERU 08] M. Beruete, M. Navarro-Cía, M. Sorolla, and I. Campillo, "Planoconcave lens by negative refraction of stacked subwavelength hole arrays," *Opt. Express* **16**, 9677 (2008).

[BERU 11] M. Beruete, M. Navarro-Cía, and M. Sorolla Ayza, "Understanding Anomalous Extraordinary Transmission From Equivalent Circuit and Grounded Slab Concepts," *Microw. Theory*, **59**, 2180 (2011).

[BERU 11b] M. Beruete, M. Navarro-Cía, S. A. Kuznetsov and M. Sorolla, "Circuit approach to the minimal configuration of terahertz anomalous extraordinary transmission," *Appl. Phys. Lett.* **98**, 014106 (2011).

[BERU 11c] M. Beruete, M. Navarro-Cía, V. Torres, and M. Sorolla, "Redshifting extraordinary transmission by simple inductance addition," *Phys. Rev. B* **84**, 1 (2011).

[BERU 13] M. Beruete, P. Rodríguez-Ulibarri, V. Pacheco-Peña, M. Navarro-Cía, and A. E. Serebryannikov, "Frozen mode from hybridized extraordinary transmission and Fabry-Perot resonances," *Phys. Rev. B* **87**, 205128 (2013).

[BETH 44] H. Bethe, "Theory of diffraction by small holes," *Phys. Rev.* **66**, 163 (1944).

[BETZ 86] E. Betzig, A. Lewis, A. Harootunian, M. Isaacson, and E. Kratschmer, "Near Field Scanning Optical Microscopy (NSOM)," *Biophys. J.* **49**, 269 (1986).

[BHAR 09] P. Bharadwaj, B. Deutsch, and L. Novotny, "Optical Antennas," *Adv. Opt. Photonics* **1**, 438 (2009).

[BIAG 12] P. Biagioni, J.-S. Huang, and B. Hecht, "Nanoantennas for visible and infrared radiation," *Rep. Prog. Phys.* **75**, 024402 (2012).

[BILO 10] F. Bilotti, S. Tricarico, and L. Vegni, "Plasmonic Metamaterial Cloaking at Optical Frequencies," *IEEE Trans. Nanotechnol.* **9**, 55 (2010).

[BOHR 98] C. F. Bohren and D. R. Huffman, *Absorption and Scattering of Light by Small Particles* (Wiley, 1998).

[BOSE 98] J. C. Bose, "On the rotation of plane of polarisation of electric waves by a twisted structure," *Proc. Roy. Soc*. **63**, 146 (1898).

[BOUH 03] A. Bouhelier, M. R. Beversluis, and L. Novotny, "Characterization of nanoplasmonic structures by locally excited photoluminescence," *Appl. Phys. Lett.* **83**, 5041 (2003).

[BOUW 54] C.J. Bouwkamp, "Diffraction theory," *Rep. Prog. Phys.* **17**, 35 (1954).

[BRAV 07] J. Bravo-Abad, A. Fernández-Domínguez, F. García-Vidal, and L. Martín-Moreno, "Theory of Extraordinary Transmission of Light through Quasiperiodic Arrays of Subwavelength Holes," *Phys. Rev. Lett.* **99**, 203905 (2007).

[BROL 04] A. G. Brolo, E. Arctander, R. Gordon, B. Leathem, and K. L. Kavanagh, "Nanohole-Enhanced Raman Scattering," *Nano Lett.* **4**, 2015 (2004).

[BROW 53] J. Brown, "Artificial dielectric having refractive indices less than unity," *Proceedings IEE* **100**, 51 (1953).

[BYKO 72] V. P. Bykov, "Spontaneous emission in a periodic structure," *Sov. Phys. JETP* **35**, 269 (1972).

C

[CAO 02] Q. Cao and P. Lalanne, "Negative Role of Surface Plasmons in the Transmission of Metallic Gratings with Very Narrow Slits," *Phys. Rev. Lett.* **88**, 057403, (2002).

[CARB 10] J. Carbonell, C. Croenne, F. Garet, E. Lheurette, J. L. Coutaz, and D. Lippens, "Lumped elements circuit of terahertz fishnet-like arrays with composite dispersion," *J. Appl. Phys.* **108**, 014907 (2010).

[CHAN 05] C.-W. Chang, A. K. Sarychev, and V. M. Shalaev, "Light diffraction by a subwavelength circular aperture," *Laser Phys. Lett.* **2**, 351 (2005).

[CHEN 71] C.-C. Chen, "Diffraction of Electromagnetic Waves by a Conducting Screen Perforated Periodically with Holes," *IEEE Trans. Microw. Theory Tech.* **19**, 475 (1971).

[CHEN 73] C.-C. Chen, "Transmission of Microwave Through Perforated Flat Plates of Finite Thickness," *IEEE Trans. Microw. Theory Tech.* **21**, 1 (1973).

[CHEN 05] X. Chen, B.-I. Wu, J. Kong, and T. Grzegorczyk, "Retrieval of the effective constitutive parameters of bianisotropic metamaterials," *Phys. Rev. E* **71**, 046610 (2005).

[CHET 07] U. K. Chettiar, A. V. Kildishev, H.-K. Yuan, W. Cai, S. Xiao, V. P. Drachev, and V. M. Shalaev, "Dual-band negative index metamaterial: double negative at 813 nm and single negative at 772 nm," *Opt. Lett.* **32**, 1671 (2007).

[COLL 61] R. E. Collin, W. H. Eggimann, "Dynamic interpretation of fields in two-dimensional lattice," *IRE T. Microw. Theory* **9**, 110 (1961).

[COLL 91] R.E. Collin, *Field Theory of Guided Waves* (Wiley, 1991).

[CRAV 66] G. Craven, "Waveguide bandpass filters using evanescent modes," *Electron. Lett.* **2**, 251 (1966).

[CURT 10] A. G. Curto, G. Volpe, T. H. Taminiau, M. P. Kreuzer, R. Quidant, and N. F. van Hulst, "Unidirectional emission of a quantum dot coupled to a nanoantenna," *Science* **329**, 930 (2010).

D

[DANC 07] M. Danckwerts and L. Novotny, “Optical Frequency Mixing at Coupled Gold Nanoparticles,” *Phys. Rev. Lett.* **98**, 026104 (2007).

[DEGI 02] A. Degiron, H. J. Lezec, W. L. Barnes, and T. W. Ebbesen, “Effects of hole depth on enhanced light transmission through subwavelength hole arrays,” *Appl. Phys. Lett.* **81**, 4327 (2002).

[DEME 08] A. Demetriadou, and J.B. Pendry, “Taming spatial dispersion in wire metamaterial,” *J. Phys-Condens. Matt.* **20**, 295222 (2008).

[DOLL 06] G. Dolling, C. Enkrich, M. Wegener, C. M. Soukoulis, and S. Linden, “Simultaneous negative phase and group velocity of light in a metamaterial,” *Science* **312**, 892 (2006).

[DRAG 04] D. Dragoman and M. Dragoman, “Terahertz fields and applications,” *Prog. Quantum Electron.* **28**, 1 (2004).

[DRUD 00] P. Drude, “Zur Elektronentheorie der Metalle,” *Ann. Phys.* **306**, 566 (1900).

E

[EBBE 98] T. W. Ebbesen, H. J. Lezec, H. F. Ghaemi, T. Thio, and P. A. Wolff, “Extraordinary optical transmission through sub-wavelength hole arrays,” *Nature* **391**, 667 (1998).

[EDWA 08] B. Edwards, A. Alù, M. Young, M. Silveirinha, and N. Engheta, “Experimental Verification of Epsilon-Near-Zero Metamaterial Coupling and Energy Squeezing Using a Microwave Waveguide,” *Phys. Rev. Lett.* **100**, 033903 (2008).

[EDWA 09] B. Edwards, A. Alù, M. Silveirinha, and N. Engheta, “Experimental Verification of Plasmonic Cloaking at Microwave Frequencies with Metamaterials,” *Phys. Rev. Lett.* **103**, 153901 (2009).

[ENGH 06] N. Engheta and R. W. Ziolkowski, *Metamaterilas. Physics and Engineering Explorations* (Wiley, 2006).

[ENGH 07] N. Engheta, “Circuits with light at nanoscales: optical nanocircuits inspired by metamaterials,” *Science* **317**, 1698 (2007).

[ENOC 08] S. Enoch, G. Tayeb, P. Sabouroux, N. Guérin, and P. Vincent, "A Metamaterial for Directive Emission," *Phys. Rev. Lett.* **89**, 213902 (2002).

[ESTE 10] R. Esteban, T. V. Teperik, and J. J. Greffet, "Optical Patch Antennas for Single Photon Emission Using Surface Plasmon Resonances," *Phys. Rev. Lett.* **104**, 026802 (2010).

F

[FALC 04] F. Falcone, T. Lopetegi, J.D. Baena, R. Marqués, F. Martín, and Mario Sorolla, "Effective negative-ε stopband microstrip lines based on complementary split ring resonators," *IEEE Microw. Wirel. Co.* **14**, 280 (2004).

[FALC 04b] F. Falcone, T. Lopetegi, M.A.G. Laso, J.D. Baena, J. Bonache, M. Beruete, R. Marqués, F. Martín, and M. Sorolla, "Babinet principle applied to metasurface and metamaterial design," *Phys. Rev. Lett.* **93**, 197401 (2004).

[FROM 04] D. P. Fromm, A. Sundaramurthy, P. J. Schuck, G. Kino, and W. E. Moerner, "Gap-Dependent Optical Coupling of Single 'Bowtie' Nanoantennas Resonant in the Visible," *Nano Lett.* **4**, 957 (2004).

G

[GARC 03] F. García-Vidal, H. Lezec, T. Ebbesen, and L. Martín-Moreno, "Multiple Paths to Enhance Optical Transmission through a Single Subwavelength Slit," *Phys. Rev. Lett.* **90**(21), 1 (2003).

[GARC 05] F. García de Abajo, R. Gómez-Medina, and J. Sáenz, "Full transmission through perfect-conductor subwavelength hole arrays," *Phys. Rev. E* **72**, 016608 (2005).

[GARC 05b] F. García-Vidal, E. Moreno, J. Porto, and L. Martín-Moreno, "Transmission of Light through a Single Rectangular Hole," *Phys. Rev. Lett.* **95**, 103901 (2005).

[GARC 07] F. J. García de Abajo, "Colloquium: Light scattering by particle and hole arrays," *Rev. Mod. Phys* **79**, 1267 (2007).

[GARC 09] C. García-Meca, R. Ortuño, F. J. Rodríguez-Fortuño, J. Martí, and A. Martínez, "Double-negative polarization-independent fishnet metamaterial in the visible spectrum," *Opt. Lett.* **34**, 1603 (2009).

[GARC 10] F. J. García-Vidal, T. W. Ebbesen, and L. Kuipers, "Light passing through subwavelength apertures," *Rev. Mod. Phys.* **82**, 729 (2010).

[GARC 11] C. García-Meca, J. Hurtado, J. Martí, A. Martínez, W. Dickson, and A. V. Zayats, "Low-Loss Multilayered Metamaterial Exhibiting a Negative Index of Refraction at Visible Wavelengths," *Phys. Rev. Lett.* **106**, 067402 (2011).

[GHAE 98] H. Ghaemi, T. Thio, D. Grupp, T. Ebbesen, and H. Lezec, "Surface plasmons enhance optical transmission through subwavelength holes," *Phys. Rev. B* **58**, 6779 (1998).

[GOLD 98] P.F. Goldsmith, *Quasioptical Systems: Gaussian Beam, Quasioptical Propagation, and Applications* (IEEE Press, 1998).

[GOME 05] J. Gómez Rivas, C. Janke, P. H. Bolivar, and H. Kurz, "Transmission of THz radiation through InSb gratings of subwavelength apertures," *Opt. Express* **13**, 847 (2005).

[GONZ 05] F. J. González and G. D. Boreman, "Comparison of dipole, bowtie, spiral and log-periodic IR antennas," *Infrared Phys. Technol.* **46**, 418 (2005).

[GRUP 99] D. E. Grupp, H. J. Lezec, T. Thio, and T. W. Ebbesen, "Beyond the Bethe Limit: Tunable Enhanced Light Transmission Through a Single Sub-Wavelength Aperture," *Adv. Mater.* **11**, 860 (1999).

[GRUP 00] D. E. Grupp, H. J. Lezec, T. W. Ebbesen, K. M. Pellerin, and T. Thio, "Crucial role of metal surface in enhanced transmission through subwavelength apertures," *Appl. Phys. Lett.* **77**, 1569 (2000).

H

[HARU 12] H. Harutyunyan, G. Volpe, R. Quidant, and L. Novotny, "Enhancing the Nonlinear Optical Response Using Multifrequency Gold-Nanowire Antennas," *Phys. Rev. Lett.* **108**, 217403 (2012).

[HESS 65] A. Hessel and A. A. Oliner, "A New Theory of Wood's Anomalies on Optical Gratings," *Appl. Opt.* **4**, 1275 (1965).

[HUPE 68] J. Hupert, “Evanescent Mode Guide Filter and Tunnel-Effect Analogy,” *IEEE Trans. Circuit Theory* **15**, 279 (1968).

I

[ISHI 90] A. Ishimaru, *Electromagnetic Wave Propagation, Radiation, and Scattering* (Prentice Hall, 1990).

J

[JACK 98] J. D. Jackson, *Classical Electrodynamics* (Wiley, 1998).

[JOAN 95] J. D. Joannopoulos, R. D. Meade, and J. N. Winn, *Photonic Crystals* (Princeton University Press, 1995).

[JOHN 72] P. B. Johnson and R. Christy, “Optical constants of the noble metals,” *Phys. Rev. B* **6**, 4370 (1972).

[JOHN 87] S. John, “Strong localization of photons in certain disordered dielectric superlattices,” *Phys. Rev. Lett.* **58**, 2486 (1987).

[JOHN 97] S. John, “Frozen light,” *Nature* **390**, 661 (1997).

K

[KAFE 07] M. Kafesaki, I. Tsiapa, N. Katsarakis, T. Koschny, C. M. Soukoulis, and E. N. Economou, “Left-handed metamaterials: The fishnet structure and its variations,” *Phys. Rev. B* **75**, 1 (2007).

[KAIP 10] C. S. R. Kaipa, A. B. Yakovlev, F. Medina, F. Mesa, C. A. M. Butler, and A. P. Hibbins, “Circuit modeling of the transmissivity of stacked two-dimensional metallic meshes,” *Opt. Express* **18**, 13309 (2010).

[KIM 99] T. J. Kim, T. Thio, T. W. Ebbesen, D. E. Grupp, and H. J. Lezec, “Control of optical transmission through metals perforated with subwavelength hole arrays,” *Opt. Lett.* **24**, 256 (1999).

[KIM 08] S. Kim, J. Jin, Y.-J. Kim, I.-Y. Park, Y. Kim, and S.-W. Kim, “High-harmonic generation by resonant plasmon field enhancement,” *Nature* **453**, 757 (2008).

[KINK 09] A. Kinkhabwala, Z. Yu, S. Fan, Y. Avlasevich, K. Müllen, and W. E. Moerner, "Large single-molecule fluorescence enhancements produced by a bowtie nanoantenna," *Nat. Photonics* **3**, 654 (2009).

[KOCK 48] W. E. Kock, "Metallic delay lenses," *Bell Sys. Tech. J.* **27**, 58 (1948).

[KRIS 01] A. Krishnan, T. Thio, T. Kim, H. Lezec, T. Ebbesen, P. Wolff, J. Pendry, L. Martín-Moreno, and F. García-Vidal, "Evanescently coupled resonance in surface plasmon enhanced transmission," *Optics Communications* **200**, 1 (2001).

L

[LEE 09] Y.-S. Lee, *Principle of Terahertz Science and Technology* (Springer, 2009).

[LEON 07] U. Leonhardt and T. G. Philbin, "Quantum levitation by left-handed metamaterials," *New J. Phys.* **9**, 254 (2007).

[LEZE 02] H. J. Lezec, A. Degiron, E. Devaux, R. a Linke, L. Martín-Moreno, F. J. García-Vidal, and T. W. Ebbesen, "Beaming light from a subwavelength aperture," *Science* **297**, 820 (2002).

[LI 08] Z. Li, H. Caglayan, E. Colak, and E. Ozbay, "Enhanced transmission and directivity from metallic subwavelength apertures with nonuniform and nonperiodic grooves," *Appl. Phys. Lett.* **92**, 011128 (2008).

[LIND 92] I. V. Lindell, A. H. Sihvola, and J. Kurkijarvi, "Karl F. Lindman: The last Hertzian, and a Harbinger of electromagnetic chirality," *IEEE Antennas Propag. Mag.* **34**, 24 (1992).

[LIU 05] C. Liu, V. Kamaev, and Z. V. Vardeny, "Efficiency enhancement of an organic light-emitting diode with a cathode forming two-dimensional periodic hole array," *Appl. Phys. Lett.* **86**, 143501 (2005).

[LIU 08] N. Liu, L. Fu, S. Kaiser, H. Schweizer, and H. Giessen, "Plasmonic Building Blocks for Magnetic Molecules in Three-Dimensional Optical Metamaterials," *Adv. Mater.* **20**, 3859 (2008).

[LIU 08b] H. Liu and P. Lalanne, "Microscopic theory of the extraordinary optical transmission," *Nature*, vol. 452, no. 7188, pp. 728–31, Apr. 2008.

[LIU 08c] R. Liu, Q. Cheng, T. Hand, J. Mock, T. Cui, S. Cummer, and D. Smith, "Experimental Demonstration of Electromagnetic Tunneling Through an Epsilon-Near-Zero Metamaterial at Microwave Frequencies," *Phys. Rev. Lett.* **100**, 023903 (2008).

[LOMA 04] V. Lomakin and E. Michielssen, "Enhanced transmission through two-period arrays of subwavelength holes," *IEEE Microw. Wirel. Components Lett.* **14**, 355 (2004).

[LOMA 05] V. Lomakin and E. Michielssen, "Enhanced transmission through metallic plates perforated by arrays of subwavelength holes and sandwiched between dielectric slabs," *Phys. Rev. B* **71**, 235117 (2005).

[LOVA 06] G. Lovat, P. Burghignoli, F. Capolino, D. R. Jackson, and D. R. Wilton, "Analysis of Directive Radiation From a Line Source in a Metamaterial Slab With Low Permittivity," *IEEE Trans. Antennas Propag.* **54**, 1017 (2006).

[LUM 14] https://www.lumerical.com.

[LUNE 66] R. K. Luneburg, *Mathematical Theory of Optics* (Cambridge University Press, 1966).

M

[MAIE 04] S. A. Maier, *Plasmonics, Fundamentals and Applications* (Springer, 2004).

[MARC 51] N. Marckuvitz, *Waveguide Handbook* (McGraw-Hill, 1951).

[MARQ 02] R. Marqués, J. Martel, F. Mesa, and F. Medina, "Left-Handed-Media Simulation and Transmission of EM Waves in Subwavelength Split-Ring-Resonator-Loaded Metallic Waveguides," *Phys. Rev. Lett.* **89**, 183901 (2002).

[MARQ 08] R. Marqués, F. Martín, and M. Sorolla, *Metamaterials with Negative Parameters: Theory, Design, and Microwave Applications* (Wiley, 2008).

[MARQ 09] R. Marqués, F. Mesa, L. Jelinek, and F. Medina, "Analytical theory of extraordinary transmission through metallic diffraction screens perforated by small holes," *Opt. Express*, **17**, 5571 (2009).

[MARQ 09b] R. Marqués, L. Jelinek, F. Mesa, and F. Medina, "Analytical theory of wave propagation through stacked fishnet metamaterials," *Opt. Express* **17**, 11582 (2009).

[MART 01] L. Martín-Moreno, F. García-Vidal, H. Lezec, K. Pellerin, T. Thio, J. Pendry, and T. Ebbesen, "Theory of Extraordinary Optical Transmission through Subwavelength Hole Arrays," *Phys. Rev. Lett.* 86, 1114 (2001).

[MART 03] L. Martín-Moreno, F. García-Vidal, H. Lezec, A. Degiron, and T. Ebbesen, "Theory of Highly Directional Emission from a Single Subwavelength Aperture Surrounded by Surface Corrugations," *Phys. Rev. Lett.* **90**(16), 1 (2003).

[MATS 07] T. Matsui, A. Agrawal, A. Nahata, and Z. V. Vardeny, "Transmission resonances through aperiodic arrays of subwavelength apertures," *Nature* **446**, 517 (2007).

[MEDI 08] F. Medina, F. Mesa, and R. Marqués, "Extraordinary Transmission Through Arrays of Electrically Small Holes From a Circuit Theory Perspective," *IEEE Trans. Microw. Theory Tech.* **56**, 3108 (2008).

[MEDI 10] F. Medina, F. Mesa, and D. C. Skigin, "Extraordinary Transmission Through Arrays of Slits: A Circuit Theory Model," *IEEE Trans. Microw. Theory Tech.* **58**, 105 (2010).

[MIE 08] G. Mie, "Beiträge zur Optik trüber Medien, speziell kolloidaler Metallösungen," *Ann. Phys.* **330** 377 (1908).

[MINI 08] I. V. Minin and O. V. Minin, *Basic Principles of Fresnel Antenna Arrays* (Springer, 2008)

[MONT 12] A. Monti, F. Bilotti, A. Toscano, and L. Vegni, "Possible implementation of epsilon-near-zero metamaterials working at optical frequencies," *Opt. Commun.* **285**, 3412 (2012).

[MONT 13] F. Monticone, N. M. Estakhri, and A. Alù, "Full Control of Nanoscale Optical Transmission with a Composite Metascreen," *Phys. Rev. Lett.* **110**, 203903 (2013).

[MUNK 00] B. A. Munk, Frequency Selective Surfaces: Theory and Design (Wiley, 2000)

N

[NAVA 08] M. Navarro-Cía, M. Beruete, M. Sorolla, and I. Campillo, "Negative refraction in a prism made of stacked subwavelength hole arrays," *Opt. Express* **16**, 560 (2008).

[NAVA 09] M. Navarro-Cía, M. Beruete, I. Campillo, and M. Sorolla, "Millimeter-Wave Left-Handed Extraordinary Transmission Metamaterial Demultiplexer," *IEEE Antennas Wirel. Propag. Lett.* **8**, 212 (2009).

[NAVA 11] M. Navarro-Cía, V. Torres Landivar, M. Beruete, and M. Sorolla Ayza, "A slow light fishnet-like absorber in the millimeter-wave," *Prog. Electromagn. Res.* **118**, 287 (2011).

[NAVA 11b] M. Navarro-Cía, M. Beruete, I. Campillo, and M. Sorolla, "Enhanced lens by ε and μ near-zero metamaterial boosted by extraordinary optical transmission," *Phys. Rev. B* **83**, 115112 (2011).

[NAVA 12] M. Navarro-Cía, M. Beruete, M. Sorolla, and N. Engheta, "Lensing system and Fourier transformation using epsilon-near-zero metamaterials," *Phys. Rev. B* **86**, 165130 (2012).

[NAVA 12b] M. Navarro-Cía and S. A. Maier, "Broad-band near-infrared plasmonic nanoantennas for higher harmonic generation," *ACS Nano* **6**, 3537 (2012).

[NEUB 08] F. Neubrech, A. Pucci, T. Cornelius, S. Karim, A. García-Etxarri, and J. Aizpurua, "Resonant Plasmonic and Vibrational Coupling in a Tailored Nanoantenna for Infrared Detection," *Phys. Rev. Lett.* **101**, 157403 (2008).

[NOVO 06] L. Novotny and S. J. Stranick, "Near-field optical microscopy and spectroscopy with pointed probes," *Annu. Rev. Phys. Chem.* **57**, 303 (2006).

[NOVO 07] L. Novotny, "Chapter 5 The history of near-field optics," *Progress in Optics* **50**, 137 (2007).

[NOVO 07b] L. Novotny, "Effective Wavelength Scaling for Optical Antennas," *Phys. Rev. Lett.* **98**, 266802 (2007).

[NOVO 11] L. Novotny and N. van Hulst, “Antennas for light,” *Nat. Photonics* **5**, 83 (2011).

O

[ORDA 85] M. A. Ordal, R. J. Bell, R. W. Alexander, Jr, L. L. Long, and M. R. Querry, “Optical properties of fourteen metals in the infrared and far infrared: Al, Co, Cu, Au, Fe, Pb, Mo, Ni, Pd, Pt, Ag, Ti, V, and W,” *Appl. Opt.* 24, 4493 (1985).

[ORTU 09] R. Ortuño, C. García-Meca, F. Rodríguez-Fortuño, J. Martí, and A. Martínez, “Role of surface plasmon polaritons on optical transmission through double layer metallic hole arrays,” *Phys. Rev. B* **79**, 1 (2009).

P

[PACH 13] V. Pacheco-Peña, B. Orazbayev, V. Torres, M. Beruete, and M. Navarro-Cía, “Ultra-compact planoconcave zoned metallic lens based on the fishnet metamaterial,” *Appl. Phys. Lett.* **103**, 183507 (2013).

[PACK 84] K. S. Packard, “The Origin of Waveguides: A Case of Multiple Rediscovery,” *IEEE Trans. Microw. Theory Tech.* **32**, 961 (1984).

[PALI 85] E. D. Palik, *Handbook of Optical Constants of Solids* (Academic Press, 1985).

[PEND 98] J.B. Pendry, A.J. Holden, D.J. Robbins and W.J. Stewart, “Low frequency plasmons in thin-wire structures,” *J. Phys-Condens. Mat.* **10**, 4785 (1998).

[PEND 99] J. B. Pendry, A.J. Holden, D.J. Robbins, and W.J. Stewart, “Magnetism from conductors and enhanced nonlinear phenomena,” *IEEE T. Microw. Theory* **47**, 2075 (1999).

[PEND 00] J. B. Pendry, “Negative refraction makes a perfect lens,” *Phys. Rev. Lett.* **85**, 3966 (2000).

[PEND 03] J. B. Pendry, “Positively negative,” *Nature* **423**, 22 (2003).

[PEND 04] J.B. Pendry, L. Martín-Moreno, and F.J. García-Vidal, “Mimicking surface plasmons with structured surfaces,” *Science* **305**, 847 (2004).

[PEND 06] J. B. Pendry and D. R. Smith, “The quest for the superlens,” *Sci. Am.* **295**, 60 (2006).

[POPO 00] E. Popov, M. Nevière, S. Enoch, and R. Reinisch, "Theory of light transmission through subwavelength periodic hole arrays," *Phys. Rev. B* **62**, 16100 (2000).

[PORT 99] J. Porto, F. García-Vidal, and J. Pendry, "Transmission Resonances on Metallic Gratings with Very Narrow Slits," *Phys. Rev. Lett.* **83**, 2845 (1999).

[POZA 05] D. M. Pozar, *Microwave Engineering* (Wiley, 2005).

[PRZY 06] F. Przybilla, C. Genet, and T. W. Ebbesen, "Enhanced transmission through Penrose subwavelength hole arrays," *Appl. Phys. Lett.* **89**, 121115 (2006).

[PRZY 08] F. Przybilla, A. Degiron, C. Genet, T. Ebbesen, F. de Léon-Pérez, J. Bravo-Abad, F. J. García-Vidal, and L. Martín-Moreno, "Efficiency and finite size effects in enhanced transmission through subwavelength apertures," *Opt. Express* **16**, 9571 (2008).

Q

R

[RAMO 94] S. Ramo, J. R. Whinnery, and T. V. Duzer, *Fields and Waves in Communication Electronics* (Wiley, 1994).

[RAYL 07] Lord Rayleigh, "On the dynamical theory of gratings," *Proceedings of the Royal Society of London A* **79**, 399 (1907).

[REDO 13] A. Redo-Sanchez, N. Laman, B. Schulkin, and T. Tongue, "Review of Terahertz Technology Readiness Assessment and Applications," *J. Infrared, Millimeter, Terahertz Waves* **34**, 500 (2013).

[ROBI 60] L.A. Robinson, "Electrical properties of metal loaded radomes," Wright air Develop. Div. Rep. WADD-TR-**60-84** (1960).

[RODR 10] R. Rodríguez-Berral, F. Mesa, and F. Medina, "Circuit model for a periodic array of slits sandwiched between two dielectric slabs," *Appl. Phys. Lett.*, **96**, 161104 (2010).

[RODR 14] F. J. Rodríguez-Fortuño, A. Vakil, and N. Engheta, "Electric Levitation Using ϵ-Near-Zero Metamaterials," *Phys. Rev. Lett.* **112**, 033902 (2014).

[ROTM 62] W. Rotman, “Plasma simulation by artificial dielectrics and parallel-plate media,” *IRE T. Antenn. Propag.* **10**, 82 (1962).

S

[SARR 03] M. Sarrazin, J.-P. Vigneron, and J.-M. Vigoureux, “Role of Wood anomalies in optical properties of thin metallic films with a bidimensional array of subwavelength holes,” *Phys. Rev. B* **67**, 085415 (2003).

[SARR 05] M. Sarrazin and J.-P. Vigneron, “Light transmission assisted by Brewster-Zennek modes in chromium films carrying a subwavelength hole array,” *Phys. Rev. B* **71**, 075404 (2005).

[SCHE 38] S. A. Schelkunoff, “The Impedance Concept and Its Application to Problems of Reflection, Refraction, Shielding and Power Absorption,” *Bell Syst. Tech. J.* **17**, 17 (1938).

[SCHW 08] L. Fu, H. Schweizer, H. Guo, N. Liu, and H. Giessen, “Synthesis of transmission line models for metamaterial slabs at optical frequencies,” *Phys. Rev. B* **78**, 11 (2008).

[SIHV 07] A. Sihvola, “Metamaterials in electromagnetics,” *Metamaterials* **1**, 2 (2007).

[SILV 05] M. G. Silveirinha and C. A. Fernandes, “Homogenization of metamaterial surfaces and slabs: the crossed wire mesh canonical problem,” *IEEE Trans. Antennas Propag.* 53, 59 (2005).

[SILV 06] M. Silveirinha and N. Engheta, “Tunneling of Electromagnetic Energy through Subwavelength Channels and Bends using ε-Near-Zero Materials,” *Phys. Rev. Lett.* **97**, 157403 (2006).

[SILV 07] M. Silveirinha and N. Engheta, “Theory of supercoupling, squeezing wave energy, and field confinement in narrow channels and tight bends using ε near-zero metamaterials,” *Phys. Rev. B* **76**, 245109 (2007).

[SILV 07b] M. Silveirinha, A. Alù, and N. Engheta, “Parallel-plate metamaterials for cloaking structures,” *Phys. Rev. E* **75**, 036603 (2007).

[SILV 07c] M. Silveirinha and N. Engheta, “Design of matched zero-index metamaterials using nonmagnetic inclusions in epsilon-near-zero media,” *Phys. Rev. B* **75**, 075119 (2007).

[SMIT 00] D. R. Smith, W. J. Padilla, D. C. Vier, S. C. Nemat-Nasser, and S. Schultz, "Composite medium with simultaneously negative permeability and permittivity," *Phys. Rev. Lett.* **84**, 4184 (2000).

[SMIT 05] D. R. Smith, D. C. Vier, T. Koschny, and C. M. Soukoulis, "Electromagnetic parameter retrieval from inhomogeneous metamaterials," *Phys. Rev. E* **71**, 036617 (2005).

[SOLY 09] L. Solymar and E. Shamonina, *Waves in Metamaterials* (Oxford University Press, 2009).

[SOMM 99] A. Sommerfeld, "Ueber die Fortpflanzung elektrodynamischer Wellen längs eines Drahtes," *Annalen der Physik und Chemie* **303**, 233 (1899).

[STAF 12] M. Staffaroni, J. Conway, S. Vedantam, J. Tang, and E. Yablonovitch, "Circuit analysis in metal-optics," *Photonics Nanostructures - Fundam. Appl.* **10**, 166 (2012).

[STUR 94] P. A. Sturrock, *Plasma Physics: An Introduction to the Theory of Astrophysical, Geophysical and Laboratory Plasmas* (Cambridge University Press, 1994).

[SUN 12] Y. Sun, B. Edwards, A. Alù, and N. Engheta, "Experimental realization of optical lumped nanocircuits at infrared wavelengths," *Nat. Mater.* **11**, 208 (2012).

[SYNG 28] E. H. Synge, "A suggested method for extending microscopic resolution into the ultra-microscopic region," *Philos. Mag. Ser. 7* **6**, 356 (1928).

T

[TAMI 07] T. H. Taminiau, R. J. Moerland, F. B. Segerink, L. Kuipers, and N. F. van Hulst, "l /4 resonance of an optical monopole antenna probed by single molecule fluorescence," *Nano Lett.* **7**, 28 (2007).

[THIO 01] T. Thio, K. M. Pellerin, R. A. Linke, H. J. Lezec, and T. W. Ebbesen, "Enhanced light transmission through a single subwavelength aperture," *Opt. Lett.* **26**, 1972, (2001).

[THYA 12] K. Thyagarajan, S. Rivier, A. Lovera, and O. J. F. Martín, "Enhanced second-harmonic generation from double resonant plasmonic antennae," *Opt. Express* **20**, 12860 (2012).

[TREA 99] M. M. J. Treacy, "Dynamical diffraction in metallic optical gratings," *Appl. Phys. Lett.* **75**, 606 (1999).

[TREA 02] M. Treacy, "Dynamical diffraction explanation of the anomalous transmission of light through metallic gratings," *Phys. Rev. B* **66**, 195105 (2002).

[TSAK 07] K. L. Tsakmakidis, A. D. Boardman, and O. Hess, "'Trapped rainbow' storage of light in metamaterials," *Nature* **450**, 397 (2007).

U

[ULRI 67] R. Ulrich, "Far-infrared properties of metallic mesh and its complementary structure," *Infrared Phys.* **7**, 37 (1967).

V

[VALE 08] J. Valentine, S. Zhang, T. Zentgraf, E. Ulin-Avila, D. A. Genov, G. Bartal, and X. Zhang, "Three-dimensional optical metamaterial with a negative refractive index," *Nature* **455**, 376 (2008).

[VESE 68] V.G. Veselago, "The electrodynamics of substances with simultaneously negative values of ε and μ," *Soviet Physics Uspekhi* **10**, 509 (1968).

W

[WALT 65] C. H. Walter, *Traveling wave antennas* (McGraw-Hill, 1965).

[WEBB 06] K. Webb and J. Li, "Analysis of transmission through small apertures in conducting films," *Phys. Rev. B* **73**, 033401 (2006).

[WEDG 04] S. Wedge, J. A. E. Wasey, W. L. Barnes, and I. Sage, "Coupled surface plasmon-polariton mediated photoluminescence from a top-emitting organic light-emitting structure," *Appl. Phys. Lett.* **85**, 182 (2004).

[WESS 85] J. Wessel, "Surface-enhanced optical microscopy," *J. Opt. Soc. Am. B* **2**, 1538 (1985).

[WEST 10] P. R. West, S. Ishii, G. V. Naik, N. K. Emani, V. M. Shalaev, and A. Boltasseva, “Searching for better plasmonic materials,” *Laser Photon. Rev.* **4**, 795 (2010).

[WILL 08] C. R. Williams, S. R. Andrews, S. A. Maier, A. I. Fernández-Domínguez, L. Martín-Moreno, and F. J. García-Vidal, “Highly confined guiding of terahertz surface plasmon polaritons on structured metal surfaces,” *Nat. Photonics* **2**, 175 (2008).

[WOOD 02] R. W. Wood, “On a Remarkable Case of Uneven Distribution of Light in a Diffraction Grating Spectrum,” *Proc. Phys. Soc. London* **18**, 269 (1902).

X

Y

[YABL 87] E. Yablonovitch, “Inhibited spontaneous emission in solid-state physics and electronics,” *Phys. Rev. Lett.* **58**, 2059 (1987).

[YABL 91] E. Yablonovitch, T. J. Gmitter, R. D. Meade, A. M. Rappe, K. D. Brommer, and J. D. Joannopoulos, “Donor and acceptor modes in photonic band-structure,” *Phys. Rev. Lett.* **67**, 3380 (1991).

[YANG 11] R. Yang, R. Rodríguez-Berral, F. Medina, and Y. Hao, “Analytical model for the transmission of electromagnetic waves through arrays of slits in perfect conductors and lossy metal screens,” *J. Appl. Phys.* **109**, 103107 (2011).

[YANG 13] X. Yang, C. Hu, H. Deng, D. Rosenmann, D. A. Czaplewski, and J. Gao, “Experimental demonstration of near-infrared epsilon-near-zero multilayer metamaterial slabs,” *Opt. Express* **21**, 23631 (2013).

Z

[ZHAN 05] S. Zhang, W. Fan, N. Panoiu, K. Malloy, R. Osgood, and S. Brueck, “Experimental Demonstration of Near-Infrared Negative-Index Metamaterials,” *Phys. Rev. Lett.* **95**, 1 (2005).

[ZIOL 04] R. W. Ziolkowski, “Propagation in and scattering from a matched metamaterial having a zero index of refraction,” *Phys. Rev. E* **70**, 046608 (2004).

Author's merits

Journal Papers

[PAPER A] V. Torres, R. Ortuño, P. Rodríguez-Ulibarri, A. Griol, A. Martínez, M. Navarro-Cía, M. Beruete, and M. Sorolla, "Mid-infrared plasmonic inductors: Enhancing inductance with meandering lines," *Sci. Rep.* **4**, 3592 (2014).

[PAPER B] V. Torres, P. Rodríguez-Ulibarri, M. Navarro-Cía, and M. Beruete, "Fishnet metamaterial from an equivalent circuit perspective," *Appl. Phys. Lett.* **101**, 244101 (2012).

[PAPER C] V. Torres, N. Sánchez, D. Etayo, R. Ortuño, M. Navarro-Cía, A. Martínez, and M. Beruete, "Compact dual-band terahertz quarter-wave plate metasurface," (under review).

[PAPER D] V. Torres, B. Orazbayev, V. Pacheco-Peña, M. Beruete, M. Navarro-Cía, and N. Engheta, "Experimental demonstration of a millimeter-wave metallic ENZ lens based on the energy squeezing principle," (under review).

[PAPER E] V. Torres, V. Pacheco-Peña, P. Rodríguez-Ulibarri, M. Navarro-Cía, M. Beruete, M. Sorolla, and N. Engheta, "Terahertz epsilon-near-zero graded-index lens," *Opt. Express* **21**, 9156 (2013).

[PAPER F] H. Aouani, M. Rahmani, H. Šípová, V. Torres, K. Hegnerová, M. Beruete, J. Homola, M. Hong, M. Navarro-Cía, and S. A. Maier, "Plasmonic Nanoantennas for Multispectral Surface-Enhanced Spectroscopies," *J. Phys. Chem. C* **117**, 18620 (2013).

[Paper 7] M. Navarro-Cía, V. Torres Landivar, M. Beruete, and M. Sorolla Ayza, "A slow light fishnet-like absorber in the millimeter-wave range," *Prog. Electromagn. Res.* **118**, 287 (2011).

[Paper 8] M. Beruete, M. Navarro-Cía, V. Torres, and M. Sorolla, "Redshifting extraordinary transmission by simple inductance addition," *Phys. Rev. B* **84**, 1 (2011).

[Paper 9] M. Beruete, A. E. Serebryannikov, V. Torres, M. Navarro-Cía, and M. Sorolla, "Toward compact millimeter-wave diode in thin stacked-hole array assisted by a dielectric grating," *Appl. Phys. Lett.* **99**, 154101 (2011).

[Paper 10] M. Navarro-Cía, P. Rodríguez-Ulibarri, V. Torres, and M. Beruete, "Quarter-Wave Plate Based on Dielectric-Enabled Extraordinary Resonant Transmission," *IEEE Photonics Technol. Lett.* **24**, 945 (2012).

[Paper 11] V. Pacheco-Peña, B. Orazbayev, V. Torres, M. Beruete, and N, Navarro-Cía, "Ultra-compact planoconcave zoned metallic lens based on the fishnet metamaterial," *Appl. Phys. Lett.* **103**, 183507 (2013).

Conferences

[Conf 1] M. Navarro-Cía, V. Torres, F. Falcone, M. Beruete, and M. Sorolla, "Extraordinary transmission lenses: different paths towards focusing enhancement," in *IEEE AP-S International Symposium on Antennas and Propagation 2011 and USNC/URSI National Radio Science Meeting 2011*, (Spokane), 2011.

[Conf 2] M. Navarro-Cía, M. Beruete, V. Torres, F. Falcone, M. Sorolla, and N. Engheta, "Epsilon-near-zero metamaterials for millimetre-wave lenses," in *33rd ESA Antenna Workshop on Challenges for Space Antenna Systems*, (Noordwijk), 2011.

[Conf 3] M. Navarro-Cía, M. Beruete, V. Torres, F. Falcone, and M. Sorolla, "Revival of metallic lenses by extraordinary transmission metamaterials," in *33rd ESA Antenna Workshop on Challenges for Space Antenna Systems*, (Noordwijk), 2011.

[Conf 4] V. Torres, M. Beruete, M. Navarro-Cía, F. Falcone, and M. Sorolla, "Extraordinary transmission frequency tuning based on meander hole arrays," in *Metamaterials'2011*, (Barcelona), 2011.

[Conf 5] V. Torres, M. Beruete, M. Navarro-Cía, F. Falcone, and M. Sorolla, "Control del fenómeno de transmisión extraordinaria mediante líneas

de meandros", in *XXVI Simposium Nacional de la Unión Científica Internacional de Radio URSI 2011*, (Leganes), 2011.

[Conf 6] M. Beruete, M. Navarro-Cía, V. Torres, F. Falcone, M. Sorolla, "Análisis circuital de la resonancia de transmisión extraordinaria anómala", in *XXVI Simposium Nacional de la Unión Científica Internacional de Radio URSI 2011*, (Leganes), 2011.

[Conf 7] V. Torres, P. Rodríguez-Ulibarri, M. Beruete, F. Falcone, M. Sorolla, and M. Navarro-Cía, "Downshifting extraordinary transmission by meander-lines in hole arrays", in *6th European Conference on Antennas and Propagation EuCAP 2012*, (Prague), 2012.

[Conf 8] M. Sorolla, M. Beruete, F. Falcone, V. Torres, and M. Navarro-Cía, "Should classical electrodynamics be leaved?," in *Advanced Electromagnetics Symposium AES 2012*, (Paris), 2012.

[Conf 9] M. Beruete, A.E. Serebryannikov, V. Torres, M. Navarro-Cía, and M. Sorolla, "Unidirectional extraordinary transmission metamaterial," in *3rd International Conference on Metamaterials, Photonic Crystals and Plasmonics META'12*, (Paris), 2012.

[Conf 10] M. Navarro-Cía, V. Torres, M. Beruete, F. Falcone, M. Sorolla, and N. Engheta, "Pencil-like radiation and spatial processing by extreme low effective electromagnetic parameters," in *3rd International Conference on Metamaterials, Photonic Crystals and Plasmonics META'12*, (Paris), 2012.

[Conf 11] V. Torres, P. Rodríguez-Ulibarri, M. Beruete, F. Falcone, M. Sorolla, and M. Navarro-Cía, "Tuning extraordinary transmission by meander-lines in hole arrays," in *4th International Conference Smart Materials, Structures, and Systems CIMTEC 2012*, (Montecatini-Terme), 2012.

[Conf 12] P. Rodríguez-Ulibarri, V. Torres, M. Beruete, and M. Navarro-Cía, "Dielectric-backed subwavelength hole arrays for terahertz polarization conversion," in *2012 IEEE International Symposium on Antennas and Propagation and USNC-URSI National Radio Science Meeting*, (Chicago), 2012.

[Conf 13] M. Beruete, A. E. Serebryannikov, V. Torres, M. Navarro-Cía, and M. Sorolla, "Diffraction inspired, polarization dependent, unidirectional transmission in thin fishnets," in *2012 IEEE International Symposium on Antennas and Propagation and USNC-URSI National Radio Science Meeting*, (Chicago), 2012.

[Conf 14] V. Torres, M. Navarro-Cía, M. Beruete, M. Sorolla, and N. Engheta, "Epsilon-near-zero waveguides for graded index lenses at terahertz frequencies," in *2012 IEEE International Symposium on Antennas and Propagation and USNC-URSI National Radio Science Meeting*, (Chicago), 2012.

[Conf 15] V. Pacheco-Peña, V. Torres, M. Navarro-Cía, M. Beruete, and N. Engheta, "Plane-plane lenses using ε near-zero stacked waveguides at millimetre waves," *Metamaterials'2012*, (St. Petersburg), 2012.

[Conf 16] M. Navarro-Cía, M. Beruete, V. Torres, F. Falcone, and M. Sorolla, "Mejora de la directividad mediante lentes metálicas con índice de refracción efectivo próximo a cero en la banda sin licencia de 60 GHz," in *XXVII Simposium Nacional de la Unión Científica Internacional de Radio URSI 2012*, (Elche), 2012.

[Conf 17] V. Pacheco-Peña, V. Torres, M. Navarro-Cía, M. Beruete, and M. Sorolla, "Lentes ENZ de perfil plano basadas en guías de onda apiladas," in *XXVII Simposium Nacional de la Unión Científica Internacional de Radio URSI 2012*, (Elche), 2012.

[Conf 18] P. Rodríguez-Ulibarri, V. Torres, M. Beruete, and M. Navarro-Cía, "Retardador de cuarto de onda basado en agrupamiento de agujeros sublambda operando en Terahercio," in *XXVII Simposium Nacional de la Unión Científica Internacional de Radio URSI 2012*, (Elche), 2012.

[Conf 19] M. Navarro-Cía, P. Rodríguez-Ulibarri, V. Torres, and M. Beruete, "Terahertz quarter-wave plate based on subwavelength hole arrays," in *7th European Conference on Antennas and Propagation EuCAP 2013*, (Gothenburg), 2013.

[Conf 20] V. Pacheco-Peña, V. Torres, M. Navarro-Cía, M. Beruete, M. Sorolla, and N. Engheta, "ε-near-zero graded index structure as a bi-concave metallic lens using stacked rectangular near cut-off waveguides," in *7th European Conference on Antennas and Propagation EuCAP 2013*, (Gothenburg), 2013.

[Conf 21] V. Torres, P. Rodríguez-Ulibarri, F. Falcone, and M. Beruete, "Equivalent circuit of the double-fishnet metamaterial," in *2013 IEEE International Symposium on Antennas and Propagation and USNC-URSI National Radio Science Meeting*, (Orlando), 2013.

[Conf 22] V. Torres, P. Rodríguez-Ulibarri, R. Ortuño, M. Navarro-Cía, and M. Beruete, "Tailoring extraordinary transmission by inductance addition

with meander–lines," in *38th International Conference on Infrared, Millimeter and Terahertz Waves IRMMW-THz 2013*, (Mainz), 2013.

[Conf 23] P. Rodríguez-Ulibarri, B. Orazbayev, V. Torres, M. Beruete, and M. Navarro-Cía, "Controlling extraordinary transmission by means of hedgehog subwavelength hole arrays," *Metamaterials'2013*, (Bordeaux), 2013.

[Conf 24] V. Torres, P. Rodríguez-Ulibarri, M. Navarro-Cía, and M. Beruete, "Equivalent circuit extraction of the double-fishnet metamaterial based on its electrodynamics," in *Metamaterials'2013*, (Bordeaux), 2013.

[Conf 25] V. Torres, B. Orazbayev, P. Rodríguez-Ulibarri, M. Beruete, and M. Navarro-Cía, "Control de la transmisión extraordinaria mediante pines metálicos ortogonales al plano de los agujeros sublambda," in *XXVIII Simposium Nacional de la Unión Científica Internacional de Radio URSI 2013*, (Santiago de Compostela), 2013.

[Conf 26] V. Torres, P. Rodríguez-Ulibarri, M. Navarro-Cía, and M. Beruete, "Circuito equivalente del metamaterial fishnet de doble capa," in *XXVIII Simposium Nacional de la Unión Científica Internacional de Radio URSI 2013*, (Santiago de Compostela), 2013.

[Conf 27] V. Pacheco-Peña, B. Orazbayev, V. Torres, M. Beruete, and M. Navarro-Cía, "Slimming the fishnet metamaterial lens," in *8th European Conference on Antennas and Propagation EuCAP 2014*, (The Hague), 2014.

[Conf 28] H. Aouani, M. Rahmani, H. Šípová, V. Torres, K. Hegnerová, M. Beruete, M. Hong, J. Homola, M. Navarro-Cía, and S. A. Maier, "Surface-enhanced spectroscopy from visible to infrared using a single plasmonic nanoantenna," in *EUROPT(R)ODE XII Conference on Optical Chemical Sensors & Biosensors*, (Athens), 2014.